PROCRUSTEAN ENTANGLEMENT CONCENTRATION, WEAK MEASUREMENTS AND OPTIMIZED STATE PREPARATION FOR CONTINUOUS-VARIABLE QUANTUM OPTICS

David Menzies

A Thesis Submitted for the Degree of PhD
at the
University of St. Andrews

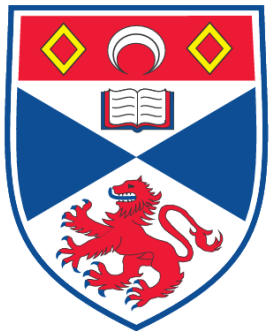

2009

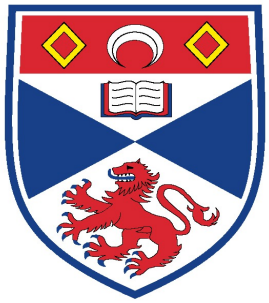

University
of
St Andrews

Procrustean entanglement concentration, weak measurements and optimized state preparation for continuous-variable quantum optics

David Menzies

PhD Thesis

School of Physics and Astronomy

University of St. Andrews

North Haugh

St. Andrews

KY16 9SS, UK.

March 30, 2009

Abstract

In this thesis, we are concerned with continuous-variable quantum optical state engineering protocols. Such protocols are designed to repair or enhance the non-classical features of a given state. In particular, we build a weak measurement model of Gaussian entanglement concentration of the two mode squeezed vacuum state. This model allows the simultaneous description of all possible ancilla system variations. In addition, it provides an explanation of the Gaussian-preserving property of these protocols while providing a success criterion which links all of the degrees of freedom on the ancilla. Following this, we demonstrate the wider application of weak measurements to quantum optical state engineering by showing that they allow probabilistic noiseless amplification of photon number. We then establish a connection between weak measurements and entanglement concentration as a fundamental result of weak measurements on entangled probes. After this, we explore the trade-off between Gaussian and non-Gaussian operations in the preparation of non-Gaussian pure states. In particular, we suggest that an operational cost for an arbitrary non-Gaussian pure state is the largest Fock state required for its approximate preparation. We consider the extent to which this non-Gaussian operational cost can be reduced by applying unitary Gaussian operations. This method relies on the identification of a minimal core state for any target non-Gaussian pure state.

Declarations

I, David Menzies, hereby certify that this thesis, which is approximately 27000 words in length, has been written by me, that it is the record of work carried out by me and that it has not been submitted in any previous application for a higher degree.

Date: 30/01/09, Signature of candidate:

I was admitted as a research student in September, 2005 and as a candidate for the degree of Doctor of Philosophy in September, 2005; the higher study for which this is a record was carried out in the University of St Andrews between 2005 and 2009.

Date: 30/01/09, Signature of candidate:

I hereby certify that the candidate has fulfilled the conditions of the Resolution and Regulations appropriate for the degree of Doctor of Philosophy in the University of St Andrews and that the candidate is qualified to submit this thesis in application for that degree.

Date: 30/01/09, Signature of supervisor:

In submitting this thesis to the University of St Andrews I understand that I am giving permission for it to be made available for use in accordance with the regulations of the University Library for the time being in force, subject to any copyright vested in the work not being affected thereby. I also understand that the title and abstract will be published, and that a copy of the work may be made and supplied to any bona fide library or research worker, that my thesis will be electronically accessible for personal or research use, and that the library has the right to migrate my thesis

into new electronic forms as required to ensure continued access to the thesis. I have obtained any third-party copyright permissions that may be required in order to allow such access and migration, or have requested the appropriate embargo below.

Date: 30/01/09, Signature of candidate:

The following is an agreed request by candidate and supervisor regarding the electronic publication of this thesis:
Access to Printed copy and electronic publication of the thesis through the University of St Andrews.

Signature of candidate:
Signature of supervisor:
Date: 30/01/09

Acknowledgements

There are a number of people without whom this thesis would not be possible. First of all, I would like to thank my supervisor Natalia Korolkova for all her encouragement, guidance and advice with my research. I would also like to thank my collaborators, Radim Filip and Sarah Croke for sharing their talent, ideas and advice with me during the course of our research projects. On top of that I'd like to thank my physics comrades Gary, Jill, Steve and Andrew for the banter over the last three years. Finally, I'd like to thank Amy for her patience, support and understanding during my PhD.

Publications and pre-prints

The following is a list of the publications that arose as a result of the research invested in this thesis:

1. D. Menzies and N. V. Korolkova, *Procrustean entanglement concentration of continuous-variable states of light*, Phys. Rev. A. **74**, 042315, (2006) [1].

2. D. Menzies and N. V. Korolkova, *Weak values and continuous-variable entanglement concentration*, Phys. Rev. A. **76**, 062310, (2007) [2].

3. D. Menzies and N. V. Korolkova, *Weak measurements on entangled probes*, Phys. Rev. A. **77**, 062105, (2008) [3].

4. D. Menzies and R. Filip, *Gaussian optimized preparation of non-Gaussian pure states*, Phys. Rev. A **79**, 012313 (2009) [4].

5. D. Menzies and S. Croke, *Noiseless amplification of photon number via weak measurements*, pre-print arXiv:0903.4181v1 (2009) [5].

Conference presentations

The following is a list of my conference presentations

1. International workshop on Continuous Variable Quantum Information Processing 2005 (CVQIP'05), Copenhagen 2005, Poster presentation.

2. Frontiers of Quantum Optics SUPA meeting 2006, St. Andrews 2006, Oral presentation.

3. International workshop on CVQIP'06 Workshop, St. Andrews 2006, Poster presentation .

4. International Conference on Coherent and Nonlinear Optics (ICONO/LAT'07), Minsk 2007, Oral presentation.

5. Workshop on Modern Trends in Quantum Optics and Quantum Information, Prague 2008, Poster presentation.

6. PHOTON'08/QEP18 Conference, Edinburgh 2008, Poster presentation.

7. QUSICO Meeting, St. Andrews 2008, Poster presentation.

Contents

Chapter 1

Introduction and overview

1.1 Motivational remarks

Historically, quantum mechanics was born from a necessity to explain a number of counter intuitive phenomena unintelligible from a classical point of view. Whilst the empirical successes of quantum mechanics are undeniable, the absence of a universally accepted physical interpretation means that the theory remains rather enigmatic. In particular, many of the key theorems of quantum mechanics such as the uncertainty principle, measurement theory and entanglement are presented in a negative light [6]. However, an alternative viewpoint has begun to emerge from the invention and development of quantum information theory. Its central tenet is the realisation that quantum mechanical systems can be exploited to perform computational and information processing tasks in a manner that could offer distinct advantages over the nearest classical counterpart. Consequently, it allows for an appreciation of the phantom properties of quantum states as potentially useful physical communication and computation resources [6]. This is the inspiration that has led to the discovery of applications such as quantum teleportation [7, 8], fast factorization algorithms [9, 10] and quantum key distribution [11–13].

Thus, the legacy of quantum information theory is the understanding that quantum mechanics can offer certain subtle advantages provided one has access to the necessary non-classical resource. This view point immediately engenders a motiva-

tion to pursue two related fields of study. The first is concerned with the conception of protocols which exploit a given non-classical resource. The second is focused on the preparation, repair and augmentation of particular non-classical features for use in the aforementioned protocols. This second branch is called state engineering and it forms a crucial part of quantum information.

While the notion of state engineering applies to any quantum system, we confine our attention to the continuous-variable quantum degrees of freedom of the light field. Ultimately, this is because the technology required to produce a variety of Gaussian quantum optical states and operations is very well developed and understood [14]. Thus, such states and operations can be implemented with relative ease. However, these successes are tempered by the limitations set by restricting ourselves to Gaussian states and operations alone. Indeed, while a number of known quantum algorithms can be implemented using just Gaussian states and operations [15], there exist a few important exceptions. These include entanglement distillation of Gaussian states [16–18] and universal quantum computing with Gaussian states [19, 20]. Both of these require additional non-Gaussian states and operations to work. These non-Gaussian states and operations are difficult to produce experimentally and lack a comprehensive theoretical understanding enjoyed by their Gaussian cousins [15, 21].

It is in this fertile area of quantum information with continuous-variable quantum optical systems that this thesis resides. In particular, this thesis is concerned with the study of state engineering protocols which require the use of non-Gaussian resources in addition to Gaussian ones to achieve the desired result. In this context, this thesis carries two main messages. Firstly, weak values and weak measurements can be an extremely useful tool in understanding the mechanism behind certain quantum optical state engineering protocols. We demonstrate this utility with respect to entanglement concentration of Gaussian states and their ability to allow probabilistic noiseless amplification of photon number for a subset of quantum optical states. Secondly, we explore non-Gaussian pure state preparation. In this context, we investigate the potential benefits of the judical application of optimized

unitary Gaussian operations in the probabilistic preparation of non-Gaussian pure states. Thus, this thesis seeks to investigate two specialized open problems of state engineering with respect to continuous-variable quantum optical information.

1.2 Overview: thesis in a nutshell

We begin this thesis with two review chapters which aim to revise a number of standard and extremely useful results from quantum optics, bipartite entanglement theory and Gaussian state entanglement concentration. These notions are discussed in chapters two and three. The latter ends with some open problems related to a particular Gaussian entanglement concentration protocol. The resolution of these outstanding issues can be found in the notion of weak values and weak measurements reviewed in chapter four. In chapter five we outline the first of our novel contributions by demonstrating a link between weak measurements and entanglement concentration. The origin of this link is found in attempting to generalize the non-linear medium protocol discussed in chapter three to arbitrary ancillary systems. In essence, the preparation and eventual measurement of the ancilla before and after its interaction with the entangled state can be interpreted as pre and post-selections. Thus, one can view the protocol as a weak measurement of the ancilla encoded onto the entangled state. The prerequisites of a weak measurement are directly responsible for the Gaussian-preserving effect manifest in such protocols.

Following our discussion of the application of the weak measurement formalism to Gaussian entanglement concentration, we present our next contribution by extending the utility of weak measurements. In particular, in chapter six we demonstrate how weak measurements allow the probabilistic realisation of the non-physical operation of noiseless amplification on a subset of quantum states. In this context, non-physical means that the probabilistic back-action applied to the probe state does not obey all of the axioms of a positive operator valued measure (POVM) for arbitrary states. Instead, these axioms are only satisfied on a reduced set of states that obey the weakness conditions. The implications of this noiseless ampli-

fication is then discussed for a variety of quantum protocols including amplifying weak Schrödinger cat states, cloning weak coherent states and weak coherent state quantum key distribution.

Further investigation in chapter six leads to our next contribution by revealing a novel and fundamental connection between weak values and the manipulation of entangled states. In particular, we show that a weak measurement where the probe state is prepared in an arbitrary pure bipartite entangled state can increase the entanglement available if the encoded weak value has a non-zero imaginary component. Ultimately, this is due to the non-unitary effect accompanying the imaginary part of the weak value. A further condition emerges on the observable acting on the probe in the interaction Hamiltonian: the probe observable must be able to distinguish between states of different Von Neumann entropies. To understand this condition, we make an appealing analogue with the notion of entanglement witnesses employed in the discussion of mixed state entanglement.

Leaving behind the weak measurement paradigm in chapter seven, we present our final contribution where we consider the possible application of deterministic Gaussian operations in the conditional state preparation of pure non-Gaussian states. This idea is based on the ability to conditionally generate a finite superposition of Fock states using an array of photon subtraction or addition measurements. One can regard this process as a way to obtain finite dimensional approximations, to a given accuracy measured by the fidelity, of a desired infinite dimensional non-Gaussian state. We suggest that unitary Gaussian operations can be used to reduce the non-Gaussian resources required for the construction of the state. The basis of this postulate is the notion of a core state, related to the target state via Gaussian unitary operations. This core state can require a smaller non-Gaussian resource overhead to construct than a direct truncation of the desired target. Thus, we suggest that one construct the core state and then apply Gaussian unitary operations to obtain the desired target to a specified accuracy. We demonstrate the utility of this method by applying it to the Schrödinger cat states.

Part I

Literature review

Chapter 2

Theoretical quantum optics

2.1 Quantisation of the field

Quantum optics provides the most accurate understanding of the electromagnetic field in the non-relativistic regime. We will begin by outlining the standard textbook canonical quantisation approach as described in [22–29], to name but a few. The starting point of quantum optics is the quantisation of the electromagnetic field by the replacing of classical fields $\mathbf{E}(\mathbf{r},t)$ and $\mathbf{B}(\mathbf{r},t)$, with quantum mechanical observables $\hat{\mathbf{E}}(\mathbf{r},t)$ and $\hat{\mathbf{B}}(\mathbf{r},t)$. In the non-relativistic regime, this task is accomplished by adopting the *Coulomb* gauge $\nabla\cdot\mathbf{A}(\mathbf{r},t)=0$, before solving the associated vacuum wave equation

$$\nabla^2\mathbf{A}(\mathbf{r},t)=c^{-2}\partial_t^2\mathbf{A}(\mathbf{r},t) \tag{2.1}$$

while imposing periodic boundary conditions. Consequently, the general solution can be written as a Fourier decomposition over plane waves

$$\mathbf{A}(\mathbf{r},t)=(\epsilon_0 V)^{-1/2}\sum_{\mathbf{k}}\sum_{s=1}^{2}\mathbf{e}_{\mathbf{k}s}\left(a_{\mathbf{k}s}e^{i\mathbf{k}\cdot\mathbf{r}-i\omega t}+a_{\mathbf{k}s}^{*}e^{-i\mathbf{k}\cdot\mathbf{r}+i\omega t}\right). \tag{2.2}$$

Where $\mathbf{e}_{\mathbf{k}s}$ are unit polarisation vectors defined by $\mathbf{k}\cdot\mathbf{e}_{\mathbf{k}s}=0$ ensuring that the field is transverse in nature. Each mode is labeled by the wavevector $\mathbf{k}$ and polarization s. The $\mathbf{k}$ is discrete since the classical field exists inside an imaginary cube of length L and volume $V=L^3$ with periodic boundary conditions at the walls.

The quantisation of this field is performed by replacing the complex coefficients $\{a_{\mathbf{k}s}, a^*_{\mathbf{k}s}\}$ with bosonic creation and annihilation operators $\{\hat{a}_{\mathbf{k}s}, \hat{a}^\dagger_{\mathbf{k}s}\}$. This is done in anticipation of the emergence of bosonic quanta of the field (photons) and is completely consistent with the linear nature of the classical field equations. The creation and annihilation operators are subject to the equal-time commutation relations

$$[\hat{a}_{\mathbf{k}s}(t), \hat{a}^\dagger_{\mathbf{k}'s'}(t)] = \delta_{\mathbf{k}\mathbf{k}'}\delta_{ss'},\ [\hat{a}_{\mathbf{k}s}(t), \hat{a}_{\mathbf{k}'s'}(t)] = [\hat{a}^\dagger_{\mathbf{k}s}(t), \hat{a}^\dagger_{\mathbf{k}'s'}(t)] = 0. \tag{2.3}$$

Thus, the quantized vacuum field solution is then

$$\hat{\mathbf{A}}(\mathbf{r}, t) = \sqrt{\frac{\hbar}{2\epsilon_0 V}} \sum_{\mathbf{k},s} \mathbf{e}_{\mathbf{k}s} \left(\hat{a}_{\mathbf{k}s} e^{i\mathbf{k}\cdot\mathbf{r} - i\omega t} + \hat{a}^\dagger_{\mathbf{k}s} e^{-i\mathbf{k}\cdot\mathbf{r} + i\omega t} \right) \tag{2.4}$$

and so, the corresponding field observables can be obtained from the quantised vector potential via the relations $\nabla \times \hat{\mathbf{A}} = \hat{\mathbf{B}}$ and $\hat{\mathbf{E}} = -\partial_t \hat{\mathbf{A}}$ and, in turn, allow the calculation of the Hamiltonian of the field

$$\hat{H} = \frac{1}{2} \int d^3\mathbf{r} \left(\varepsilon_0 \hat{\mathbf{E}}^2 + \frac{1}{\mu_0} \hat{\mathbf{B}}^2 \right) = \sum_{\mathbf{k}} \sum_{s=1}^{2} \omega_{\mathbf{k}} \hbar (\hat{a}^\dagger_{\mathbf{k}s} \hat{a}_{\mathbf{k}s} + 1/2). \tag{2.5}$$

The interpretation of this equation is clear - the quantum electromagnetic field is analogous to an infinite set of independent quantum harmonic oscillators. Consequently, most of the physics of the field can be understood through the properties of these oscillators and the quantum mechanical formalism associated with them.

Quantum mechanics requires an association between each mode and an appropriately defined Hilbert space [30]. In this case, each mode is a simple harmonic oscillator labeled by wavevector $\mathbf{k}$ and polarization s and has a state space $\mathcal{H}_{\mathbf{k}s}$. The entire state space of the field is then given as:

$$\mathcal{H} = \bigotimes_{\mathbf{k}} \bigotimes_{s=1}^{2} \mathcal{H}_{\mathbf{k}s} = \bigotimes_{\mathbf{k}} \mathcal{H}_{\mathbf{k}1} \otimes \mathcal{H}_{\mathbf{k}2}. \tag{2.6}$$

From now on, we will only consider very simple fields composed of one or two modes. Accordingly, we will drop the index notation for brevity.

Following the derivation of the Hamiltonian of the field, we use its eigenstates to define the associated Hilbert space of each mode. These aforementioned eigenstates are the *Fock* or photon number states

$$\hat{n}|n\rangle = \hat{a}^\dagger \hat{a}|n\rangle = n|n\rangle. \tag{2.7}$$

In the standard analysis of the quantum harmonic oscillator, the number states correspond to a definite energy of the oscillator labeled by the quantum number n. A similar interpretation applies here, which follows from the conventional wisdom of second quantized field theories, namely that the field operators $\hat{\mathbf{E}}(\mathbf{r},t)$ and $\hat{\mathbf{B}}(\mathbf{r},t)$ create and annihilate their associated quanta. This follows from the action of the creation and annihilation operators on Fock states as

$$\hat{a}|n\rangle = \sqrt{n}|n-1\rangle, \;\; \hat{a}^{\dagger}|n\rangle = \sqrt{n+1}|n+1\rangle, \tag{2.8}$$

i.e. the operators $\hat{a}$ and $\hat{a}^{\dagger}$ reduce or increase the number of photons by one. Consequently, the states $|n\rangle$ describe the case when the field is composed of n photons with a well defined energy $E_n = \hbar\omega(n+1/2)$. Thus, the ground or *vacuum* state of the field describes the complete absence of photons i.e. $\hat{a}|0\rangle = 0$ and so the energy in the vacuum state is just the zero-point energy of the field $E_0 = \hbar\omega/2$.

The excited states $|n\rangle$ can be obtained from the vacuum by the application of the creation and annihilation operators

$$\frac{(\hat{a}^{\dagger})^n}{\sqrt{n!}}|0\rangle = |n\rangle, \;\; \frac{(\hat{a})^n}{\sqrt{n!}}|n\rangle = |0\rangle. \tag{2.9}$$

Mathematically, the Fock states are complete meaning that they allow a resolution of the identity

$$\sum_{n=0}^{\infty} |n\rangle\langle n| = \hat{I}, \tag{2.10}$$

and can, consequently, allow the linear decomposition of any other state of the field

$$\hat{\rho} = \sum_{m,n=0}^{\infty} \langle n|\hat{\rho}|m\rangle |n\rangle\langle m| = \sum_{m,n=0}^{\infty} \rho_{nm}|n\rangle\langle m| \tag{2.11}$$

and for pure states we get $|\psi\rangle = \sum_{n=0}^{\infty} \psi_n |n\rangle$. The existence of Fock states is the precise manifestation of particulate behaviour of light. That is, the Fock states describe the quantized excitations, photons, of the underlying quantum field, i.e. the particulate nature of the field. However, caution must be exercised when employing this picture since the photons are not particles in the traditional sense as they are delocalized over the quantisation volume of the field [28, 29].

2.2 Phase space description

2.2.1 Wigner functions

To aid in the visualization of quantum optical states it is useful to consider their phase-space representation in order to exploit intuition gained from classical physics [15]. This phase space representation of states and operations follows from the mathematical description employed by quantum mechanics. On one level, pure states are represented as normalised vectors in a Hilbert space $\mathcal{H}$ equipped with an inner product $(|\psi\rangle, |\phi\rangle) := \langle\psi|\phi\rangle$. However, the operators which act on these states also form their own larger Hilbert space which has its own inner product defined by $(\hat{A}, \hat{B}) := \mathrm{Tr}(\hat{A}^\dagger \hat{B})$. Consequently, in analogue to decomposing a vector in terms of a basis, we can equally decompose any operator in terms of a basis of this larger space. For example, suppose the operators $\{\hat{\omega}\}_{\omega\in\Omega}$ form such a basis, then any operator $\hat{A}$ can be decomposed as

$$\hat{A} = \sum_{\omega\in\Omega} (\hat{\omega}, \hat{A})\hat{\omega} = \sum_{\omega\in\Omega} \mathrm{Tr}(\hat{\omega}^\dagger \hat{A})\hat{\omega}. \tag{2.12}$$

This notion of decomposing operators also applies to quantum states $\hat{\rho}$ allowing $\hat{\rho} = \sum_{\omega\in\Omega} \mathrm{Tr}(\hat{\omega}^\dagger\hat{\rho})\hat{\omega}$. The phase space description of states and operations then follows from a particular choice of basis operators [31]

$$\hat{O} = \frac{1}{\pi} \int d^2\alpha \, \mathrm{Tr}(\hat{D}(\alpha)\hat{O})\hat{D}^\dagger(\alpha), \tag{2.13}$$

where $\alpha = (q - ip)/\sqrt{2}$. Then (q, p) are the canonical coordinates of phase space and

$$\hat{D}(\alpha) = \exp\left(\alpha\hat{a}^\dagger - \alpha^*\hat{a}\right), \tag{2.14}$$

is the unitary Weyl or *displacement* operator and obeys $\hat{D}^\dagger(\alpha)\hat{D}(\alpha) = \hat{D}(-\alpha^*)\hat{D}(\alpha) = \hat{I}$. In addition, the displacement operator also obeys [31] $\mathrm{Tr}(\hat{D}(\alpha)) = \mathrm{Tr}(\hat{D}^\dagger(\alpha)) = \pi\delta^2(\alpha) = \pi\delta(\Re(\alpha))\delta(\Im(\alpha))$ and $\hat{D}(\alpha_1)\hat{D}(\alpha_2) = e^{(\alpha_1\alpha_2^* - \alpha_1^*\alpha_2)/2}\hat{D}(\alpha_1 + \alpha_2)$.

Thus, just as a particular pure state $|\psi\rangle$ can be described by a continuous-variable wave-function $\psi(q) = \langle q|\psi\rangle$, an operator $\hat{O}$ admits a phase space function $O(q, p) = \mathrm{Tr}(\hat{D}(\alpha)\hat{O})$. Furthermore, since quantum states can also be described as

density operators $\hat{\rho}$, then we can replace the wave-function description with that of a characteristic function [15]

$$\chi(\alpha) = \mathrm{Tr}\left(\hat{\rho}\,\hat{D}(\alpha)\right). \tag{2.15}$$

Where the *Fourier* transform of this characteristic function yields the associated quasi-probability distribution

$$\mathcal{P}(\alpha) = (2\pi)^{-1}\int d^2\beta\, e^{i(\alpha\beta^* + \alpha^*\beta)}\chi(\beta), \tag{2.16}$$

where $\alpha = 2^{-1/2}(q+ip)$. This quasi-probability distribution is known as the Wigner function [32] and the above can be re-written [27] in the form

$$W_\rho(q,p) = \frac{1}{2\pi}\int_{-\infty}^{\infty} dx e^{ipx}\left\langle q - \frac{x}{2}\right|\hat{\rho}\left|q + \frac{x}{2}\right\rangle. \tag{2.17}$$

Since the Wigner function is a quasi-probability distribution then it obeys [27]

$$W_\rho(q,p) = W_\rho^*(q,p), \quad \int_{-\infty}^{\infty}\int_{-\infty}^{\infty} dq\, dp\, W_\rho(q,p) = 1, \tag{2.18}$$

whilst allowing the calculation of the marginal distributions [27]

$$\langle q|\hat{\rho}|q\rangle = \int_{-\infty}^{\infty} dp\, W_\rho(q,p), \quad \langle p|\hat{\rho}|p\rangle = \int_{-\infty}^{\infty} dq\, W_\rho(q,p). \tag{2.19}$$

Both of these attributes are shared with actual classical joint probability distributions, however the distinguishing feature of the Wigner function that grants it the status of a quasi-probability distribution is its potential for negativity. Thus, there are some quantum states $\hat{\rho}$ which have associated Wigner functions that have negative regions and so cannot be considered proper probability distributions [28].

There are several motivations for employing the Wigner function description of quantum states. Firstly, Wigner functions allow an immediate visualisation of a particular state $\hat{\rho}$ in terms as a distribution over a phase space with canonical coordinates (q,p) from $\alpha = 2^{-1/2}(q+ip)$. This picture can aid in both the definition and identification of certain characteristics of quantum states. For example, Wigner functions allow a classification of quantum states as either Gaussian or non-Gaussian depending on their shape [15]. Secondly, the fact that some quantum states can have

negative or ill-behaved Wigner functions has led to the notion of non-classicality (i.e. the degree by which the Wigner function cannot be considered a proper probability distribution) of the associated state [33–36] and the ability to quantify this non-classicality via the negativity of the Wigner function. Thirdly, the Wigner function allows the calculation of operator moments on phase space by making use of the trace rule

$$\mathrm{Tr}(\hat{\rho}\hat{A}) = 2\pi \int_{-\infty}^{\infty} dq\, dp\, W_\rho(q,p) W_A(q,p), \tag{2.20}$$

with $W_\rho(q,p)$ being the Wigner function of $\hat{\rho}$ and $W_A(q,p)$ begin the analogous object for $\hat{A}$:

$$W_A(q,p) = \frac{1}{2\pi} \int_{-\infty}^{\infty} dx e^{ipx} \left\langle q - \frac{x}{2} \right| \hat{A} \left| q + \frac{x}{2} \right\rangle. \tag{2.21}$$

In particular, the Wigner function is ideally suited to the calculation of the average of any symmetric polynomial of $\hat{q}$ and $\hat{p}$ denoted by $\mathcal{S}(\hat{q}^m, \hat{p}^n)$, for example $\mathcal{S}(\hat{q},\hat{p}) = (\hat{q}\hat{p} + \hat{p}\hat{q})/2$, as

$$\mathrm{Tr}\left(\hat{\rho}\mathcal{S}(\hat{q}^m, \hat{p}^n)\right) = 2\pi \int dq\, dp\, W(q,p) q^m p^n. \tag{2.22}$$

Finally, we note that the single mode Wigner function can be generalized to a field of N modes with

$$\begin{aligned} W(q_1, p_1, \ldots, q_N, p_N) = \frac{1}{(2\pi)^N} \int_{\infty}^{\infty} \cdots \int_{\infty}^{\infty} \prod_{j=1}^{N} dx_j e^{ip_j x_j} \\ \times \left\langle q_1 - \frac{x_1}{2}, \ldots, q_N - \frac{x_N}{2} \right| \hat{\rho} \left| q_1 + \frac{x_1}{2}, \ldots, q_N + \frac{x_N}{2} \right\rangle \end{aligned} \tag{2.23}$$

being the Wigner function for the N mode field state $\hat{\rho}$. For example, the Wigner function of the single mode vacuum state is $W_0(q,p) = (\pi)^{-1} \exp(-q^2 - p^2)$ [27] and the N mode vacuum is $W_0(q_1, p_1, \ldots, q_N, p_N) = (\pi)^{-N} \prod_{j=1}^{N} \exp(-q_j^2 - p_j^2)$.

2.2.2 Quadratures

The phase space picture of quantum states provide by the Wigner function is also directly related to the canonical position and momentum observables of each field mode. These observables follow from the mathematical description of field modes as quantum harmonic oscillators and are called the quadratures of the field

$$\hat{Q}_{\mathbf{k}s} = \sqrt{\frac{\hbar}{2\omega_{\mathbf{k}}}} (\hat{a}_{\mathbf{k}s}(t) + \hat{a}^\dagger_{\mathbf{k}s}(t)), \quad \hat{P}_{\mathbf{k}s} = i\sqrt{\frac{\hbar\omega_{\mathbf{k}}}{2}} (\hat{a}^\dagger_{\mathbf{k}s}(t) - \hat{a}_{\mathbf{k}s}(t)). \tag{2.24}$$

These operators observe the usual commutation relations

$$[\hat{Q}_{\mathbf{k}s}(t), \hat{P}_{\mathbf{k}'s'}(t)] = i\hbar\delta_{\mathbf{k}'\mathbf{k}}\delta_{ss'}, \;\; [\hat{Q}_{\mathbf{k}s}(t), \hat{Q}_{\mathbf{k}'s'}(t)] = [\hat{P}_{\mathbf{k}s}(t), \hat{P}_{\mathbf{k}'s'}(t)] = 0, \tag{2.25}$$

and can be understood, physically, as the *Fourier* components of the electromagnetic field observables [27] and not the position and momentum of the underlying quanta. To see this, consider the electric field observable of a single mode field (with constant polarization):

$$\hat{E}(\mathbf{r}, t) = iE_0 \left(\hat{a}e^{i(\mathbf{k}\cdot\mathbf{r}-\omega t)} + \hat{a}^\dagger e^{-i(\mathbf{k}\cdot\mathbf{r}-\omega t)}\right). \tag{2.26}$$

Next substitute for the relation: $\hat{a} = 2^{-1/2}(\hat{q} + i\hat{p})$, where we defined the dimensionless quadratures $\hat{q} = \sqrt{\frac{\omega}{\hbar}}\hat{Q}$ and $\hat{p} = \frac{1}{\sqrt{\hbar\omega}}\hat{P}$ to give

$$\hat{E}(\mathbf{r}, t) = E_0\sqrt{2}\left(\hat{q}\sin(\mathbf{k}\cdot\mathbf{r} - \omega t) - \hat{p}\cos(\mathbf{k}\cdot\mathbf{r} - \omega t)\right). \tag{2.27}$$

Thus, the $(\hat{q}, \hat{p})$ operators can be interpreted as the *Fourier* components of $\hat{E}(\mathbf{r}, t)$ which accompany the $\sin(\mathbf{k}\cdot\mathbf{r} - \omega t)$ and $\cos(\mathbf{k}\cdot\mathbf{r} - \omega t)$ plane waves, respectively.

These operators have eigenstates defined as $\hat{q}|q\rangle = q|q\rangle$, $\hat{p}|p\rangle = p|p\rangle$. Moreover, since $[\hat{q}, \hat{p}] = i$ then both $\hat{q}$ and $\hat{p}$ are unbounded operators with continuous spectra and so their eigenstates are complete

$$\int_{-\infty}^{\infty} |q\rangle\langle q| dq = \int_{-\infty}^{\infty} |p\rangle\langle p| dp = \hat{I}, \tag{2.28}$$

but not normalisable; They do not actually exist inside the configuration space of the field as they are not square integrable $\langle q'|q\rangle = \delta(q' - q)$, $\langle p'|p\rangle = \delta(p' - p)$. However, they can still be accommodated by extending the Hilbert space to include them [25, 31]. Furthermore, we can represent these eigenstates as a function of the creation operator on the vacuum [25, 31]

$$|q\rangle = \pi^{-1/4}\exp\left(-q^2/2 + \sqrt{2}q\hat{a}^\dagger - (\hat{a}^\dagger)^2/2\right)|0\rangle, \tag{2.29}$$

$$|p\rangle = \pi^{-1/4}\exp\left(-p^2/2 + i\sqrt{2}p\hat{a}^\dagger + (\hat{a}^\dagger)^2/2\right)|0\rangle. \tag{2.30}$$

These quadrature operators and eigenstates are directly related to the phase space picture mentioned earlier with the Wigner functions of the quadrature observables corresponding to the canonical coordinates of the phase space

$$W_q(q, p) = q, \;\; W_p(q, p) = p. \tag{2.31}$$

This means that the Wigner function of a particular state $\hat{\rho}$ can be reconstructed by repeated measurement of the quadrature observables on an identically prepared ensemble in a process known as quantum tomography [27].

Finally, we also note a useful generalization of quadrature operators from the standard canonical $\{\hat{q}, \hat{p}\}$ operators to [25, 31]

$$\hat{x}_\theta = \cos\theta\hat{q} + \sin\theta\hat{p} = \frac{\hat{a}e^{-i\theta} + \hat{a}^\dagger e^{i\theta}}{\sqrt{2}}. \tag{2.32}$$

These generalized quadratures simply correspond to a rotation of phase space by an angle θ since

$$W_{x_\theta}(q,p) = \cos\theta q + \sin\theta p, \quad W_{x_{\theta+\pi/2}}(q,p) = \cos\theta p - \sin\theta q. \tag{2.33}$$

In addition, they obey the commutation relation

$$[\hat{x}_\phi, \hat{x}_\theta] = \cos\phi\sin\theta[\hat{q},\hat{p}] + \sin\phi\cos\theta[\hat{p},\hat{q}] = i\sin(\theta-\phi), \tag{2.34}$$

where each $\hat{x}_\theta$ admits a complete eigenbasis $\{|x_\theta\rangle\}_{x_\theta\in(-\infty,\infty)}$

$$\int dx_\theta |x_\theta\rangle\langle x_\theta| = \hat{I}, \tag{2.35}$$

and are not normalisable since $\langle x_\theta|x'_\theta\rangle = \delta(x_\theta - x'_\theta)$. They can, however, be expressed as a function of creation operators on the vacuum state [25]

$$|x_\theta\rangle = \pi^{-1/4}\exp\left(-x_\theta^2/2 + \sqrt{2}e^{i\theta}\hat{a}^\dagger - e^{2i\theta}(\hat{a}^\dagger)^2/2\right)|0\rangle. \tag{2.36}$$

2.3 Gaussian and non-Gaussian states

The phase space description of quantum states allows one to immediately recognize the reality of two varieties of quantum optical state: Gaussian and non-Gaussian. The former are states with Gaussian characteristic functions and corresponding Gaussian quasi-probability distributions. Thus, for example, an N mode field state $\hat{\rho}$ is Gaussian if its associated Wigner function is a Gaussian function of the canonical coordinates of phase space [21]

$$W(q_1,p_1,\ldots,q_N,p_N) = \frac{\exp\left(-\frac{1}{2}(\xi-\mathbf{d})^T\,\gamma\,(\xi-\mathbf{d})\right)}{\sqrt{(2\pi)^N \det\gamma}}. \tag{2.37}$$

Here ξ is a $2N$ dimensional phase space vector labeling phase space events $\xi^T = (q_1, p_1, \ldots, q_N, p_N)$, related to the corresponding phase space vector operator $\hat{\xi}^T = (\hat{q}_1, \hat{p}_1, \ldots, \hat{q}_N, \hat{p}_N)$ and $\mathbf{d} = \langle\hat{\xi}\rangle = (\Re(d_1), \Im(d_1), \Re(d_2), \Im(d_2), \ldots, \Re(d_N), \Im(d_N))^T$ is a $2N$ dimensional vector representing the possible displacement from the origin of phase space. The covariance matrix γ is the $2N \times 2N$ dimensional matrix whose components are given by

$$\gamma_{jk} = \langle\{\hat{\xi}_j, \hat{\xi}_k\}\rangle - 2\langle\hat{\xi}_j\rangle\langle\hat{\xi}_k\rangle. \tag{2.38}$$

A covariance matrix must obey the generalized Heisenberg inequality $\gamma + iJ^{\oplus N} \geq 0$, where

$$J = \begin{pmatrix} 0 & 1 \\ -1 & 0 \end{pmatrix}, \tag{2.39}$$

is the symplectic matrix [15]. The physical meaning of this inequality is that γ must reflect the requisite conditions of both the density operator and Heisenberg's uncertainty relation for non-commuting quadrature observables. The latter follows since the matrix $iJ^{\oplus N}$ comprises the commutation relations of $[\xi_j, \xi_k]$ [15, 21]. From the above definition of Gaussian states, one immediately notes the key properties of this class of states. Firstly, Gaussian states are exhaustively described by their first and second order phase space moments. This follows since each Gaussian state is exhaustively defined by its corresponding correlation matrix, which only contains information about the first and second order moments of $\hat{q}$ and $\hat{p}$. Secondly, the Wigner function of a Gaussian state is always positive and behaves as a bona-fide probability distribution. Thirdly, Gaussian states can only be generated by Hamiltonians which are quadratic in quadrature operators, since if this were not the case, then we would require additional knowledge of higher order moments to specify the state.

The distinction between Gaussian and non-Gaussian states and operations is important because of the resource paradigm of quantum information theory. Under this philosophy, Gaussian and non-Gaussian states and operations are regarded as different types of resource to be used in various information protocols. Moreover, it is clear that non-Gaussian resources are required for the successful and efficient

implementation of certain information processing tasks. For example, proposals for universal quantum computation using continuous-variables require Hamiltonians that are polynomials of quadrature operators with degree > 2 [19].

2.4 Useful Gaussian states and operations

2.4.1 Coherent states

A radiation field can be prepared in a coherent state as a result of interacting with a classical electric current. In particular, a quantized field described by $\hat{\mathbf{A}}(\mathbf{r},t)$ interacts with a classical current $\mathbf{J}(\mathbf{r},t)$ via the Hamiltonian [28] (in the interaction picture)

$$\hat{H}_I(t) = \int_V d^3\mathbf{r}\, \mathbf{j}(\mathbf{r},t)\cdot\hat{\mathbf{A}}(\mathbf{r},t). \tag{2.40}$$

where $\mathbf{J}(\mathbf{r},t) = \int_V d^3\mathbf{r}\, \mathbf{j}(\mathbf{r},t)$ relates the current $\mathbf{J}(\mathbf{r},t)$ to its associated current density $\mathbf{j}(\mathbf{r},t)$. After much algebra [28], this interaction Hamiltonian can be shown to generate the evolution operator

$$\hat{U}_I = \prod_{\mathbf{k}s} \exp\left(\alpha(t)^*_{\mathbf{k}s}\hat{a}^\dagger_{\mathbf{k}s} - \alpha(t)_{\mathbf{k}s}\hat{a}_{\mathbf{k}s}\right), \tag{2.41}$$

where $\alpha(t)_{\mathbf{k}s} = -\frac{i}{\hbar}\sqrt{\frac{\hbar}{2\epsilon_0 V}}\int_0^t d\tau e^{-i\omega\tau}\tilde{\mathbf{j}}(\mathbf{k},\tau)\cdot\mathbf{e}_{\mathbf{k}s}$. This evolution operator on the vacuum state generates a coherent state

$$|\alpha(t)\rangle = \hat{U}_I\bigotimes_{\mathbf{k}s}|0\rangle_{\mathbf{k}s} = \bigotimes_{\mathbf{k}s}\exp\left(\alpha(t)^*_{\mathbf{k}s}\hat{a}^\dagger_{\mathbf{k}s} - \alpha(t)_{\mathbf{k}s}\hat{a}_{\mathbf{k}s}\right)|0\rangle_{\mathbf{k}s}. \tag{2.42}$$

The properties of coherent states are easily established in the simplifying case of a single field mode with constant polarization $|\alpha\rangle = \hat{D}(\alpha)|0\rangle$ where $\hat{D}(\alpha) = e^{\alpha\hat{a}^\dagger - \alpha^*\hat{a}}$ is an aforementioned Weyl operator and is also known as the unitary displacement operator. Coherent states are eigenstates of the annihilation operator since [25]

$$\hat{a}|\alpha\rangle = \hat{D}(\alpha)\hat{D}^\dagger(\alpha)\hat{a}\hat{D}(\alpha)|0\rangle = \hat{D}(\alpha)\left(\hat{a}+\alpha\hat{I}\right)|0\rangle = \alpha|\alpha\rangle, \tag{2.43}$$

which means that subtracting a photon will leave the state invariant since the post-subtraction state

$$\alpha \to \frac{\hat{a}|\alpha\rangle}{\sqrt{\langle\alpha|\hat{a}^\dagger\hat{a}|\alpha\rangle}} = \frac{\alpha|\alpha\rangle}{|\alpha|} = e^{i\theta}|\alpha\rangle \tag{2.44}$$

is identical to the original coherent state up to an unobservable global phase. Consequently, the average energy in a field mode prepared in a coherent state is invariant under photon subtraction. Furthermore, decomposing the unitary displacement operator using the Campbell-Baker-Hausdroff (CBH) decomposition [25]

$$\hat{D}(\alpha) = e^{\alpha\hat{a}^\dagger - \alpha^*\hat{a}} = e^{-|\alpha|^2/2} e^{\alpha\hat{a}^\dagger} e^{-\alpha^*\hat{a}}, \tag{2.45}$$

reveals the photon number distribution of the state $|\alpha\rangle$ to be

$$|\alpha\rangle \propto e^{\alpha\hat{a}^\dagger}|0\rangle = \sum_{n=0}^{\infty} \frac{\alpha^n e^{-|\alpha|^2/2}}{\sqrt{n!}}|n\rangle, \tag{2.46}$$

which has a Poissonian photon number probability distribution

$$p_n = |\langle n|\alpha\rangle|^2 = \frac{|\alpha|^{2n} e^{-|\alpha|^2}}{n!}. \tag{2.47}$$

These states are also regarded as the most classical of the quantum optical states since they are exhaustively described by the evolution of a complex number $\alpha(t)$

$$\begin{aligned} e^{-i\kappa t\hat{n}}|\alpha\rangle &= e^{-|\alpha|^2/2} \sum_{m=0}^{\infty} \frac{\alpha^m e^{-i\kappa t m}}{\sqrt{m!}}|m\rangle \\ = e^{-|\alpha e^{-i\kappa t}|^2/2} \sum_{m=0}^{\infty} \frac{\alpha^m e^{-i\kappa t m}}{\sqrt{m!}}|m\rangle &= |\alpha e^{-i\kappa t}\rangle = |\alpha(t)\rangle, \end{aligned} \tag{2.48}$$

like the equivalent case in classical optics [28]. This is also the reason for their name "coherent" as an evolving coherent state will maintain the coherence of its superposition.

The fact that coherent states are eigenstates of a non-Hermitian operator means that they do not form an orthonormal basis. Instead they are mathematically overcomplete [25]

$$\frac{1}{\pi}\int d^2\alpha |\alpha\rangle\langle\alpha| = \hat{I}, \tag{2.49}$$

meaning that we can decompose field states in terms of coherent states

$$|\psi\rangle = \pi^{-1}\int d^2\alpha\, \psi(\alpha, \alpha^*)|\alpha\rangle \tag{2.50}$$

and

$$\hat{\rho} = \pi^{-2}\int d^2\alpha\, d^2\beta\, \rho(\alpha, \alpha^*, \beta, \beta^*)|\alpha\rangle\langle\beta| \tag{2.51}$$

and that they are non-orthogonal with

$$\langle\alpha|\beta\rangle = \exp\left(-\frac{|\alpha|^2}{2} - \frac{|\beta|^2}{2} + \alpha^*\beta\right). \tag{2.52}$$

In addition, coherent states are minimum uncertainty states as they reduce the quadrature uncertainty principle

$$V_\psi(\hat{q})V_\psi(\hat{p}) \geq \frac{1}{4} \tag{2.53}$$

to an equality

$$V_\alpha(\hat{q})V_\alpha(\hat{p}) = \frac{1}{4}, \tag{2.54}$$

where $V_\psi(\hat{A}) = \langle\psi|\hat{A}^2|\psi\rangle - \langle\psi|\hat{A}|\psi\rangle^2$. Consequently, such states allow for the smallest error in the simultaneous measurement of $\hat{q}$ and $\hat{p}$. In addition to this, coherent states also have a symmetric noise profile that is independent of the amplitude α with $V_\alpha(\hat{p}) = V_\alpha(\hat{q}) = 1/2$. Thus, all coherent states have the same quadrature noise profile of the vacuum state i.e. they all possess the same shot noise [27]. Accordingly, all coherent states are regarded as displaced vacuum states since they only differ from the vacuum in their first moments with

$$\langle\alpha|\hat{q}|\alpha\rangle = \sqrt{2}\Re(\alpha), \quad \langle\alpha|\hat{p}|\alpha\rangle = \sqrt{2}\Im(\alpha). \tag{2.55}$$

This can also be seen from a phase space point of view where displacing a state $|\psi\rangle$ i.e. $\hat{D}(\alpha)|\psi\rangle$ is described by a canonical transformation with $W_{D(\alpha)\psi}(q,p) = W_\psi(q+\sqrt{2}\Re(\alpha), p+\sqrt{2}\Im(\alpha))$ [27] and so the location of the distribution is displaced from the origin. Thus, the Wigner function of a coherent state is

$$W_\alpha(q,p) = \frac{1}{\pi}e^{-(q-\sqrt{2}\Re(\alpha))^2-(p-\sqrt{2}\Im(\alpha))^2}, \tag{2.56}$$

and can be easily identified as a Gaussian state.

2.4.2 Linear optical devices

Linear optics is the study of the linear interactions between light and matter. The linear term follows from the particular response of the medium in question. A dielectric medium responds to the presence of an electric field by generating a

polarization vector $\mathbf{P}(\mathbf{r},t)$ and so the propagating field is the displacement field $\mathbf{D}(\mathbf{r},t) = \epsilon\mathbf{E}(\mathbf{r},t) + \mathbf{P}(\mathbf{r},t)$ [37, 38]. The polarization of the field can be expanded as a function of the vacuum electric field

$$\mathbf{P} = \epsilon_0 \left(\chi^{(1)}\mathbf{E} + \chi^{(2)}\mathbf{EE} + \chi^{(3)}\mathbf{EEE} + \ldots\right). \tag{2.57}$$

Where mathematical consistency demands that $\chi^{(2)}$ and $\chi^{(3)}$ are tensor quantities. Consequently, any optical device constructed from a homogenous dielectric material whose response to external electric fields is dominated by a $\chi^{(1)}$ interaction is a linear device [15, 37]. In this section we consider lossless transmission of the field meaning that we assume that $\chi^{(1)}$ is entirely real. Linear optical elements are also characterized by their passive nature with respect to the propagating field mode i.e. they do not change the total number of photons. Thus, the creation and annihilation of photons in such elements is balanced to ensure that the total number of photons in all the interacting modes is conserved [37, 38]. Another crucial property of linear optical interactions is that they are Gaussian operations. That is, they preserve the Gaussian character of any Gaussian input states. This stems from the fact that the Hamiltonians which generate such interactions are quadratic functions of the quadrature operators [38].

Phase shifter

The phase shifter [37] is described by the following unitary operator

$$\hat{U}_\theta = e^{i\theta\hat{n}}, \tag{2.58}$$

which acts to change the relative phase between each Fock state term in a superposition

$$\hat{U}_\theta|\psi\rangle = \sum_{n=0}^{\infty} \psi_n \hat{U}_\theta|n\rangle = \sum_{n=0}^{\infty} \psi_n e^{i\theta n}|n\rangle. \tag{2.59}$$

In phase space, such an operation corresponds to an active rotation of the state around the origin.

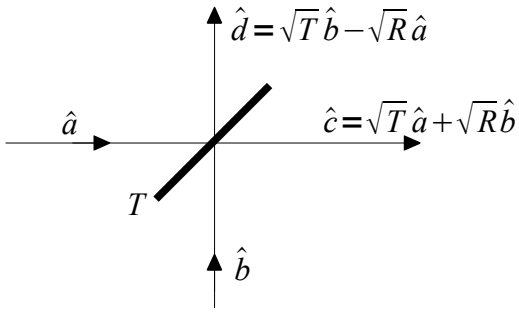

Figure 2.1: *The lossless beam splitter is a four port linear optical device which transforms input mode operators into outputs that are linear combinations of the inputs.*

Lossless beam splitter

The next linear optical element considered here is the lossless beam splitter [27, 37]. This device allows a linear coupling between two distinct field modes, labeled by operators $(\hat{a}, \hat{b})$, and is governed by the interaction Hamiltonian

$$\hat{H}_{BS}(t) = \hbar\kappa(\hat{a}(t)^\dagger \hat{b}(t) + \hat{a}(t)\hat{b}(t)^\dagger), \tag{2.60}$$

then the corresponding unitary operator generating this evolution is given by

$$\hat{U}_{BS} = \exp\left(\xi \hat{a}^\dagger \hat{b} - \xi^* \hat{a}\hat{b}^\dagger\right). \tag{2.61}$$

Each beam splitter is characterized by its reflection and transmission coefficients $R = \sin^2|\xi|$ and $T = \cos^2|\xi|$, which determine the proportion of the mixture of the input modes available in each output port of the device as illustrated in Fig.2.1. Thus, when $T = 1$ or $R = 1$ then the beam splitter is completely transparent for one mode while being perfectly reflecting for the other.

Direct application of the above unitary operator to a global input state vector $|\Psi\rangle_{AB}$ can be difficult to calculate even if we employ its Campbell-Baker-Hausdroff (CBH) decomposition [15]:

$$\hat{U}_{BS} = e^{e^{i\theta}\sqrt{R/T}\hat{a}^\dagger \hat{b}}\, T^{\hat{b}^\dagger \hat{b} - \hat{a}^\dagger \hat{a}}\, e^{-e^{-i\theta}\sqrt{R/T}\hat{a}\hat{b}^\dagger}. \tag{2.62}$$

However, there is an alternative method that exploits the Heisenberg transformation of the mode operators that allows a potentially easier method for calculating the

output states [27, 37]. In the Heisenberg picture, the input mode operators $\{\hat{a}, \hat{b}\}$ transform according to

$$\hat{U}_{BS}^{\dagger} \begin{pmatrix} \hat{a} \\ \hat{b} \end{pmatrix} \hat{U}_{BS} = \begin{pmatrix} \sqrt{T} & -e^{-i\theta}\sqrt{R} \\ e^{i\theta}\sqrt{R} & \sqrt{T} \end{pmatrix} \begin{pmatrix} \hat{a} \\ \hat{b} \end{pmatrix}. \tag{2.63}$$

Consequently, the inverse of the above can be employed to calculate the transformation of the state $|\Psi\rangle = \sum_{n=0}^{\infty}\sum_{m=0}^{\infty}(m!n!)^{-1/2}\Psi_{mn}(\hat{a}^{\dagger})^m(\hat{b}^{\dagger})^n|0,0\rangle$ to

$$\hat{U}_{BS}|\Psi\rangle = \sum_{n=0}^{\infty}\sum_{m=0}^{\infty}\Psi_{mn}\frac{(\sqrt{T}\hat{a}^{\dagger} + e^{-i\theta}\sqrt{R}\hat{b}^{\dagger})^m}{\sqrt{m!}}\frac{(\sqrt{T}\hat{b}^{\dagger} - e^{i\theta}\sqrt{R}\hat{a}^{\dagger})^n}{\sqrt{n!}}|0,0\rangle. \tag{2.64}$$

After some algebra, the final state can be written as

$$\hat{U}_{BS}|\Psi\rangle = \sum_{n=0}^{\infty}\sum_{m=0}^{\infty}\frac{\Psi_{mn}}{\sqrt{n!m!}}\sum_{\ell=0}^{n}\sum_{k=0}^{m}\begin{pmatrix} m \\ k \end{pmatrix}\begin{pmatrix} n \\ \ell \end{pmatrix}(\sqrt{T})^{k+\ell}e^{-i(m-k)\theta}e^{i(n-\ell)\theta}$$
$$\times(-1)^{n-\ell}(\sqrt{R})^{m+n-k-\ell}\sqrt{(k+\ell)!(m+n-k-\ell)!}|k+\ell, m+n-k-\ell\rangle.$$

Essentially, the lossless beam splitter will act to distribute the photons in each input mode into the two output modes since it must conserve energy and, hence, mean photon number.

2.4.3 Squeezed states

A pure quadrature squeezed state is a state $|\psi\rangle$ which exhibits a quadrature noise level below the threshold set by the vacuum shot noise i.e. $V_{\psi}(\hat{x}_{\theta}) < V_0(\hat{x}_{\theta})$ for a given $\hat{x}_{\theta}$. Its name is derived from its property of "squeezing" the uncertainty in a particular quadrature [15]. In addition, such squeezed states are also minimum uncertainty states, like the coherent states, and exhibit an asymmetric quadrature noise profile as a result of their squeezing with

$$V_{\psi}(\hat{q}) = cV_0(\hat{q}) < V_0(\hat{q}), \;\; V_{\psi}(\hat{p}) = c^{-1}V_0(\hat{p}) > V_0(\hat{p}). \tag{2.65}$$

Physically, such states can be generated by nonlinear optical processes. For example, single mode squeezed states can be formed from the interaction between a light field and a non-linear medium with a $\chi^{(2)}$ non-linearity in a process called degenerate

parametric down-conversion. Essentially, a pump field of frequency 2ω is incident on a non-linear medium, which responds by emitting two photons of frequency ω for every pump photon that it absorbs. If we treat the pump beam as classical then the corresponding unitary evolution operator for this process is

$$\hat{S}(re^{i\phi}) = \exp\left(\frac{r}{2}\{e^{i\phi}(\hat{a}^\dagger)^2 - e^{-i\phi}\hat{a}^2\}\right). \tag{2.66}$$

The real parameter r, which is dependant on the intensity of the pump beam and the coupling constant of the medium, is known as the squeezing parameter since it ultimately dictates the magnitude of the ratio between the squeezed state and the vacuum shot noise. The $\hat{S}(re^{i\phi})$ is called the single mode unitary squeezing operator and it obeys $\hat{S}^\dagger(re^{i\phi}) = \hat{S}(-re^{-i\phi})$ and $\hat{S}(re^{i\phi})\hat{S}(-re^{-i\phi}) = \hat{I}$ and it can be decomposed as [25, 31]

$$\hat{S}(re^{i\phi}) = \exp\left(\frac{e^{i\phi}\tanh r}{2}\{\hat{a}^\dagger\}^2\right) e^{-\frac{1}{2}(\hat{a}^\dagger\hat{a}+\hat{a}\hat{a}^\dagger)\ln(\cosh r)} \exp\left(\frac{-e^{-i\phi}\tanh r}{2}\hat{a}^2\right). \tag{2.67}$$

If the signal mode is initially in the vacuum state then this interaction results in the so-called squeezed vacuum state

$$|re^{i\phi}\rangle \propto e^{\frac{e^{i\phi}\tanh r}{2}\{\hat{a}^\dagger\}^2}|0\rangle = \frac{1}{\sqrt{\cosh r}}\sum_{n=0}^{\infty}\frac{\sqrt{(2n)!}}{n!}\left(\frac{e^{i\phi}\tanh r}{2}\right)^n|2n\rangle. \tag{2.68}$$

When $\phi = 0$ the above state is squeezed in the $\hat{q}$ quadrature as it exhibits a smaller variance than the vacuum state

$$V_r(\hat{q}) = \frac{e^{-2r}}{2} < V_0(\hat{q}), \quad V_r(\hat{p}) = \frac{e^{2r}}{2} > V_0(\hat{p}). \tag{2.69}$$

The squeezing operation is a Gaussian operation, which can easily be seen replacing the creation and annihilation operators with the corresponding quadrature operators [24]

$$\hat{S}(r) = \exp\left(-i\frac{r}{2}(\hat{q}\hat{p} + \hat{p}\hat{q})\right). \tag{2.70}$$

Alternatively, this fact is also obvious from phase space where the Wigner function of $\hat{S}(r)|\psi\rangle$ is related to the Wigner function of $|\psi\rangle$ by the canonical phase space transformation $W_{S(r)\psi}(q,p) = W_\psi(e^{-r}q, e^r p)$. For example, the Wigner function of a squeezed vacuum state given as

$$W(r,q,p) = \frac{1}{\pi}\exp\left(-e^{-2r}q^2 - e^{2r}p^2\right). \tag{2.71}$$

Thus, the state has an elliptical cross section corresponding to the asymmetric quadrature noise profile with one quadrature exhibiting a lower noise level than the vacuum.

The notion of squeezing and squeezed states is not confined to quadrature squeezing or to minimum uncertainty states and it can be generalised as $V_{SQ} < V_{Coh}$ where V_{Coh} is the variance of a coherent state with respect to some observable and V_{SQ} is the variance of the squeezed state. For example, this very general definition allows the notion of polarisation squeezed states with respect to the Stoke's observables [39]. In this thesis, we shall restrict our attention to quadrature squeezed states and we will refer to them simply as squeezed states.

2.4.4 Homodyne detection

Balanced homodyne detection

Balanced homodyne detection [27, 31, 37] involves the measurement of one of the quadratures of the input field and requires both a beam splitter and photo-detection. Essentially, the signal field is incident on a 50-50 beam splitter with a very intense local oscillator field as shown in Fig.2.2. The local oscillator field is assumed to be so intense that we can neglect its quantum fluctuations and treat it as a purely classical field. Consequently, this means that we can replace the mode operators of the local oscillator field with a complex amplitude $\hat{b} \rightarrow \alpha_{LO}$. This semi-classical treatment is desirable because it leads to a very simple result in contrast to a quantum treatment of the pump [40].

Each output field then falls onto a photo-detector that responds to the intensity of each of the electric fields. Consequently, each detector measures the current observable associated with the intensity of the incident field mode i.e. $\hat{I} \propto \hat{n}$. These currents are then subtracted electronically and so in the case where an input quantum field $\hat{a}$ is mixed with a classical local oscillator field $\hat{b} \rightarrow \alpha_{LO}$ the detector approximately measures the observable [27]

$$\hat{I} \approx |\alpha_{LO}|(e^{-i\theta}\hat{a} + e^{i\theta}\hat{a}^{\dagger}) = \sqrt{2}|\alpha_{LO}|\hat{x}_{\theta}. \tag{2.72}$$

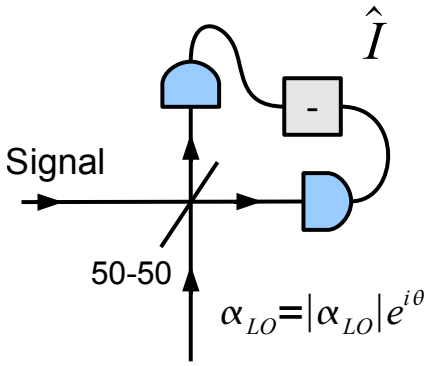

Figure 2.2: *The balanced homodyne detector measures the difference in current between the signal state and a semi-classical local oscillator field. In this limit, the homodyne detector is allows the measurement of the quadrature observable* $\hat{x}_\theta$.

Where we note that the phase of the local oscillator field θ is experimentally accessible and can be tuned at will [27] to select one of the quadratures from the set $\{\hat{x}_\theta\}_{\theta\in[0,2\pi]}$. The homodyne detection is dependent on a well defined phase relationship between the signal and local oscillator fields. This is normally taken care of by ensuring that the signal and local oscillator field originate from the same source [27]. The balanced homodyne detector approximately induces the probabilistic transformation

$$|\psi\rangle \rightarrow \langle x_\theta|\psi\rangle, \tag{2.73}$$

where $|x_\theta\rangle$ is the un-normalised field state registered by the detector [31]. Following this measurement the field mode is projected onto the vacuum state and so balanced homodyne detection is a Gaussian transformation.

Double Homodyne detection

While a balanced homodyne detector allows the measurement of a single quadrature observable $\hat{x}_\phi$, a double homodyne detector allows the measurement of pairs of incompatible quadratures on two input field modes, i.e. $\hat{U}_\phi = \hat{x}_{\phi,A} - \hat{x}_{\phi,B}$ and $\hat{V}_\phi = \hat{x}_{\pi/2+\phi,A} + \hat{x}_{\pi/2+\phi,B}$, i.e. a measurement of relative position and total momentum.

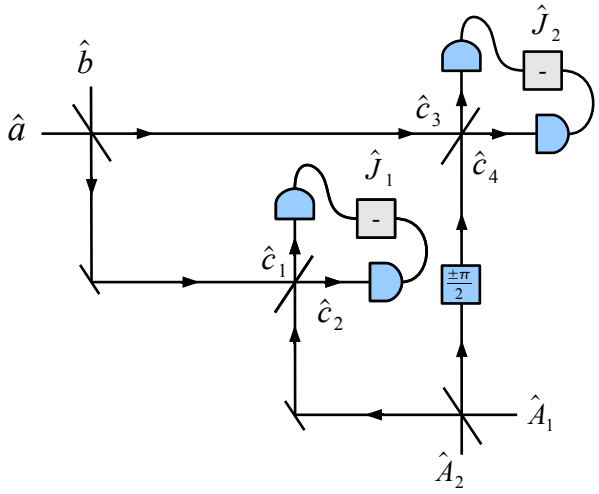

Figure 2.3: *The double homodyne detector allows the joint measurement of the sum and difference of incompatible quadrature observables.*

Such a measurement is possible since

$$[\hat{U}_\phi, \hat{V}_\phi] = [\hat{x}_{\phi,A}, \hat{x}_{\pi/2+\phi,A}] - [\hat{x}_{\phi,B}, \hat{x}_{\pi/2+\phi,B}] = i - i = 0, \tag{2.74}$$

meaning that these global operators commute even though the local operators do not. This linear optical device is composed of two balanced homodyne detectors and two additional beam splitters with two input modes $\{\hat{a}, \hat{b}\}$ and two local oscillators $\{\hat{A}_1, \hat{A}_2\}$ as shown in Fig.2.3. This detector measures the currents $\hat{J}_1 = \hat{c}_1^\dagger \hat{c}_1 - \hat{c}_2^\dagger \hat{c}_2$ and $\hat{J}_1 = \hat{c}_3^\dagger \hat{c}_3 - \hat{c}_4^\dagger \hat{c}_4$. After expressing these currents in terms of the input modes and their accompanied local oscillators and assuming $\hat{A}_1 \to |\alpha| e^{i\phi}$ with $|\alpha| >> 1$ while leaving $\hat{A}_2$ unexcited allows the above currents to be given as [31]

$$\hat{J}_1 = \frac{|\alpha| \left(\hat{x}_{\phi,A} - \hat{x}_{\phi,B}\right)}{\sqrt{2}}, \quad \hat{J}_2 = \frac{|\alpha| \left(\hat{x}_{\pi/2+\phi,A} + \hat{x}_{\pi/2+\phi,B}\right)}{\sqrt{2}}, \tag{2.75}$$

thus allowing us to simultaneously measure $\hat{U}_\phi$ and $\hat{V}_\phi$.

Double homodyne detection is an example of an entangling measurement since it measures an observable with entangled eigenstates i.e. it projects onto entangled states. In this case, the double homodyne detector projects onto the maximally entangled and un-physical EPR states, which can be written for $\phi = 0$ as [31]

$$|z\rangle\rangle = \frac{1}{\sqrt{\pi}} \left(\hat{D}(z) \otimes \hat{I}\right) \sum_{k=0}^{\infty} |k, k\rangle. \tag{2.76}$$

These states form a basis in the product configuration space $\mathcal{H}_A \otimes \mathcal{H}_B$ by allowing a resolution of the identity $\int d^2z|z\rangle\rangle\langle\langle z| = \hat{I}_A \otimes \hat{I}_B$, and $\langle\langle z|z'\rangle\rangle = \delta^2(z - z')$. Furthermore, these states are the eigenstates of the $\hat{U}_0$ and $\hat{V}_0$ [31], with

$$\hat{U}_0|z\rangle\rangle = \sqrt{2}\Re(z)|z\rangle\rangle, \quad \hat{V}_0|z\rangle\rangle = \sqrt{2}\Im(z)|z\rangle\rangle, \tag{2.77}$$

and so the real and imaginary parts of z are the simultaneous eigenvalues of $\hat{U}_0$ and $\hat{V}_0$, respectively. The measurement postulate for the double homodyne detector is given as

$$|\Psi\rangle_{AB} \rightarrow \langle\langle z|\Psi\rangle_{AB}. \tag{2.78}$$

However, if one of the input modes to the detector is in the vacuum state, then the detector measures the remaining field mode in a random coherent state instead of an EPR state [31]. This follows since $\langle\langle z|0,\psi\rangle \propto \sum_{k=0}^{\infty}\langle k|\hat{D}(-z^*)|0\rangle\langle k|\psi\rangle \propto \langle z|\psi\rangle$. The double homodyne detector is Gaussian since it projects the incident field modes onto the vacuum state. One of the main applications of the double homodyne detector is as an entangled measurement for continuous-variable teleportation [41].

2.5 Useful non-Gaussian states and operations

2.5.1 Binary photo-detectors

A binary photo-detector is a device which can distinguish between the presence and absence of photons. An avalanche photo-diode is a physical example of such a device where incident photons ionize a number of atoms in the detector and the liberated electrons then promote the further release of more electrons, thereby building up a measurable voltage. In the ideal case of unit quantum efficiency, such a detector is mathematically described as [31]

$$\hat{\Pi}_{noclick} = |0\rangle\langle 0|, \;\; \hat{\Pi}_{click} = \hat{I} - |0\rangle\langle 0|. \tag{2.79}$$

This measurement is non-Gaussian since $\hat{\Pi}_{click} = \sum_{k=1}^{\infty}|k\rangle\langle k|$ and, therefore, by linearity, has a Wigner function $W_{click}(q,p) = \sum_{k=1}^{\infty} W_k(q,p)$ where $W_k(q,p)$ is the

associated Wigner function for the Fock state $|k\rangle$ which is [27]

$$W_k(q,p) = \frac{1}{\pi} e^{-q^2-p^2}(-1)^k L_k(2(q^2+p^2)), \tag{2.80}$$

where $L_k(x)$ is a Laguerre polynomial. Incidently, this also reveals that the Fock states are non-Gaussian states. Consequently,

$$W_{click}(q,p) = \frac{1}{\pi}\left(1 - e^{-q^2-p^2}\right), \tag{2.81}$$

which is also clearly non-Gaussian [31].

2.5.2 Photon subtraction

The probabilistic photon subtraction operation is a useful resource in state engineering and has been used in continuous-variable entanglement distillation protocols [42], de-gaussification protocols [43], the preparation of non-Gaussian states [44], quantum optical universal quantum computing with single photons [45] and in the construction of arbitrary finite dimensional superpositions of Fock states [46]. Conditional photon subtraction on the state $|\psi\rangle$ can be achieved by combining $|\psi\rangle$ on a beam-splitter with the vacuum before measuring the reflected port with a binary photo-detector as shown in Fig.2.4(a). This will subtract the vacuum from the state $|\psi\rangle$ to a very good approximation provided that $\sqrt{T} \approx 1$ i.e. provided the beam splitter is highly transmitting. The subtraction succeeds when the photo-detector clicks. In this presentation we will restrict ourselves to ideal resources and assume that the detector has unit quantum efficiency.

If $|\psi\rangle|0\rangle = \sum_{n=0}^{\infty} \psi_n |n,0\rangle$ is incident on the input ports of the beam splitter then the global state at the output ports is given by

$$|\Psi\rangle = \sum_{n=0}^{\infty} \psi_n \sum_{k=0}^{n} \sqrt{\frac{n!}{k!(n-k)!}} \sqrt{T}^{n-k} \sqrt{R}^{k} |n-k,k\rangle. \tag{2.82}$$

However, since the beam-splitter is highly transmitting and weakly reflective then $\sqrt{R}^k \approx \delta_{0k} + \sqrt{R}\delta_{1k}$ and so

$$|\Psi\rangle \approx \sum_{n=0}^{\infty} \psi_n \sqrt{T}^{n} |n\rangle|0\rangle + \sum_{n=1}^{\infty} \psi_n \sqrt{\frac{n!}{1!(n-1)!}} \sqrt{T}^{n-1} \sqrt{R} |n-1,1\rangle. \tag{2.83}$$

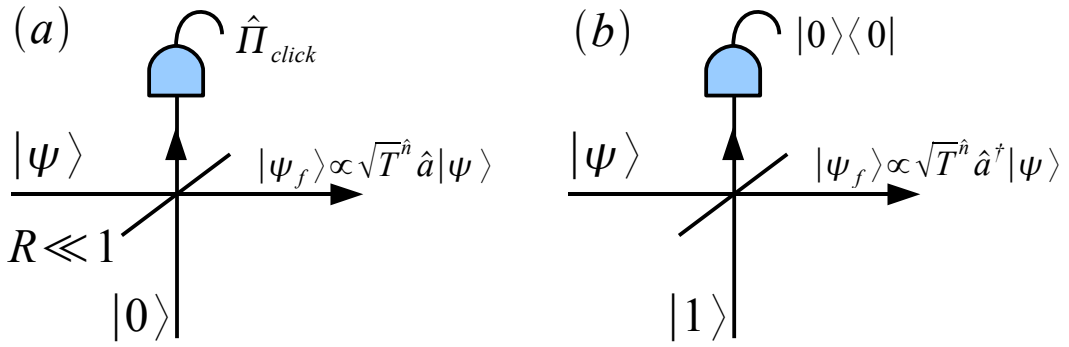

Figure 2.4: *Photon subtraction shown in* (a) *requires the binary photon detector to register the presence of photons, while in photon addition in* (b)*, the measurement must project onto the vacuum.*

In the event that the detector clicks the final state of field mode and detector is $|\Psi'\rangle \propto \hat{\Pi}_{click}|\Psi\rangle$, with

$$\hat{\Pi}_{click} = \hat{I} - |0\rangle\langle 0| = \sum_{k=1}^{\infty} |k\rangle\langle k|, \tag{2.84}$$

and so the vacuum term in (2.83) disappears and

$$|\Psi'\rangle \propto \sum_{n=1}^{\infty} \psi_n \sqrt{n} \sqrt{T}^{n-1} \sqrt{R} |n-1, 1\rangle. \tag{2.85}$$

After tracing out the state of the detector, the final field state is

$$|\psi_f\rangle \propto \sum_{n=1}^{\infty} \psi_n \sqrt{n} \sqrt{T}^{n-1} \sqrt{R} |n-1\rangle \propto \sqrt{R} \sqrt{T}^{\hat{n}} \hat{a} \left(\sum_{n=0}^{\infty} \psi_n |n\rangle \right). \tag{2.86}$$

Thus, we denote the conditional photon subtraction operation by the operator $\hat{X} = \sqrt{R}\sqrt{T}^{\hat{n}}\hat{a}$. Accordingly, this conditional operation can be viewed as the annihilation of a photon in the field mode followed by noiseless decay by a factor of $\sqrt{T}$. This is the reason for the name photon subtraction.

The probability of success of this operation is dependant on the probability of the detector clicking. This is $P_S = \langle\Psi|(\hat{\Pi}_{click} \otimes \hat{I})|\Psi\rangle$ and after substituting $\hat{\Pi}_{click} = \sum_{k=1}^{\infty} |k\rangle\langle k|$ we can obtain $P_S = R \sum_{n=0}^{\infty} |\psi_n|^2 T^{n-1} n$. Hence, this reveals a trade-off between our ability to perform this photon-subtraction operation and the probability of success since we require $R \approx 0$.

2.5.3 Photon addition

Given a field mode in state $|\psi\rangle$, we can conditionally perform the converse operation to photon subtraction. This is called photon addition and it requires an ancillary single photon state and a noiseless beam splitter in addition to a measurement scheme that allows the projection onto the vacuum state as shown in Fig.2.4(b). Photon addition operations are also useful in generating non-classical states of light [47, 48], the preparation of finite dimensional superpositions of Fock states [49] and in measurement-induced non-linearities [50]. In this case, the initial global state incident on the beam splitter is $|\psi\rangle|1\rangle = \sum_{n=0}^{\infty} \psi_n |n\rangle|1\rangle$, which transforms into the global output state $|\Psi\rangle = \hat{U}|\psi, 1\rangle$ with

$$|\Psi\rangle = \sum_{n=0}^{\infty} \psi_n \frac{(\sqrt{T}\hat{a}^\dagger + \sqrt{R}\hat{b}^\dagger)^n (\sqrt{T}\hat{b}^\dagger - \sqrt{R}\hat{a}^\dagger)}{\sqrt{n!}} |0,0\rangle. \tag{2.87}$$

Following this interaction the ancilla output port is conditionally projected onto the vacuum state $|0\rangle\langle 0|$. This can either be done with a binary photo-detection or by double homodyne detection. In the former case, the protocol succeeds when the detector does not click. The latter method is successful when the double homodyne current is zero or very close to zero. In this case, the homodyne measurement projects onto a coherent state very close to the vacuum. These different measurement strategies lead to different probabilities of success which we will consider later. Assuming the vacuum projection is successful, the global state of the field mode and detector is $|\Psi'\rangle \propto (\hat{I} \otimes |0\rangle\langle 0|)|\Psi\rangle$. This is given by

$$|\Psi'\rangle \propto \sum_{n=0}^{\infty} \frac{\psi_n \sqrt{T}^n (-\sqrt{R})(\hat{a}^\dagger)^{n+1}}{\sqrt{n!}} |0,0\rangle, \tag{2.88}$$

and after tracing out the state of the detector, the final field mode state is

$$|\psi_f\rangle \propto \sqrt{\frac{R}{T}} \sqrt{T}^{\hat{n}} \hat{a}^\dagger |\psi\rangle \propto \hat{Y}|\psi\rangle. \tag{2.89}$$

Where we denote $\hat{Y}$ as the conditional photon addition operator. Thus, this conditional operation is equivalent to adding a photon followed by noiseless decay of the state.

As noted above, the probability of success of this protocol is dependant on the measurement strategy used to project onto the vacuum state. If we use a binary photo-detector then the probability of success is $P_S = \langle\Psi|(|0\rangle\langle 0| \otimes \hat{I})|\Psi\rangle$ which is explicitly given as

$$P_S = R\sum_{n=0}^{\infty} |\psi_n|^2 T^n \langle n|\hat{a}\hat{a}^\dagger|n\rangle = R\sum_{n=0}^{\infty} |\psi_n|^2 T^n (1+n) = R\langle\psi|T^{\hat{n}}(1+\hat{n})|\psi\rangle. \quad (2.90)$$

In contrast, if we use double homodyne detection to project onto a coherent state $|re^{i\theta}\rangle$ that is very close to the vacuum, then the probability of success is given by

$$P_S = \int_0^{\epsilon} dr \int_0^{2\pi} d\theta \langle\Psi|re^{i\theta}\rangle\langle re^{i\theta}|\Psi\rangle, \quad (2.91)$$

with $\epsilon \approx 0$. Thus, in this latter case the probability of projecting onto the vacuum using homodyne detection can only be obtained approximately. This is because the probability of projecting onto a single state from a continuum is necessarily zero. Instead, we can associate a probability density of projecting near the vacuum as $\rho(\epsilon, \theta) = \langle\Psi|(|re^{i\theta}\rangle\langle re^{i\theta}| \otimes \hat{I})|\Psi\rangle$. In either case, this configuration allows a probabilistic photon addition operation.

2.5.4 Cross-Kerr effect

The cross-Kerr effect is a non-linear optical effect between two field modes propagating through a material with a $\chi^{(3)}$ non-linear response. Essentially, each of the traveling field modes experience a refractive index that is dependant on the intensity of the electric field of the co-propagating mode. Thus, if we label the modes A and B then the refractive index as experienced by mode A is $n_A = n_0 + \gamma|E_B|^2$ and the index experienced by mode B is $n_B = n_0 + \gamma|E_A|^2$ with γ being a function of the intrinsic parameters of the medium. Consequently, each field mode experiences a phase shift that is dependant on the number of photons in the co-propagating beam. The quantum mechanical Hamiltonian which generates this interaction is

$$\hat{H}_{Kerr} = \hbar\kappa\hat{n}_A\hat{n}_B \quad (2.92)$$

with κ as the strength of coupling between the two modes. The corresponding evolution operator for this interaction is

$$\hat{U}_K = e^{-i\kappa T \hat{n}_A \hat{n}_B}, \tag{2.93}$$

and so, this interaction is non-Gaussian because it is not quadratic in the quadrature operators. In quantum information, the cross-Kerr effect has many potential applications and is a vital component in photon number resolving detectors [51], photonic Fredkin gates [52], photonic C-NOT gates [53], Gaussian entanglement concentration [1, 54], quantum state conversion [55] and in the generation of non-Gaussian quantum states of light [56, 57].

2.5.5 The Schrödinger cat states

The Schrödinger cat state is the quantum optical version of the hypothetical state dreamt up by Schrödinger in his famous thought experiment, where the cat is prepared in is a superposition of macroscopically distinguishable states such as $|\psi\rangle = (|alive\rangle + |dead\rangle)/\sqrt{2}$. In quantum optics, the coherent states $\{|\alpha\rangle, |-\alpha\rangle\}$ play the role of the macroscopically distinguishable states since $|\langle\alpha|-\alpha\rangle|^2 = e^{-2|\alpha|^2}$ and so as $|\alpha| \to \infty$ then $\{|\alpha\rangle, |-\alpha\rangle\}$ become distinguishable. The even and odd Schrödinger cat states are then defined as

$$|\psi_{\pm}(\alpha)\rangle = \frac{|\alpha\rangle \pm |-\alpha\rangle}{\sqrt{2(1 \pm e^{-2|\alpha|^2})}}, \tag{2.94}$$

and both of these states have associated symmetries [28]. In the case of the even parity cat, only the even number Fock states make a contribution to the state

$$\begin{aligned} |\psi_{+}(\alpha)\rangle &= (2 + 2e^{-2|\alpha|^2})^{-1/2} \sum_{n=0}^{\infty} \frac{e^{-|\alpha|^2/2}}{\sqrt{n!}} (\alpha^n + (-\alpha)^n)|n\rangle \\ &= \frac{1}{\sqrt{\cosh|\alpha|^2}} \sum_{n=0}^{\infty} \frac{\alpha^{2n}}{\sqrt{(2n)!}} |2n\rangle, \end{aligned} \tag{2.95}$$

since all the odd n terms vanish. In the odd parity cat, the opposite is true and all the even Fock state contributions cancel out

$$|\psi_{-}(\alpha)\rangle = (2 - 2e^{-2|\alpha|^2})^{-1/2} \sum_{n=0}^{\infty} \frac{e^{-|\alpha|^2/2}}{\sqrt{n!}} (\alpha^n - (-\alpha)^n)|n\rangle$$

$$= \frac{1}{\sqrt{\sinh|\alpha|^2}} \sum_{n=0}^{\infty} \frac{\alpha^{2n+1}}{\sqrt{(2n+1)!}} |2n+1\rangle, \tag{2.96}$$

and so these states are orthogonal $\langle\psi_-(\alpha)|\psi_+(\alpha)\rangle = 0$. They are also non-Gaussian since their Wigner functions, are given by [28]

$$W_{\psi_\pm(\alpha)}(q,p) = \frac{e^{-(q-\sqrt{2}\alpha)^2-p^2} + e^{-(q+\sqrt{2}\alpha)^2-p^2} \pm e^{-q^2-p^2}\cos(2\sqrt{2}\alpha q)}{2\pi(1 \pm e^{-2\alpha^2})}. \tag{2.97}$$

We also note that these cat states are considered non-classical since their Wigner functions have negative values in some regions of phase space [27]. In quantum information, the Schrödinger cat states allow for universal quantum computation with linear optics [58, 59], and are therefore regarded as a valuable resource in continuous-variable quantum computing. Schrödinger cat states can be conditionally generated either by off-resonance interaction with ions in cavity quantum-electrodynamics [28] or by the linear optics and a weak self Kerr state [60]. To date, these cat states have been generated experimentally for $|\alpha| < 1$ and are the so-called kitten states [61].

Chapter 3

Gaussian state entanglement concentration

3.1 Bipartite pure state entanglement

3.1.1 Historical evolution

Entanglement like most other predictions of quantum mechanics has had an interesting evolution. Originally noted by Schrödinger as the essential quantum characteristic, it was subsequently was employed by Einstein, Podolsky and Rosen [62] as a device to argue for the incompleteness of quantum mechanics. Following this, entanglement languished in obscurity for decades, ignored by physicists for its seemingly purely philosophical character. This remained the case until Bell revisited the concept and went on to derive the inequality that now bears his name. His contribution was to show that the predictions of quantum mechanics, in particular the measurement statistics of entangled subsystems, could not be duplicated by a hidden-variable theory that obeyed Einstein causality [63]. This result was catapulted into mainstream physics following the experimental verification by Aspect [64]. Today entanglement is viewed as a resource to be consumed in various quantum information protocols. For example, entanglement can be readily used to teleport unknown quantum states [7]. To understand the mechanics behind such exploita-

tions, requires a mastery over the underlying mathematics of entangled states.

3.1.2 Mathematical definition

Let A and B be two physical systems of interest with associated state spaces $\mathcal{H}_A$ and $\mathcal{H}_B$, respectively, then the state space for the total system $A + B$ is given by the tensor product rule [9, 13, 65]:

$$\mathcal{H}_{AB} = \mathcal{H}_A \otimes \mathcal{H}_B. \tag{3.1}$$

Consequently, the states living in $\mathcal{H}_{AB}$ fall into one of two classes. *Separable states* are given by product states $|\psi\rangle = |\phi\rangle \otimes |\varphi\rangle = |\phi, \varphi\rangle = |\phi\rangle|\varphi\rangle$, such states describe systems with no non-local correlations. In contrast, *entangled states* are those which cannot be represented as a product of subsystem states $|\Psi\rangle \neq |\psi\rangle \otimes |\phi\rangle$.

A particularly powerful tool used in the understanding of entangled states is provided by the Schmidt decomposition [9, 13, 65]. Obviously, we can decompose any $|\Psi\rangle \in \mathcal{H}_A \otimes \mathcal{H}_B$ into a superposition of basis elements of $\mathcal{H}_A \otimes \mathcal{H}_B$. If $\{|i\rangle\}_{i=1}^{M}$ and $\{|j\rangle\}_{j=1}^{N}$ are orthonormal bases of $\mathcal{H}_A$ and $\mathcal{H}_B$, then $\{|i, j\rangle\}_{i,j=1}^{M,N}$ forms an orthonormal basis for $\mathcal{H}_{AB}$. Accordingly, any vector $|\Psi\rangle \in \mathcal{H}_{AB}$ can be represented as an unique expansion relative to this basis:

$$|\Psi\rangle = \sum_{i=1}^{M} \sum_{j=1}^{N} \Psi_{ij} |i, j\rangle. \tag{3.2}$$

The coefficients Ψ_{ij} are the components of a $M \times N$ complex matrix that describe the projection of $|\Psi\rangle$ onto the basis element $|i, j\rangle$. However, because of a remarkable theorem due to Schmidt it is always possible to find a change of basis of $\mathcal{H}_{AB}$ such that any $|\Phi\rangle$ can be expressed as

$$|\Psi\rangle = \sum_{k=1}^{K} s_k |e_k, f_k\rangle, \tag{3.3}$$

with $K = \min(M, N)$. The derivation of this result is both simple and compelling and follows from the singular value decomposition of complex matrices [9]. The values of s_k are unique to each vector and they obey $s_k \in \Re$, $\sum_{k=1}^{K} s_k^2 = 1$ and $s_k \geq 0$.

These coefficients are called the Schmidt coefficients and the orthonormal basis $\{|e_k, f_k\rangle\}_{k=1}^{K}$ is called the Schmidt basis. The number of non zero Schmidt coefficients of a vector is called its Schmidt rank. The power and elegance of the Schmidt decomposition is that it allows an immediate identification of the separability of a state via its Schmidt rank. In particular, separable states must have a Schmidt rank of one, while any entangled state must have a Schmidt rank greater than one.

3.1.3 Entanglement as a resource

The central reason for the resource interpretation of entangled states is due to their remarkable non-local properties. In particular, a composite system prepared in an entangled state will display non-local correlations between locally performed measurements on the entangled subsystems [9]. This leads to the conclusion that the outcomes of local measurements are interdependent even if the subsystems are separated by a spacelike interval. For example, suppose two observers shared an identically prepared ensemble of spin singlet states

$$|\Psi\rangle_{AB} = 2^{-1/2}(|\uparrow,\downarrow\rangle_{AB} - |\downarrow,\uparrow\rangle_{AB}) \tag{3.4}$$

and each observer measures the spin on their local particle while recording the results. After comparing their measurement data via classical communication, they discover perfect anti-correlation in their results where spin up for one observer is always accompanied by spin down for the other and vice versa. Furthermore, these correlations exist even though the local measurements on each subsystem could have no casual influence on each other. It is the exploitation of this non-casual connection between entangled subsystems that allows all of the celebrated applications of entanglement.

The non-local correlations manifest in entangled states are a direct result of the non-separable nature of such states and while the question of separability of a given composite pure state is binary, the degree by which a given non-separable state is considered entangled is not. Thus, different entangled states with different Schmidt coefficients have different degrees of non-separability. The degree of non-separability

is the mathematical expression of the lack of individuality of the entangled subsystems, i.e. if a composite system is in a pure entangled state then the subsystems cannot be assigned pure quantum states. They can, however, be assigned mixed states, called reduced density matrices. These are obtained by tracing out the other subsystem. For example, if we assume our composite system is in the state $|\Psi\rangle_{AB}$ then we can obtain the reduced density matrices by

$$\begin{aligned}\hat{\rho}_A = \mathrm{Tr}_B(|\Psi\rangle\langle\Psi|) &= \sum_k \sum_j s_k s_j \mathrm{Tr}_B \left(|e_k\rangle\langle e_j| \otimes |f_k\rangle\langle f_j|\right) \\ &= \sum_k \sum_j s_k s_j \mathrm{Tr}\left(|f_k\rangle\langle f_j|\right) |e_k\rangle\langle e_j| = \sum_k s_k^2 |e_k\rangle\langle e_k|, \end{aligned} \tag{3.5}$$

where $\hat{\rho}_B = \mathrm{Tr}_A(|\Psi\rangle\langle\Psi|)$ can also be done by tracing out subsystem A. The interpretation of the disorder of these reduced density matrices is due to the lack of individuality of each subsystem as a result of their non-local connection.

Thus, the degree of disorder in the states of the subsystems quantifies the the strength of the non-local correlations [9, 66] between these systems. This disorder or lack or purity in a given $\hat{\rho}$ can be measured by the Von Neumann entropy $\mathcal{S}_{VN}$:

$$\mathcal{S}_{VN}(\hat{\rho}) = -\mathrm{Tr}\left(\hat{\rho} \ln \hat{\rho}\right). \tag{3.6}$$

This entropy is zero if $\hat{\rho}$ is a pure state, since if $\hat{\rho}$ is pure then there exists some $|\phi\rangle$ such that $\hat{\rho} = |\phi\rangle\langle\phi|$ and so

$$\mathcal{S}_{VN}(\hat{\rho}) = -\ln(1)\langle\phi|\phi\rangle = 0. \tag{3.7}$$

On the other hand, assuming that $\hat{\rho}$ is mixed with $\hat{\rho} = \sum_{j=1}^{K} p_j |\varphi_j\rangle\langle\varphi_j|$ then $\mathcal{S}_{VN}(\hat{\rho}) = -\sum_{k=1}^{K} p_k \ln p_k$ is maximized when all the weights are equal $p_1 = p_2 = \ldots = p_K = 1/K$. This can be easily verified using Lagrange multipliers on $\mathcal{S}_{VN}(\hat{\rho})$ with respect to the normalization condition $\sum_{k=1}^{K} p_k = 1$. Such maximally mixed states are proportional to the identity operator

$$\hat{\rho}_{max} = K^{-1}\hat{I}. \tag{3.8}$$

This has the maximum degree of disorder because it does not favour any of the individual pure states involved in its convex decomposition. Thus, it is equally

unlike any possible pure state. This statement can be made rigorous by appealing to the fidelity of states. The fidelity of any two states $\hat{\rho}$ and $\hat{\sigma}$ is defined as $\mathcal{F}(\hat{\rho},\hat{\sigma}) = (\mathrm{Tr}\sqrt{\hat{\rho}^{1/2}\hat{\sigma}\hat{\rho}^{1/2}})^2$ and is the probability of confusing $\hat{\rho}$ with $\hat{\sigma}$ if one can perform only a single measurement in an attempt to distinguish them [13]. Then $\mathcal{F}(|\psi\rangle\langle\psi|,\hat{\rho}_{max}) = \langle\psi|\hat{\rho}|\psi\rangle = K^{-1}$ for any pure state $|\psi\rangle$.

Returning to entanglement, the Von Neumann entropy forms the basis of an entanglement measure for bipartite pure states. This measure is called the entropy of entanglement [9, 65, 67]:

$$\mathcal{E}(|\Psi\rangle\langle\Psi|) = \{\mathcal{S}_{VN}\circ \mathrm{Tr}_j\}(|\Psi\rangle\langle\Psi|), \tag{3.9}$$

where Tr_j is the partial trace with respect to the jth subsystem with $j = (A, B)$. The Schmidt decomposition allows an immediate calculation of the entropy of entanglement associated with each state

$$\mathcal{E}(|\Psi\rangle\langle\Psi|) = -\sum_{k=1}^{K} s_k^2 \ln s_k^2. \tag{3.10}$$

Note that $\mathcal{E}(|\Psi\rangle\langle\Psi|) = 0$ if $|\Psi\rangle$ is separable because the Von Neumann entropy of the reduced density matrices of the subsystem is zero. Thus, if $A + B$ is in a separable state then $\hat{\rho}_A$ and $\hat{\rho}_B$ are in pure states and the VN entropy is zero. Conversely, the VN entropy has a maximum $S_{max} = \ln(K)$ when A and B have the states

$$\hat{\rho}_A = \frac{1}{K}\hat{I}_A, \quad \hat{\rho}_B = \frac{1}{K}\hat{I}_B, \tag{3.11}$$

which leads to the definition of *maximally entangled states*

$$|\Psi\rangle = \frac{1}{\sqrt{K}}\sum_{i=1}^{K} |e_k, f_k\rangle. \tag{3.12}$$

Physically, maximally entangled states correspond to the case where the states of the subsystems are completely undefined and hence correspond to maximum entropy.

It is this connection between local disorder and non-local correlations together with the proven ability of harnessing these correlations to achieve an information processing effect [7, 8] that leads to the resource interpretation of entanglement. Simply put, entanglement allows the execution of tasks which cannot be completed

by solely relying on local quantum operations and classical communication (LOCC) between agents [68]. Consequently, entanglement allows the implementation of protocols that would otherwise be impossible to perform if limited to LOCC. Ergo, any measure of the degree of entanglement must be non-increasing under LOCC. Operationally, an entanglement measure is a real valued function $\mathcal{E}(|\Psi\rangle\langle\Psi|)$ on the state space of the composite system $A + B$ which obeys

1. $\mathcal{E}(|\Psi\rangle\langle\Psi|) = 0$ if $|\Psi\rangle$ is seperable.

2. Entanglement is invariant under local unitary operations on each subsystem:

$$\mathcal{E}(|\Psi\rangle\langle\Psi|) = \mathcal{E}(\hat{U}_A \otimes \hat{U}_B|\Psi\rangle\langle\Psi|\hat{U}_A^\dagger \otimes \hat{U}_B^\dagger). \tag{3.13}$$

3. Entanglement should not increase on average under operations involving local measurements and classical communication only

$$\mathcal{E}(|\Psi\rangle\langle\Psi|) \leq \sum_{\omega\in\Omega} p_\omega \, \mathcal{E}\left(\frac{\hat{A}_\omega|\Psi\rangle\langle\Psi|\hat{A}_\omega^\dagger}{p_\omega}\right). \tag{3.14}$$

   Here $p_\omega = \mathrm{Tr}(\hat{A}_w^\dagger \hat{A}_\omega|\Psi\rangle\langle\Psi|)$ is the probability of obtaining the ω outcome and $\{\hat{A}_\omega = \hat{A}_{\omega,A} \otimes \hat{A}_{\omega,B}\}_{\omega\in\Omega}$ are the corresponding *Kraus* [68] operators for the general POVM measurement [68].

In the case of pure bipartite entangled states, any one of the entropic measures of density matrices, including the Von Neumann entropy and the linear entropy $\mathcal{S}_L(\hat{\rho}) = 1 - \mathrm{Tr}(\hat{\rho}^2)$, can be shown to obey these constraints [69]. In addition, more general manifestations of entanglement including mixed state entanglement and multipartite entanglement rely on these and other axioms to define a resource theory of entanglement [65].

3.1.4 Procrustean entanglement concentration

Traditionally viewed as a source of contention over the completeness of quantum mechanics [62], entanglement has undergone a change in perception. The turning point came with the discovery of the teleportation of quantum states [7]. For the first

time, it was realised that entangled states could transfer unknown quantum states between potentially space-like separated systems. However, the efficiency of such protocols is governed by the degree of entanglement present in the shared state. Optimized performance comes with the use of maximally entangled states. The difficult part is in the distributing of the shared entangled state to the observers who require it. Ultimately, this requires the propagation of the physical carriers prepared in the entangled state, whether it be a pair of spin half particles or radiation modes. The rest of the universe then makes its presence felt by corrupting the initially pure state via decoherence and dissipation processes. Such processes conspire to reduce both the purity and available entanglement, thereby reducing the efficiency of the non-local protocol the entangled state is destined to be consumed in.

Fortunately, the observers Alice and Bob are not defenceless against this assault and can employ entanglement distillation protocols to counteract the consequences of unwanted environmental interactions. Such protocols allow for the probabilistic repair of the state back to its former glory by purification and replenishing lost entanglement. In this thesis, we restrict our attention to the considerably simpler task of entanglement concentration, where the input state of the protocol is a pure entangled state. The goal is then to probabilistically increase the entanglement content of the input state using only local quantum operations and classical communication on each of the entangled subsystems. The restriction to LOCC allows the entanglement to be modified after it has been distributed to the agents.

In this thesis, we investigate entanglement concentration where the entangled state has been distributed to the spatially separated observers and has suffered a loss of purity and entanglement as a result. It is then assumed that the observers employ some conditional purification procedure to restore the purity of a sub-ensemble of all the distributed states. At this point, the Alice and Bob are left with an ensemble of pure, possibility reduced, entangled states. To optimize the performance of the entanglement-aided protocol that they wish to execute, they apply an entanglement concentration protocol to their remaining sub-ensemble. One such method is the Procrustean method [70] where Alice and Bob use LOCC to conditionally transform

the *Schmidt* coefficients of each input entangled state to obtain a more entangled output state. Whether an individual run of the protocol is successful is dependant on the probabilities inherent to the particular scheme being used. Symbolically, such protocols can be represented by the state transformation

$$|\psi_{in}\rangle = \sum_{k=1}^{K} s_k |e_k\rangle \otimes |f_k\rangle \longrightarrow |\psi_{out}\rangle = \sum_{k=1}^{K} t_k |e_k\rangle \otimes |f_k\rangle, \tag{3.15}$$

where the post-protocol state must exhibit a higher degree of entanglement than the original state. Such protocols must have a success condition to allow Alice and Bob to distinguish between success and failure outcomes of the protocol.

Procrustean Entanglement concentration protocols are unavoidably probabilistic due to a fundamental theorem by Nielsen concerning entanglement transformations [71]. This idea makes use of the concept of majorization [72] which measures the degree of disorder between two normalised vectors $\mathbf{a} = (a_0^2, a_1^2, \ldots a_K^2)^T$ and $\mathbf{b} = (b_0^2, b_1^2, \ldots b_K^2)^T$, where the elements of these vectors are arranged in descending numerical order, i.e. $a_0^2 \geq a_1^2 \geq \ldots \geq a_K^2$ and $b_0^2 \geq b_1^2 \geq \ldots \geq b_K^2$. Then $\mathbf{a}$ is said to be *majorized* by $\mathbf{b}$, denoted $\mathbf{a} \prec \mathbf{b}$, if

$$\sum_{k=\ell}^{K} b_k^2 > \sum_{k=\ell}^{K} a_k^2, \tag{3.16}$$

for $1 \leq \ell \leq K$. This means that the components of $\mathbf{b}$ are more alike than the components of $\mathbf{a}$ and is therefore a more globally disordered vector than $\mathbf{a}$. This latter point follows since the majorization order is preserved by a set of functions called the *Shur convex* [69]

$$\mathbf{a} \prec \mathbf{b} \Longrightarrow f(\mathbf{b}) > f(\mathbf{a}), \tag{3.17}$$

of which, Von Neumann's entropy

$$S(\mathbf{a}) = -\sum_{k=0}^{K} a_k^2 \ln a_k^2, \tag{3.18}$$

is a member.

In Nielsen's theorem [71], our ability to transform one pure bipartite entangled state into another via deterministic local operations (i.e. local unitary operations)

and classical communication is determined by the majorization relation between the eigenvalues of the reduced density matrices of the input and output states. Thus, if $\mathbf{s} = (s_0^2, s_1^2, \ldots s_K^2)^T$ is the ordered vector of the eigenvalues of the reduced density matrices for $|\psi_{in}\rangle$ and $\mathbf{t} = (t_0^2, t_1^2, \ldots t_K^2)^T$ is the equivalent quantity for $|\psi_{out}\rangle$ then the latter can be transformed into the former via deterministic LOCC if

$$\mathbf{t} \prec \mathbf{s}. \tag{3.19}$$

Consequently, this means that we can only transform $|\psi_{in}\rangle \longrightarrow |\psi_{out}\rangle$ by deterministic LOCC if the input state is more entangled than the output state. This follows since $\mathbf{t}$ must have a smaller entropy than $\mathbf{s}$ and, therefore, has a smaller degree of entanglement. Thus, since entanglement concentration aims to proceed in the opposite manner it must be probabilistic. Generalizations of this theorem to entanglement transformations under probabilistic LOCC places restrictions on any single-copy entanglement concentration protocol [73–75]. In particular, in [74], the probabilistic transformation of $|\psi_{in}\rangle \longrightarrow |\psi_{out}\rangle$ can only occur if

$$\sum_j p_j \mathbf{t}_j \prec \mathbf{s}, \tag{3.20}$$

where p_j is the probability that the entanglement concentration protocol yields the entangled state characterised by $\mathbf{t}_j$ and denoted by $|\psi_{out}(j)\rangle$. Physically this means that on average entanglement concentration cannot occur i.e. for every $|\psi_{out}(j)\rangle$ which is more entangled than $|\psi_{in}\rangle$ there is another which is less entangled than the input state. Thus, such protocols come with a success condition that is dependant on achieving a particular outcome j. This is in accordance with the defining properties of an entanglement measure where LOCC cannot increase the entanglement on average.

3.2 Gaussian state Procrustean entanglement concentration

So far, entanglement has only been discussed in the regime of finite dimensional quantum systems. However, as noted earlier, the experimental ease of preparation

of Gaussian states and operations motivates the development of quantum information protocols that exploit these resources. It is therefore natural to explore the continuous-variable entangled states and the equivalent non-local protocols they can be exploited in. Moreover, Gaussian entangled states are natural candidates for such protocols since they are readily producible and can be exploited to perform teleportation [8], dense coding [41] and entanglement-assisted communication [76]. Thus, in accepting the utility of such entangled states we are forced to consider protocols which increase or repair entangled states as they are distributed. This is the subject of this section.

3.2.1 No maximally entangled states

While most of the intuition of entanglement developed from finite dimensional pure bipartite states equally applies to infinite dimensional Gaussian entangled states, there are nonetheless a few eccentricities. The Schmidt decomposition still holds meaning that entangled states can be decomposed as

$$|\Psi\rangle = \sum_{k=1}^{\infty} s_k |e_k\rangle |f_k\rangle, \tag{3.21}$$

where $\{|e_k\rangle\}_k$ and $\{|f_k\rangle\}_k$ are bases for the spaces $\mathcal{H}_A$ and $\mathcal{H}_B$. Furthermore, Von Neumann entropy of its reduced density matrices serve to quantify the degree of entanglement available in the state with

$$\hat{\rho}_A = \mathrm{Tr}_B \left(|\Psi\rangle\langle\Psi| \right) = \sum_{k=1}^{\infty} s_k^2 |e_k\rangle\langle e_k|, \tag{3.22}$$

and so

$$\mathcal{E}(|\Psi\rangle) = -\sum_{k=1}^{\infty} s_k^2 \ln s_k^2. \tag{3.23}$$

This is where the first peculiarity of Gaussian entangled states emerges, namely that there are no physical maximally entangled states. This fact follows from the standard definition of maximally entangled states

$$|\Psi_{max}\rangle = \frac{1}{\sqrt{K}} \sum_{k=1}^{K} |e_k\rangle |f_k\rangle, \tag{3.24}$$

and so in the limit of $K \to \infty$ these states become undefined. Consequently, since the Schmidt decomposition applies, by design, to normalisable states then maximally entangled infinite dimensional states must be non-normalisable.

This property follows from the fact that infinite dimensional states, unlike finite dimensional states can be eigenstates of operators with continuous spectra. In particular, maximally entangled Gaussian states are simultaneous eigenstates of relative canonical position $\hat{U}_0 = \hat{q}_B - \hat{q}_A$ and total canonical momenta $\hat{V}_0 = \hat{p}_A + \hat{p}_B$ [31]. These EPR states exhibit perfect correlations between the local conjugate position and momentum at the price of being non-physical. Indeed, the Wigner function for such an EPR state is $W_{EPR}(q_1, p_1, q_2, p_2) = \delta(q_2 - q_1)\delta(p_2 + p_1)$ and so

$$\int dq_1 dq_2 dp_1 dp_2 \, \delta(q_2 - q_1)\delta(p_1 + p_2) = \int dq_2 dp_2 = \infty. \tag{3.25}$$

Ultimately, this fact has profound implications for any continuous-variable entanglement concentration protocol because it means that maximally entangled states are unobtainable. Instead, one need content oneself to use partially entangled continuous variable states and therefore never achieve optimal performance from any entanglement based protocols. This disadvantage of continuous-variable entanglement is to be contrasted with the ease at which Gaussian entangled states can be obtained experimentally [14].

3.2.2 The necessity of non-Gaussian operations

The second interesting feature of Gaussian state entanglement concentration is that it cannot be achieved by involving local Gaussian operations and classical communication alone. This fundamental result applies to all Gaussian entangled states both mixed and pure as detailed in [16–18]. Consequently, all Gaussian entanglement distillation protocols will always require the inclusion of a non-Gaussian operation in order to work. Thus, the only examples of Gaussian distillation or concentration protocols known either involve a non-Gaussian operation or the inclusion of non-Gaussian noise. In the context of entanglement concentration, this theorem means that either non-linear optical devices or photon subtraction/addition techniques are

required to increase the shared entanglement.

3.2.3 The two mode squeezed vacuum

The Gaussian entangled two mode squeezed vacuum state (TMSV) is a finite entangled version of the EPR state which exhibits non-local correlations in the variances of the relative canonical position $\hat{U}_0$ and total momenta $\hat{V}_0$ observables. Its optical realisation is generated by a nonlinear process called non-degenerate parametric down-conversion [14], where photons in an intense pump beam of frequency ω_p are absorbed by the medium and re-emitted as pairs of entangled photons (traditionally called *signal* and *idler* photons) with frequencies ω_s and ω_i, such that $\omega_p = \omega_s + \omega_i$. Mathematically, the two mode squeezed vacuum state is related to the vacuum by a suitable unitary evolution in the limit of a classical pump field $\zeta = re^{i\theta}$ [25]

$$\hat{S}_{AB}(\zeta) = \exp\left(\zeta \hat{a}^\dagger \hat{b}^\dagger - \zeta^* \hat{a}\hat{b}\right), \tag{3.26}$$

and can be decomposed into

$$\hat{S}_{AB}(\zeta) = \exp\left(\hat{a}^\dagger \hat{b}^\dagger \, e^{i\theta} \tanh r\right) \exp\left\{-\ln(\cosh r)(\hat{a}^\dagger \hat{a} + \hat{b}\hat{b}^\dagger)\right\} \exp\left(-\hat{a}\hat{b} \, e^{-i\theta} \tanh r\right).$$

Here r is the so-called squeezing parameter and it is a function of the probe of intensity and the coupling constant of the medium, while the second equality follows from a CBH decomposition [25]. The TMSV with $\theta = 0$ is given, in its Schmidt decomposition, as

$$|\zeta\rangle \propto e^{\tanh r \hat{a}^\dagger \hat{b}^\dagger} |0,0\rangle = \frac{1}{\cosh r} \sum_{n=0}^{\infty} \tanh^n r |n\rangle |n\rangle, \tag{3.27}$$

and so it contains all amplitudes for obtaining different numbers of photons in the signal and idler modes. Consequently, the Fock basis is the Schmidt basis for this state and $(\tanh r)^n / \cosh r$ are the Schmidt coefficients of $|\zeta\rangle$. It is also very useful to introduce the parameter $\lambda = \tanh r$, which transforms the *Schmidt* coefficients into $c_n = \sqrt{(1-\lambda^2)}\lambda^n$ for reasons discussed later. Alternatively, this state can be described via its Wigner function [15]

$$W(q_1, p_1, q_2, p_2) = \frac{4}{\pi} e^{-e^{-2r}(q_2+q_1)^2 - e^{-2r}(p_2-p_1)^2 - e^{2r}(q_2-q_1)^2 - e^{2r}(p_1+p_2)^2}, \tag{3.28}$$

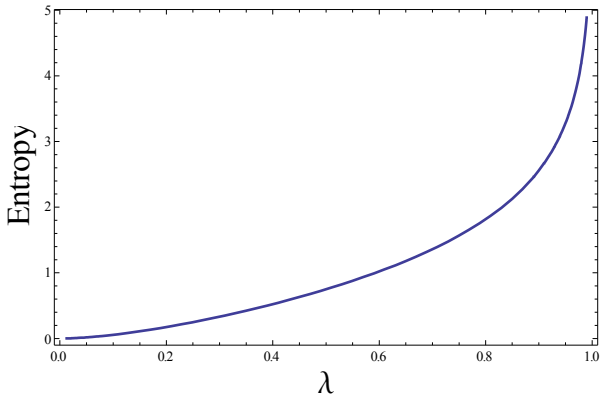

Figure 3.1: *The degree of entanglement in the TMSV is a monotonically increasing function of λ since the greater lambda, the more energy injected in the signal and idler modes and the flatter the Schmidt components become.*

and so, we can identify the TMSV as a Gaussian entangled pure state.

The entanglement content of the TMSV can be measured by calculating its Von Neumann entropy. In this case we get [31]

$$\mathcal{E}(|\zeta\rangle) = -\sum_{n=0}^{\infty} c_n^2 \ln c_n^2 = -\frac{2\lambda^2 \ln \lambda}{1-\lambda^2} - \ln(1-\lambda^2), \tag{3.29}$$

which as illustrated in Fig.3.1 is a monotonic increasing function of λ and tends to infinity as $\lambda \to 1$, which is the reason for employing the λ parametrisation in the first place. This occurs because λ is a re-scaling of the pump intensity r which controls the number of photons available in each of the signal and idler modes. Thus, by increasing the pump intensity we increase the energy injected into the signal and idler modes and increase the probability of detecting ever larger number of photons in each mode. This also increases the entanglement since it flattens the Schmidt components i.e. more energy means that the amplitude for $|n,n\rangle$ for $n > 0$ increases at the expense of the vacuum contribution $|0,0\rangle$. This also explains the non-physical nature of the maximally entangled EPR states which are related to the TMSV in the limit $\lambda \to 1$, since reaching this limit requires an infinite amount of energy. This follows from the expectation value of the free Hamiltonian, while ignoring the zero

point contributions, of the single and idler modes

$$\langle E(\lambda)\rangle = \langle\zeta(\lambda)|(\hat{n}_A + \hat{n}_B)|\zeta(\lambda)\rangle = \frac{2\lambda^2}{1-\lambda^2}, \tag{3.30}$$

and so $\langle E(\lambda)\rangle \to \infty$ as $\lambda \to 1$, i.e. the average energy available in the state tends to infinity.

3.2.4 Photon-subtraction protocol

Non-Gaussian operations are a vital prerequisite for the concentration of Gaussian continuous-variable entanglement. To date, the only technologically feasible non-Gaussian entanglement concentration protocol of the TMSV involves photon subtraction via binary photo-detectors [42]. In this protocol, Alice and Bob both attempt to subtract a photon from the entangled mode in their possession. This requires each agent to propagate their entangled mode through a noiseless beam splitter with the vacuum before subjecting one of the output modes to binary photo-detection [42]. This protocol is deemed successful if both register a click corresponding to the presence of photons in each detector and provided that they share their results then the final shared state between Alice and Bob is given by

$$|\Psi_f\rangle \propto \left(\hat{\Pi}_{click} \otimes \hat{I}_{BC} \otimes \hat{\Pi}_{click}\right) \hat{U}_{BS} \otimes \hat{U}_{BS} |0, \zeta(\lambda), 0\rangle_{ABCD}, \tag{3.31}$$

where $\hat{\Pi}_{click} = \sum_{k=1}^{\infty} |k\rangle\langle k|$ is the POVM element corresponding to the detection of a single photon state and $\{\hat{a}, \hat{b}, \hat{c}, \hat{d}\}$ are the mode operators for modes A, B, C and D. This entanglement transformation is actually Procrustean, since $|\Psi_f\rangle \propto \hat{X}_b \otimes \hat{X}_c |\zeta(\lambda)\rangle$, where $\hat{X}_b = \sqrt{R}\sqrt{T}^{\hat{n}}\hat{b}$ with a similar expression for $\hat{X}_c$ as noted in chapter two, and thus

$$|\Psi_f\rangle \propto \sum_{n=1}^{\infty} T^n \lambda^n n |n-1, n-1\rangle = \sqrt{\frac{(1-T^2\lambda^2)^3}{1+T^2\lambda^2}} \sum_{n=0}^{\infty} \lambda^n T^n (1+n)|n, n\rangle. \tag{3.32}$$

The protocol is probabilistic and succeeds with the probability [21]

$$P_S = \frac{(1-T)^2\lambda^2(1-\lambda^2)(1+T^2\lambda^2)}{(1-T^2\lambda^2)^3}. \tag{3.33}$$

The verification of entanglement concentration is done by comparing the entanglement content of the initial state with the final state. This can be demonstrated

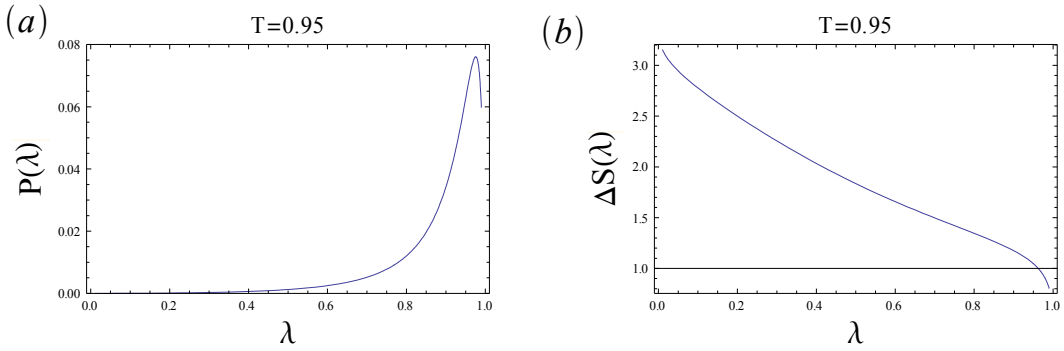

Figure 3.2: *The features of the photon subtraction protocol can be understood considering the relationship between (a) probability of success and (b) the increase in entanglement for* $T = 0.95$.

by considering the ratio of the Von Neumann entropies $\mathcal{S}_i = \mathcal{S}(\hat{\rho}_i)$ and $\mathcal{S}_f = \mathcal{S}(\hat{\rho}_f)$ where

$$\hat{\rho}_i = (1 - \lambda^2) \sum_{n=0}^{\infty} \lambda^{2n} |n\rangle\langle n|, \tag{3.34}$$

and

$$\hat{\rho}_f = \frac{(1 - T^2\lambda^2)^3}{1 + T^2\lambda^2} \sum_{n=0}^{\infty} (T\lambda)^{2n} (1 + n)^2 |n\rangle\langle n|. \tag{3.35}$$

Thus, entanglement concentration occurs when $\Delta\mathcal{S} = \mathcal{S}_f/\mathcal{S}_i > 1$. This protocol can be characterised by the behaviour of this ratio together with the behaviour of the probability of success. The behaviour and efficiency of this protocol is shown in Fig.3.2 for $T = 0.95$. In particular, we note from Fig.3.2(b) that, for $T = 0.95$, the entanglement concentration succeeds for $0 < \lambda < 0.97$ i.e. the photon subtracted state is almost always more entangled that the initial TMSV unless $\lambda > 0.97$. Thus, the relative increase in entanglement is most dramatic for very weakly entangled input states and decreases as the entanglement in the initial TMSV increases. Furthermore, we also note from Fig.3.2(a) the tradeoff between entanglement increase $\Delta\mathcal{S}$ with the probability of success, with greater increases occurring when the probability of success is at its smallest. Nevertheless, the current technological state of art has meant that this entanglement concentration protocol has been experimentally verified [77].

3.2.5 Cross-Kerr protocol

An alternative scheme [54] relies on the use of a non-Gaussian coupling between one of the entangled modes of light and an ancillary light mode prepared in a coherent state $|\alpha \in \Re\rangle$, i.e. the global input state is $|\psi_{in}(0)\rangle = |\zeta(\lambda), \alpha\rangle$. The coherent state and Bobs half of the squeezed state are fed into a nonlinear medium that exhibits the cross-Kerr effect with a κ_T phase shift per photon. This interaction results in entanglement between the coherent beam and Alice and Bobs beams:

$$\begin{aligned}
|\psi_{in}(t)\rangle &= \left(\hat{I}_A \otimes e^{-i\kappa_T\, \hat{b}^\dagger \hat{b} \hat{c}^\dagger \hat{c}}\right) |\psi_{in}(0)\rangle \\
&= \sum_{m=0}^{\infty}\sum_{n=0}^{\infty} \frac{c_n e^{-\alpha^2/2}\alpha^m e^{-i\kappa_T nm}}{\sqrt{m!}} |n, n, m\rangle \\
&= \sum_{n=0}^{\infty} c_n |n, n\rangle \otimes \sum_{m=0}^{\infty} e^{-|\alpha \exp(-in\kappa_T)|^2/2} \frac{\left(\alpha e^{-i\kappa_T n}\right)^m}{\sqrt{m!}} |m\rangle \\
&= \sum_{n=0}^{\infty} c_n |n, n, \alpha e^{-in\kappa_T}\rangle. \qquad (3.36)
\end{aligned}$$

A local double homodyne measurement is then performed on the coherent state, which ultimately projects it onto a random coherent state $|\beta\rangle$. Consequently, the final state shared between Alice and Bob is given by

$$|\psi_f\rangle \propto \sum_{n=0}^{\infty} \lambda^n \langle\beta|\alpha e^{-i\kappa_T n}\rangle |n, n\rangle, \qquad (3.37)$$

and in the regime of weak non-linearity $\kappa_T << 1$, the induced back-action is given by

$$|\psi_f\rangle \propto \sum_{n=0}^{\infty} \lambda^n e^{-i\kappa_T n\alpha\beta^*} |n, n\rangle. \qquad (3.38)$$

Thus, if the measurement results in a $\Im(\beta) < 0$ then the squeezing and entanglement is increased since

$$\lambda \to \lambda e^{\kappa_T \alpha \Im(\beta)}. \qquad (3.39)$$

The impossibility theorem of distillation of Gaussian entanglement means that the non-Gaussian coupling, i.e. the cross-Kerr interaction, between the modes must be maintained. However, a number of open questions remain with regard to this protocol.

1. Are there other measurement strategies on the ancilla that will achieve entanglement concentration, possibly to a greater degree, in this weak nonlinear regime?

2. What is the fundamental mechanism that is responsible for the Gaussian-preserving entanglement modification effect in this weak regime?

3. How accurate is the output entangled state given here for the weak limit $\kappa_T << 1$ and how constraining is the requirement of weak non-linearities?

4. Can this scheme be extended to non-optical ancilla systems and interactions?

5. What is the origin of the measurement based success criterion?

Surprisingly, all of these open questions can be answered rather elegantly in a single entanglement concentration model based on the weak measurement formalism. However, to understand this we must first review the notion of weak values and weak measurements. This is the subject of chapter four and then in chapter five we apply these notions to entanglement concentration.

3.3 Other methods

3.3.1 Schmidt projection

For completeness, we note that the Procrustean method is not the only method to be suggested that allows entanglement concentration. An alternative method is called Schmidt projection [70], where the protocol takes a ensemble of weakly entangled states and projects onto a maximally entangled state on a subspace of the initial entangled states. In the context of Gaussian entanglement concentration, this method has been employed by Duan *et. al.* [78, 79] for the two mode squeezed vacuum, with Alice and Bob initially sharing K copies of the entangled state $|\zeta(\lambda)\rangle = \sqrt{1-\lambda^2}\sum_{n=0}^{\infty}\lambda^n|n,n\rangle$ which can be written as

$$|\Psi_{in}(\lambda)\rangle = \bigotimes_{i=1}^{K}|\zeta(\lambda)\rangle_{A_i,B_i} = (1-\lambda^2)^{K/2}\sum_{L=0}^{\infty}\lambda^L\sqrt{d_L^{(K)}}|L\rangle_{A_i,B_i}. \tag{3.40}$$

The $|L\rangle_{A_i,B_i}$ states are finite dimensional maximally entangled states

$$|L\rangle_{A_i,B_i} = \frac{1}{\sqrt{d_L^{(K)}}} \sum_{i_1,i_2,\ldots,i_K}^{i_1+i_2+\ldots+i_K=L} |i_1, i_2, \ldots i_K\rangle_{A_i} |i_1, i_2, \ldots i_K\rangle_{B_i}, \tag{3.41}$$

with $d_L^{(K)} = (L+K-1)!/(L!(K-1)!$. Thus, this entanglement concentration protocol requires a non-demolition measurement of the total photon number in Alice's modes and it yields the final shared state $|L\rangle$ with a probability $P_L^{(K)} = (1-\lambda^2)^K \lambda^{2L} d_L^{(K)}$. This non-Gaussian non-demolition measurement can be accomplished by using an array of noiseless beam splitters and photon counting [78, 79].

3.3.2 Non-Gaussian noise approach

Another alternative method of entanglement distillation for continuous-variable states lies in the introduction of a source of non-Gaussian noise which can then be corrected by Gaussian operations. Such schemes have recently been experimentally realised [80–82].

Chapter 4

Weak measurements and weak values

The previous chapter ended with the desire to generalise the optical entanglement concentration protocol to include arbitrary ancilla systems. In attempting to do so, we are faced with two immediate problems: What measurement strategies can be employed to allow conditional entanglement concentration? And: What are the general constraints required to produced Gaussian preserving entanglement concentration? Both of these issues have a common resolution in the framework of weak measurements. Indeed, one can consider the previous entanglement concentration protocols as examples of weak measurements where the probe state is initially entangled. This realisation is surprisingly powerful as it yields a criterion for selecting different ancillary ingredients.

4.1 Weak Values

4.1.1 Definition of weak values

Any physical theory makes contact with empirical observations through the observable numbers it predicts. In quantum theories, there are three types of observable numbers: eigenvalues or measurement results, expectation values and weak values

[83]. The first set of numbers follow from the basic formulation of observables and measurements in quantum mechanics. Simply put, the results of a measurement of an observable $\mathcal{A}$ coincide the eigenvalues of its associated self-adjoint operator

$$\hat{A} = \sum_j a_j |a_j\rangle\langle a_j|. \tag{4.1}$$

These numbers are observable in a single measurement on a quantum mechanical system. Next is the notion of an expectation value, i.e. the statistical average of an observable on a particular quantum state

$$\langle A\rangle = \langle\psi|\hat{A}|\psi\rangle. \tag{4.2}$$

Expectation values only emerge on a statistical level following measurements performed on an identically prepared ensemble. These numbers are also used to establish a correspondence with classical theories [30].

The final set of observable numbers in quantum mechanics are a recent addition called weak values [83, 84]. A weak value, like an expectation value, is only a statistically observable number, but unlike an expectation value or eigenvalue, it can be complex. Weak values are only applicable to quantum systems which have been both pre and post-selected in particular quantum states. Thus, the weak value of the observable $\mathcal{A}$ on a system which is pre-selected in the state $|\Phi_1\rangle$ and post-selected in $|\Phi_2\rangle$ is defined as

$$A_W = \frac{\langle\Phi_2|\hat{A}|\Phi_1\rangle}{\langle\Phi_2|\Phi_1\rangle}, \tag{4.3}$$

where it is assumed that $|\Phi_1\rangle$ and $|\Phi_2\rangle$ are non-orthogonal. From a physical point of view, weak values are regarded as the possible values of the observable at intermediate times between the pre and post-selections [85].

4.1.2 Some properties of weak values

To gain a better appreciation for weak values it is worthwhile to consider how they are related to both eigenvalues and expectation values of a given observable. In the

first case, the weak value of $\hat{A}$ coincides with an eigenvalue if either of $\{|\Phi_1\rangle, |\Phi_2\rangle\}$ coincide with an eigenstate of $\hat{A}$:

$$A_W = \frac{\langle a_j|\hat{A}|\Phi_1\rangle}{\langle a_j|\Phi_1\rangle} = a_j \frac{\langle a_j|\Phi_1\rangle}{\langle a_j|\Phi_1\rangle} = a_j, \tag{4.4}$$

$$A_W = \frac{\langle \Phi_2|\hat{A}|a_k\rangle}{\langle \Phi_2|a_k\rangle} = a_k \frac{\langle \Phi_2|a_k\rangle}{\langle \Phi_2|a_k\rangle} = a_k. \tag{4.5}$$

The weak value becomes undefined if both the pre and post-selected states are distinct eigenstates of $\hat{A}$ (assuming that $\hat{A}$ has a completely non-degenerate eigenvalue spectrum). On the other hand, a weak value of $\hat{A}$ coincides with an expectation value of $\hat{A}$ if the pre and post-selected states are identical:

$$A_W = \frac{\langle \psi|\hat{A}|\psi\rangle}{\langle \psi|\psi\rangle} = \langle \psi|\hat{A}|\psi\rangle = \langle A\rangle. \tag{4.6}$$

Furthermore, any expectation value of $\hat{A}$ can be linearly decomposed into a sum of different weak values of $\hat{A}$ [85, 86] since

$$\langle \psi|\hat{A}|\psi\rangle = \langle \psi| \left(\sum_j |j\rangle\langle j| \right) \hat{A}|\psi\rangle = \sum_j |\langle \psi|j\rangle|^2 \frac{\langle j|\hat{A}|\psi\rangle}{\langle j|\psi\rangle} = \sum_j P(\psi|j) A_W(j), \tag{4.7}$$

where the complete basis used in the above does not coincide with the eigenbasis of $\hat{A}$ and $P(\psi|j)$ is the probability of obtaining $|\psi\rangle$ given $|j\rangle$. This allows an alternative interpretation of expectation values as a probabilistic mixture of weak values [86]. In addition, it demonstrates two possibilities for the imaginary components of weak values, either $\Im(A_W(j)) = 0$ for all j or they are mixed with some positive for some j and others negative. This follows from

$$\Im\left(\langle \psi|\hat{A}|\psi\rangle\right) = 0 \Rightarrow \sum_j P(\psi|j)\Im(A_W(j)) = 0. \tag{4.8}$$

Thus, since not all of the $P(\psi|j)$s can be zero then either $\Im(A_W(j)) = 0$ for all j or they are mixed. So, in contrast to both eigenvalues and expectation values, weak values can assume complex numerical values whilst remaining observable at the statistical level. To understand the process by which this is possible, we now discuss the notion of weak measurements [83].

4.2 Weak measurements

4.2.1 General configuration

Operator weak values are observable, but only in an indirect sense on the statistical level [83]. To illustrate this point, we recall the standard concept of a weak measurement. A weak measurement can be regarded as a modification of the conventional model of an indirect quantum measurement. Historically, such indirect measurement models were were originally introduced by *Von Neumann* [87] in order to describe the process of quantum measurement in a more realistic manner, the idea being that we displace the "Heisenberg" cut [63] between the classical and quantum world by one system. Hence, there are two quantum systems of interest. The first system, called the signal, possesses the property that is to be measured. The other, called the probe, is an additional system required to witness the property of interest. In this original context, the probe is regarded as the degree of freedom of the measurement apparatus which interacts with the system to be measured (the signal). Consequently, the measurement is regarded as the entangling of the pointer degrees of freedom of the probe with the eigenstates of the chosen observable of the system. In the original model [87], the cut is reintroduced by the postulating the collapse of the probe into one of its pointer eigenstates.

Weak measurements represent a departure from this traditional model in two respects. Firstly, the signal system is required to be both pre and post-selected by completely independent processes to the one that mediates its interaction with the probe. Secondly, the coupling strength between the probe and signal must be weak. A quantitative expression for this requirement of weakness will be presented in due course. If these vital pre-requisites are not met then the weak measurement will fail and the probe will not be able to witness the desired weak value. The general configuration of a weak measurement is portrayed in Fig.4.1. In the context of measurement theory, we can regard a weak measurement as a very low resolution indirect quantum measurement where the signal is both pre and post-selected. That is, the coupling and the initial state of the probe are tuned to ensure that there is

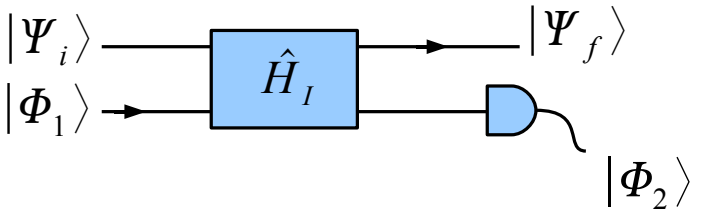

Figure 4.1: *The general schematic of a weak measurement involves a system which is both pre and post selected in particular states. In this diagram, the probe system is the top system and the signal is the bottom one. The signal is mixed with the probe at intermediate times between the selections and if the coupling is weak then the probe encodes the weak value of an observable.*

insufficient resolution to indirectly observe the eigenvalue spectrum of the observable imprinted on the probe and it can be regarded as an unsharp measurement [30].

4.2.2 Actual implementation

It is worth considering the actual implementation of a weak measurement [85]. Clearly this cannot be done in a single measurement since the processes which underly the pre and post-selection procedures will almost certainly be probabilistic in nature. As a consequence, a weak measurement of a weak value can only be implemented on an identically prepared ensemble. Thus, suppose that we have such an ensemble of signal and probe systems. The pre- and post-selection of the signal states can be achieved by initially measuring the observable $\mathcal{X}$ on every signal and only keeping systems which correspond to the result $\mathcal{X} = x$. This sub-ensemble is then allowed to interact with the ensemble of probe states. After this, we measure $\mathcal{Y}$ on every remaining signal system in the sub-ensemble and only keep systems corresponding to $\mathcal{Y} = y$. $\mathcal{X}$ and $\mathcal{Y}$ are chosen such that $[\hat{X}, \hat{Y}] \neq 0$ and $[\hat{A}, \hat{X}] \neq 0$ and $[\hat{A}, \hat{Y}] \neq 0$ where the observable $\mathcal{A}$ is the operator acting on the signal in the interaction Hamiltonian. Consequently, this sub-ensemble contains only signal systems that are pre-selected in $|\mathcal{X} = x\rangle$ and post-selected in $|\mathcal{Y} = y\rangle$. Then the desired

weak value

$$A_W = \frac{\langle \mathcal{Y} = y|\hat{A}|\mathcal{X} = x\rangle}{\langle \mathcal{Y} = y|\mathcal{X} = x\rangle}, \tag{4.9}$$

can be obtained from the sub-ensemble of final probe states i.e. the statistical distribution of the results of the probe pointer measurements allow the recovery of the probe's final wavefunction.

4.2.3 Encoding the weak value

We now demonstrate that a weak measurement leads to the encoding of a given weak value. Following Fig.4.1, we consider the case where the signal is pre-selected in the state $|\Phi_1\rangle$ and post-selected in the state $|\Phi_2\rangle$. We assume that the dynamics of this model follow the interaction picture and that the probe system has an infinite dimensional Hilbert space with canonical observables $\hat{q}, \hat{p}$ where $[\hat{q}, \hat{p}] = i\hbar$. We interpret $\hat{q}$ as the pointer position observable i.e. as representing the position of the pointer of the measuring device's gauge. Accordingly, $\hat{p}$ is viewed as the pointer's canonical momentum and the interaction between signal and probe is mediated by the Hamiltonian

$$\hat{H}_I = \hbar\kappa(t)\hat{A} \otimes \hat{p}, \tag{4.10}$$

where $\hat{A}$ is the observable of interest, i.e. we want to measure the weak value of $\hat{A}$. For simplicity, we assume that $\kappa(t) = \text{const}$ and that interaction persists for $T = t_f - t_i$ seconds. It is assumed that all of the systems have vanishing free Hamiltonians. This can be done provided we note that all results are unique up to a suitable local unitary transformation.

In addition, we also assume that the probe is initially prepared in a Gaussian superposition of pointer eigenstates

$$|\Psi_i\rangle \propto \int dq \, \exp\left(-\frac{q^2}{4\Delta^2 q}\right)|q\rangle, \tag{4.11}$$

where $\Delta^2 q$ is the uncertainty in pointer observable. This is another departure from the original indirect model offered by Von Neumann. In the original, the probe was assumed to be initially prepared in a pointer eigenstate. However, in this case, the

finite width of the probe state is also important as we shall see later. The interaction is generated via

$$\hat{U}_I = \exp\left(-i\kappa \int_{t_i}^{t_f} \hat{A} \otimes \hat{p}\, dt\right) = e^{-i\kappa T \hat{A}\hat{p}}. \tag{4.12}$$

The final state of the probe following both the interaction with the system and the final post-selection is

$$|\Psi_f\rangle \propto \langle \Phi_2 | e^{-i\kappa T \hat{A}\otimes\hat{p}} |\Phi_1\rangle |\Psi_i\rangle \propto \sum_{n=0}^{\infty} \frac{(-i\kappa T)^n}{n!} \langle \Phi_2|\hat{A}^n|\Phi_1\rangle \hat{p}^n |\Psi_i\rangle. \tag{4.13}$$

Assuming $\langle \Phi_2|\Phi_1\rangle \neq 0$ and defining

$$A_W = \langle \Phi_2|\hat{A}|\Phi_1\rangle / \langle \Phi_2|\Phi_1\rangle, \tag{4.14}$$

we obtain:

$$\begin{aligned} |\Psi_f\rangle &\propto \sum_{n=0}^{\infty} \frac{(-i\kappa T)^n}{n!} (A_W)^n \hat{p}^n |\Psi_i\rangle \\ &+ \sum_{m=2}^{\infty} \frac{(-i\kappa T)^m}{m!} \left(\frac{\langle \Phi_2|\hat{A}^m|\Phi_1\rangle}{\langle \Phi_2|\Phi_1\rangle} - (A_W)^m \right) \hat{p}^m |\Psi_i\rangle. \end{aligned} \tag{4.15}$$

The state of the probe records the so-called weak value only if the second term in (4.15) vanishes. This condition constrains both the magnitude of the coupling constant and the noise in the initial state of the measuring device. This follows from considering the momentum wavefunction of $|\Psi_i\rangle$ given by $\tilde{\Psi}_i(p) = e^{-p^2\Delta^2 q}$. Thus, the second term in (4.15) vanishes if

$$e^{-p^2\Delta^2 q} \left(\frac{\langle \Phi_2|e^{-i\kappa T \hat{A}p}|\Phi_1\rangle}{\langle \Phi_2|\Phi_1\rangle} - e^{-i\kappa T A_W p} \right) \approx 0 \;\; \forall\, p \;\in\; (-\infty, \infty), \tag{4.16}$$

is true. If the coupling constant is small ($\kappa_T << 1$) then (4.16) is satisfied for small p. For large p, the above can only be satisfied if the noise in the initial state of the measuring device is large i.e. $\Delta^2 q >> 1$ and so the superposition is broad. The measuring device then receives little information about the observable $\mathcal{A}$ on the system. This, in conjunction with the weak coupling, is required in order to allow the weak value to be encoded on the state of the probe.

Consequently, the weak value is only observable if a combination of factors are realized together. Thus, we need both the weakness of the coupling and the noise in

the probe for the weak value to be encoded and we can gain some intuition about this by considering the following. Note that the pre and post-selected states of the probe admit the decompositions $|\Phi_1\rangle = \sum_k c_k|a_k\rangle$ and $|\Phi_2\rangle = \sum_k d_k|a_k\rangle$ where $\hat{A}|a_k\rangle = a_k|a_k\rangle$. To understand the emergence of weak values, we must first consider what happens to the probe state in general. In this case, each probe and signal evolves according to

$$\int_{-\infty}^{\infty} dq e^{-q^2/4\Delta^2 q}|q\rangle|\Phi_1\rangle \rightarrow \sum_k \int_{-\infty}^{\infty} dq e^{-q^2/4\Delta^2 q} c_k|q+\kappa T a_k\rangle|a_k\rangle, \tag{4.17}$$

where we assume that the interaction lasts for T seconds and ignore normalization for the moment. Thus, in this regime (i.e. no restriction on the size of the coupling constant) the probe pointer degrees of freedom become entangled with the eigenvalues of $\hat{A}$. Following this evolution, the signal (for all members in this sub-ensemble) is post-selected as $|\Phi_2\rangle$:

$$\sum_k \int_{-\infty}^{\infty} dq\, e^{-q^2/4\Delta^2 q} c_k|q+\kappa T a_k\rangle|a_k\rangle \rightarrow \int_{-\infty}^{\infty} dq \sum_k c_k d_k^* e^{-q^2/4\Delta^2 q}|q+\kappa T a_k\rangle. \tag{4.18}$$

Hence, the wavefunction of the final probe state is a summation of Gaussian functions centered around a particular eigenvalue of $\mathcal{A}$:

$$\Psi_f(q) \propto \sum_k c_k d_k^* \exp\left(-\frac{(q-\kappa T a_k)^2}{4\Delta^2 q}\right) \tag{4.19}$$

and the associated probability density is

$$\rho_f(q) = \frac{\left|\sum_k c_k d_k^* \exp\left(-\frac{(q-\kappa T a_k)^2}{4\Delta^2 q}\right)\right|^2}{\int_{-\infty}^{\infty} dq \left|\sum_k c_k d_k^* \exp\left(-\frac{(q-\kappa T a_k)^2}{4\Delta^2 q}\right)\right|^2}. \tag{4.20}$$

Thus, the measurement statistics of the probe's pointer position will reveal a series of Gaussian peaks centered at (up to a scalar multiple) the eigenvalues of the observable $\mathcal{A}$.

In contrast, if we restrict ourselves to the weak value regime then the final probe state is given by

$$|\Psi_f\rangle \propto \exp\left(-i\kappa T A_W \hat{p}\right)|\Psi_i\rangle \propto \int_{-\infty}^{\infty} dp\, e^{-p^2\Delta^2 q} e^{-i\kappa T\, \Re(A_W)p + \kappa T\, \Im(A_W)p}|p\rangle, \tag{4.21}$$

and so the momentum probability density yields

$$\tilde{\rho}_W(p) = \frac{|\tilde{\Psi}_f(p)|^2}{\int_{-\infty}^{\infty} dp\, |\tilde{\Psi}_f(p)|^2} = \sqrt{\frac{2\Delta^2 q}{\pi}}\, e^{-2\Delta^2 q\left(p - \kappa T\, \Im(A_W)/2\Delta^2 q\right)^2}, \tag{4.22}$$

and the position probability density

$$\rho_W(q) = \frac{|\Psi_f(q)|^2}{\int_{-\infty}^{\infty} dq\, |\Psi_f(q)|^2} = \frac{1}{\sqrt{2\pi\Delta^2 q}}\, e^{-(q - \kappa T\, \Re(A_W))^2/2\Delta^2 q}. \tag{4.23}$$

The pointer position and its conjugate momentum are both displaced by the components of the weak value of observable $\mathcal{A}$ and not any of its eigenvalues. In particular, in the weak value regime the expectation value of the canonical variables of the probe change in response to the weak value [86, 88–90]

$$\langle q \rangle_f = \int_{-\infty}^{\infty} dq\, q\, \rho_W(q) = \kappa T \Re(A_W), \quad \langle p \rangle_f = \int_{-\infty}^{\infty} dp\, p\, \tilde{\rho_W}(p) = \frac{\kappa T \Im(A_W)\Delta^2 q}{2}.$$

Hence, the change of these first order moments of the probe encode the components of the weak values

$$\Delta\langle q \rangle = \kappa T \Re(A_W), \quad \Delta\langle p \rangle = \frac{\kappa T \Im(A_W)\Delta^2 q}{2}. \tag{4.24}$$

It is in this sense that both the real and imaginary components of the weak value are observable, albeit in an indirect manner on a statistical level.

4.2.4 An example of a weak measurement

To make this discussion of weak measurements and values concrete, we will consider the following example [85, 91]. We assume that the signal system is a spin-1/2 particle and that the observable of interest is the z-component of spin

$$\hat{S}_z = \frac{1}{2}|\uparrow\rangle\langle\uparrow| - \frac{1}{2}|\downarrow\rangle\langle\downarrow|, \tag{4.25}$$

where we assume $\hbar = 1$. Accordingly, the pre and post-selected states are superpositions of the eigenstates of $\hat{S}_z$

$$|\Phi_1\rangle = \frac{1}{\sqrt{2}}|\uparrow\rangle + \frac{1}{\sqrt{2}}|\downarrow\rangle, \tag{4.26}$$

$$|\Phi_2\rangle = \frac{1}{\sqrt{3}}|\uparrow\rangle + \sqrt{\frac{2}{3}}|\downarrow\rangle. \tag{4.27}$$

The probe is once again prepared as a Gaussian superposition of pointer eigenstates

$$|\Psi_i\rangle \propto \int dq\, e^{-q^2/4\Delta^2 q}|q\rangle, \tag{4.28}$$

with $\Delta^2 q$ defining the width of the superposition. The interaction Hamiltonian which mediates the interaction between signal and probe is given by

$$\hat{H}_I = \kappa \hat{S}_z \hat{p}. \tag{4.29}$$

Physically, such and interaction describes the coupling of the spin of the signal to momentum shifts in the probe.

To illustrate the circumstances for which the weak measurement model is valid, we will compare it to the general case of indirect measurement with pre and post-selection which results in a final probe state that is a superposition of Gaussians centered around the eigenvalues of $\hat{S}_z$

$$\Psi_f(q) \propto \frac{1}{\sqrt{6}} e^{-\frac{(q-\kappa T/2)^2}{4\Delta^2 q}} + \sqrt{\frac{2}{6}} e^{-\frac{(q+\kappa T/2)^2}{4\Delta^2 q}}, \tag{4.30}$$

and so the position probability density for this final state is then

$$\rho_f(q) \propto \left(\frac{1}{\sqrt{6}} e^{-\frac{(q-\kappa T/2)^2}{4\Delta^2 q}} + \sqrt{\frac{2}{6}} e^{-\frac{(q+\kappa T/2)^2}{4\Delta^2 q}} \right)^2, \tag{4.31}$$

up to a normalization factor.

However, if we perform the above indirect measurement in the weakness regime then the state of the probe encodes the weak value of $\hat{S}_z$ corresponding to the particular choice of pre and post-selection. In this case, the weak value is real and is given by

$$(S_z)_W = \frac{\langle \Phi_2 | \hat{S}_z | \Phi_1 \rangle}{\langle \Phi_2 | \Phi_1 \rangle} = \frac{1/\sqrt{6} - \sqrt{2}/\sqrt{6}}{2/\sqrt{6} + 2\sqrt{2}/\sqrt{6}} = -\frac{3}{2} + \sqrt{2}. \tag{4.32}$$

The weak measurement of this weak value is portrayed in Fig.4.2 and leads to a final probe state

$$\Psi_f(q) \propto \exp\left(-\frac{(q - \kappa T (S_z)_W)^2}{4\Delta^2 q} \right), \tag{4.33}$$

and so the pointer position probability density of the final probe state in the weak measurement regime is (up to a normalization factor):

$$\rho_W^f(q) \propto \exp\left(-\frac{(q - \kappa T (S_z)_W)^2}{2\Delta^2 q} \right). \tag{4.34}$$

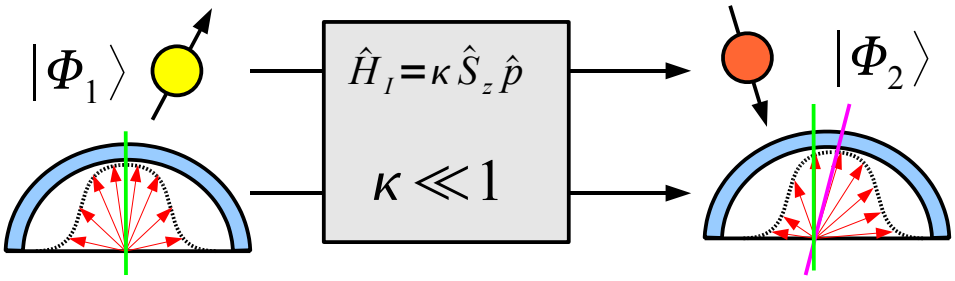

Figure 4.2: *This diagram portrays the features of the weak measurement regime for the previous indirect measurement. This regime is only reached provided the coupling is sufficiently weak. The probe is initially prepared in a Gaussian superposition of pointer states with a mean position of zero (green line). After the weak measurement, the probe has experienced a shift in average position (pink line) that is directly proportional to the real part of the weak value of interest.*

Clearly, the two cases lead to very different measurement statistics for their final probe states (4.31) and (4.34). However, in the limit of weak coupling both give identical results as shown in Fig.4.3.

Consequently, this demonstrates that the results of weak measurements, i.e. the measuring of weak values are only correct in the limit of weak coupling combined with finite $\Delta^2 q$. This is clearly illustrated in Fig.4.3 where the distinct Gaussian peaks of (4.31) represented by the blue curve merge into a single Gaussian which coincides with (4.34) represented by the red curve as the coupling strength is decreased. Furthermore, this approximate equivalence between (4.31) and (4.34) can only occur provided $\Delta^2 q$ is sufficiently large otherwise the distinct peaks of (4.31) would remain forever distinct for all non-zero coupling strengths. Thus, the measurement of weak values in weak measurements occur if the indirect measurement is very inefficient - the resolution of the probe state is low and the interaction between signal and probe is weak. We will see this combination of effects arising whenever we wish to discuss weak values.

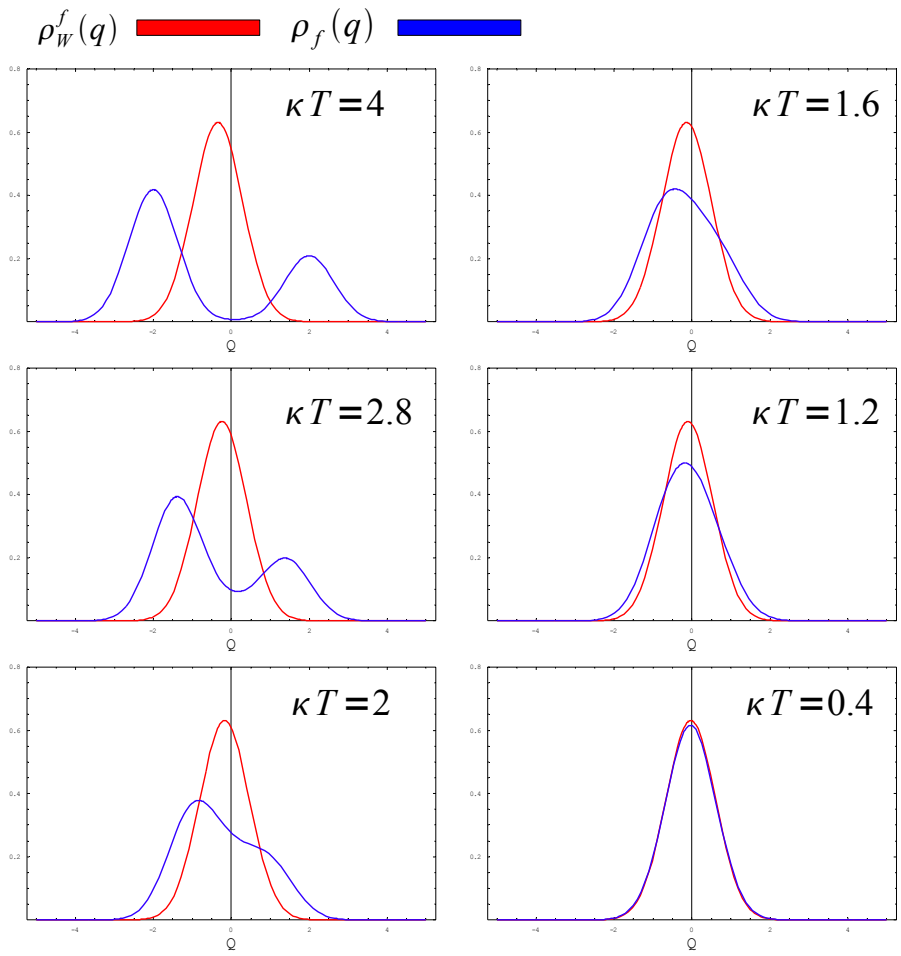

Figure 4.3: *This diagram shows that weak measurements emerge as a special example of indirect measurements with pre and post-selection where the coupling is weak and the probe has sufficiently poor resolution. Here, $\rho_f(q)$ in the general indirect measurement is plotted in blue and for large κT exhibits distinguishable peaks corresponding to the eigenvalues of $\hat{S}_z$. This case coincides with the equivalent pointer position probability density of the final probe state for the weak measurement regime represented by the red curve in the limit of weak coupling. This demonstrates the appropriate conditions for which weak measurements provide a valid description.*

4.3 The development and application of weak values

The concept of weak values and weak measurements began in the context of obtaining spin values outside the eigenvalue spectrum of the corresponding Pauli operators [84]. That is, it was shown that a weak indirect measurement on a pre and post-selected ensemble of spins can result in very large observed values of spin. Elements of this original proposal proved to be erroneous [92], but the overall concept was shown to be sound [92]. It was *Aharonov* and *Vaidman* [83] who developed and refined weak values and weak measurements into its currently understood form. Since their original conception, weak values have enjoyed a great deal of theoretical investigation and eventual experimental confirmation.

The former has revealed the great versatility of weak values and weak measurements in providing an explanatory basis for a number of physical phenomena. Indeed, weak values and weak measurements explain or appear in: fast and slow light effects [93], superluminal quantum tunneling effects [94, 95], optical telecommunications networks [96], the quantum back-action of charged particles on a classical field [97], an approach to a time-symmetric formulation of quantum mechanics [98–101]. Furthermore, their contextual nature and relation to hidden variables has been explored [102] as has their semi-classical approximation [103]. In the context of quantum information theory, weak values have found application in communication protocols [104], so-called "weak cloning" [105] and in the control of transitions between different states [106]. This theoretical investigation has also given away to eventual experimental observation of weak values in quantum optical systems [107–111].

In relation to entanglement concentration, there are two aspects of weak values and weak measurements that could be of potential use. The first point to notice is that weak measurements engender a simple back-action on the probe as a consequence of imprinting the weak value. Ultimately, the real part of the weak value accompanies a unitary back action on the state of the probe, whereas, the imaginary

part induces a non-unitary back action [83, 88]. This back action has be thoroughly investigated in the case of the interaction Hamiltonian $\hat{H}_I = \hbar\kappa\hat{O}\hat{p}$ for a variety of different single mode probe states in [86, 88]. In such investigations, the back action is analyzed via the measurement statistics of the pointer and momentum observables of the probe. Secondly, other authors have shown that weak measurements can also apply to mixed probe states [112]. Thus, this understanding immediately inspires two questions: can weak measurements be generalized to entangled probe states and can the back-action of the weak value be related to the non-classicality properties of the probe? Both of these questions have positive answers and they allow us to use the weak value as a calculation tool in entanglement concentration protocols.

Part II

Original research

Chapter 5

Weak values and Gaussian entanglement concentration

5.1 Introduction

We now begin to detail the first of our original contributions in this thesis. Chapter three ended with a discussion of open questions surrounding the indirect measurement entanglement concentration approach. Perhaps unexpectedly, weak measurements can account for all of these issues in single coherent explanation as outlined in this chapter. That is, we demonstrate that the previous family of entanglement concentration protocols are actually examples of weak measurements where the probe state is initially prepared in an entangled state. Indeed, we have discovered that [1, 54] are special cases of a general weak measurement interaction. Using the weak value paradigm, we demonstrate how to construct a general model of such Procrustean protocols. Moreover, we identify that the features of these protocols, namely success conditions and Gaussian preservation are not unique to the particular choices advocated in both [1, 54]. Instead, our general analysis reveals that the origin of these features lie with the consequences of performing a weak measurement. Furthermore, our model constrains the pre and post-selected ancilla states whilst providing a method for determining which possible combinations work.

5.2 Weak measurement induced entanglement concentration

5.2.1 The protocol

Our weak measurement model is based on the following configuration. As depicted in Fig.5.1, the entangled state in modes A and B is coupled to ancilla state in mode C by means of a unitary evolution between B and C. The requirements of the *Procrustean* method dictate that the interaction Hamiltonian describing this process must be of the form

$$\hat{H}_I = \hbar\kappa(t)\hat{n}_B \otimes \hat{O}_C. \tag{5.1}$$

The form of this interaction Hamiltonian is required to preserve the *Schmidt* basis of the TMSV, i.e. the *Fock* basis. In addition, we assume vanishing free Hamiltonians for all modes, meaning that our results are unique up to a suitable unitary transformation. Assuming the interaction persists for T seconds, then the corresponding unitary evolution operator is

$$\hat{U} = e^{-i\int_0^T \kappa(t)\hat{n}_B\hat{O}_c} = e^{-i\kappa_T\hat{n}_B\hat{O}_C}, \tag{5.2}$$

where $\kappa_T = \kappa(T) - \kappa(0)$.

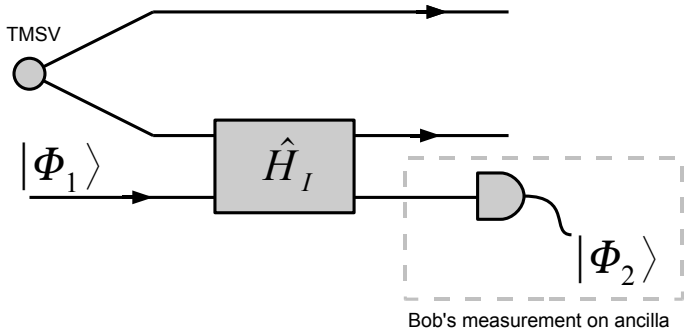

Figure 5.1: *Bob mixes his half of the TMSV with an ancillary mode pre-selected in* $|\Phi_1\rangle$ *via an non-linear interaction described by the Hamiltonian* $\hat{H}_I$*. The ancilla mode is then subjected to a post-selected measurement leaving it in the state* $|\Phi_2\rangle$*.*

Following this, Bob performs a measurement on the ancilla and post-selects it in

the state $|\Phi_2\rangle$. Consequently, the state shared between Alice and Bob is given by

$$|\psi_f\rangle = \mathcal{N}\langle\Phi_2|e^{-i\kappa_T\hat{n}_B\hat{O}_C}|\zeta(\lambda)\rangle|\Phi_1\rangle = \mathcal{N}'\sum_{m=0}^{\infty}\frac{(-i\kappa_T)^m}{m!}\frac{\langle\Phi_2|\hat{O}_C^m|\Phi_1\rangle}{\langle\Phi_2|\Phi_1\rangle}\hat{n}_B^m|\zeta(\lambda)\rangle. \quad (5.3)$$

The weak value of $\hat{O}_C$ is defined as

$$O_W = \frac{\langle\Phi_2|\hat{O}_C|\Phi_1\rangle}{\langle\Phi_2|\Phi_1\rangle}, \quad (5.4)$$

and so the final state of the system is given by

$$|\psi_f\rangle = \mathcal{N}'\exp\left(-i\kappa_T O_W\hat{n}_B\right)|\zeta(\lambda)\rangle, \quad (5.5)$$

if the weakness condition

$$\sum_{m=2}^{\infty}\frac{(-i\kappa_T)^m}{m!}\left\{O_W^m - (O_W)^m\right\}\hat{n}_b^m|\zeta(\lambda)\rangle \approx 0|\phi\rangle \quad (5.6)$$

is obeyed. Here $|\phi\rangle$ is an arbitrary vector in $\mathcal{H}_A \otimes \mathcal{H}_B$ and

$$O_W^m = \langle\Phi_2|\hat{O}_C^m|\Phi_1\rangle/\langle\Phi_2|\Phi_1\rangle. \quad (5.7)$$

By using the linear independence of the *Schmidt* basis of the TMSV we can express (5.6) as set of equations:

$$\lambda^n\left(\frac{\langle\Phi_2|e^{-i\kappa_T n\hat{O}_C}|\Phi_1\rangle}{\langle\Phi_2|\Phi_1\rangle} - e^{-i\kappa_T n O_W}\right) \approx 0 \;\; \forall n \in [0,\infty). \quad (5.8)$$

Assuming that the above weakness condition is satisfied means that the output state is another TMSV as (5.5) yields

$$|\psi_f\rangle = \sqrt{1-\lambda^2 e^{2\kappa_T\Im(O_W)}}\sum_{n=0}^{\infty}\lambda^n e^{-i\kappa_T O_W n}|n,n\rangle, \quad (5.9)$$

This only holds subject to $\lambda^2 e^{2\Im(O_W)\kappa_T} < 1$, otherwise the output state is un-physical as the normalisation constant will not converge. From (5.9) it can be seen that the real part O_W induces a phase shift on the TMSV whereas the imaginary part modifies the average number of photons in the state. Put succinctly, the induced transformation is $\lambda \to \lambda' = \lambda e^{-i\kappa_T O_W}$. Thus, the average number of photons has been altered [25],

$$\frac{2\lambda^2}{1-\lambda^2} \to \frac{2\lambda^2 e^{2\kappa_T\Im(O_W)}}{1-\lambda^2 e^{2\kappa_T\Im(O_W)}}, \quad (5.10)$$

meaning that we can subtract or add an indefinite number of photons to our target state.

5.2.2 Verification of concentration and configuration selection

The use of the weak value in our entanglement concentration model is entirely different to the usual presentation of weak measurements, where the goal is to observe the weak value from a sub-ensemble of final probe states. However, in our model the weak value is a function of the measurement result on the ancilla $O_W = O_W(\omega)$, where ω is the measurement outcome. Thus, in each run of the protocol a different ω is obtained and a different weak value $O_W(\omega)$ is imprinted on the shared entangled state. So the aim is not to observe the weak value of the ancilla system, but to use it as a calculational aid to understand the general nature of the back action on the entangled state. This point is crucial to avoid confusion over the application of weak values and measurements here. With this in mind, we now show how the encoded weak value can transform the entanglement content of the TMSV.

To determine if entanglement concentration has occurred in a particular run of the protocol requires that we establish whether the transformation

$$\lambda \to \lambda e^{-i\kappa_T O_W} \tag{5.11}$$

between initial and final states increases the shared entanglement. Thus, we must calculate the entanglement entropy (3.9) for both states and then determine which has a larger degree of entanglement. Mathematically, this requires demonstrating

$$\frac{\mathcal{S}(\hat{\rho}_f(O_W))}{\mathcal{S}(\rho_i)} > 1, \tag{5.12}$$

where $\hat{\rho}_f = \mathrm{Tr}_j(|\psi_f\rangle\langle\psi_f|)$ and $\hat{\rho}_i = \mathrm{Tr}_j(|\zeta(\lambda)\rangle\langle\zeta(\lambda)|)$ and translating it into a condition that constrains the weak value imprinted onto the entangled state. Unfortunately, attempting to translate this into a condition on O_W is algebraically nontrivial.

Instead we adopt the method of *Majorization* [72] to derive an appropriate condition. Let $\mathbf{c} = (c_0^2, c_1^2, \ldots)^T$ be the ordered vector of the eigenvalues of the input TMSV and $\mathbf{d} = (d_0^2, d_1^2, \ldots)^T$ be the analogues object for (5.9). Then the final entangled state is more entangled than the initial one if $\mathbf{c}$ is *majorized* by $\mathbf{d}$, which is

written as $\mathbf{c} \prec \mathbf{d}$ and defined by [68, 69]

$$\sum_{k=\ell}^{\infty} d_k^2 > \sum_{k=\ell}^{\infty} c_k^2, \tag{5.13}$$

for $\ell \in [1, \infty)$. This follows since measures of bipartite pure state entanglement such as the *Von Neumann* entropy belong to the *Shur convex* [69] and hence, preserve the majorization order

$$\mathbf{c} \prec \mathbf{d} \Longrightarrow f(\mathbf{d}) > f(\mathbf{c}). \tag{5.14}$$

It is sufficient for entanglement concentration to show that the eigenvalues of the reduced density matrices of the output state majorize those of the input state. The majorization expression for the input entangled state is given by:

$$\sum_{k=\ell}^{\infty} c_k^2 = (1-\lambda^2) \sum_{k=\ell}^{\infty} \lambda^{2k} = \lambda^{2\ell}. \tag{5.15}$$

The proof of this is expression provided by induction. Note that (5.15) holds for $\ell = 1$ and $\ell = 2$ terms since

$$(1-\lambda^2) \sum_{k=1}^{\infty} \lambda^{2k} = (1-\lambda^2) \left(\sum_{k=0}^{\infty} \lambda^{2k} - 1 \right) = 1 - (1-\lambda^2) = \lambda^{2\times 1} \tag{5.16}$$

and

$$(1-\lambda^2) \left(\sum_{k=0}^{\infty} \lambda^{2k} - 1 - \lambda^2 \right) = 1 - (1-\lambda^2)(1+\lambda^2) = \lambda^{2\times 2}. \tag{5.17}$$

Thus, we assume that the expression is true for $k = m$ then and it check for $k = m+1$:

$$\begin{aligned} (1-\lambda^2) \sum_{k=m+1}^{\infty} \lambda^{2k} &= (1-\lambda^2) \left(\sum_{k=m}^{\infty} \lambda^{2k} - \lambda^{2m} \right) \\ &= \lambda^{2m} - (1-\lambda^2)\lambda^{2m} = \lambda^{2\times(m+1)}. \end{aligned} \tag{5.18}$$

Hence, by induction it holds for all m and so

$$\sum_{k=\ell}^{\infty} c_k^2 = \lambda^{2\ell}, \tag{5.19}$$

is true. Accordingly, (5.13) becomes

$$\lambda^{2\ell} e^{2\kappa_T \ell \Im(O_W)} > \lambda^{2\ell} \tag{5.20}$$

for all $\ell \in [1, \infty]$. The only way to satisfy (5.20) is if the imaginary part of O_W is positive for all ℓ (assuming $\kappa_T > 0$). Entanglement concentration can then occur if the imaginary weak value is positive

$$\Im\left(\frac{\langle\Phi_2|\hat{O}_C|\Phi_1\rangle}{\langle\Phi_2|\Phi_1\rangle}\right) > 0. \tag{5.21}$$

This condition allows the selection of working configurations of the ancilla ingredients i.e. on the combination of initial state, interaction Hamiltonian and measurement strategy. That is it provides a number of constraints that the interaction Hamiltonian $\hat{H}_I$, the pre-selected and post-selected ancilla states $|\Phi_1\rangle$ and $|\Phi_2\rangle$ and the observable $\hat{O}_C$ must obey in order to produce entanglement concentration of the TMSV. It is interesting to note that the weak condition (5.8) coupled with the requirements of the *Procrustean* method are all that is required to preserve the Gaussian character of the TMSV.

5.2.3 Measurement based success condition

Consequently, $\Im(O_W) > 0$ can be theoretically calculated by the agents participating in the protocol to select working configurations required for Gaussian-preserving entanglement concentration. What is still needed is the measurement-based success condition that allows Alice and Bob to decide whether they keep the shared entangled state or not. However, such a condition is hidden in the selection criterion above. To see this, let $|\Psi\rangle$ be a fixed pre-selected state of the ancilla and assume that the interaction Hamiltonian is fixed with $\hat{H}_I = \hbar\kappa\hat{n}\hat{O}$. We further assume that the post-selected state in each run of the protocol is one of the eigenstates of an operator $\hat{\omega}$ i.e. $|\omega\rangle$. Different runs of the protocol result in different measurement outcomes ω and imprint a different weak value on the shared entangled state:

$$\lambda \to \lambda \exp\left(\kappa_T \Im(O_W(\omega))\right), \tag{5.22}$$

where $O_W(\omega) = \langle\omega|\hat{O}|\Psi\rangle/\langle\omega|\Psi\rangle$. Thus, we can establish a measurement-based success condition from

$$\langle\Psi|\hat{O}|\Psi\rangle = \sum_{\omega\in\Omega}\langle\Psi|\omega\rangle\langle\omega|\hat{O}|\Psi\rangle = \sum_{\omega\in\Omega} P(\omega|\Psi)O_W(\omega), \tag{5.23}$$

where $P(\omega|\Psi) = |\langle\Psi|\omega\rangle|^2$ is the probability of finding $|\Psi\rangle$ given $|\omega\rangle$. Now, given

$$\Im(\langle\Psi|\hat{O}|\Psi\rangle) = \sum_{\omega\in\Omega} P(\omega|\Psi)\Im(O_W(\omega)) = 0, \tag{5.24}$$

and since $P(\omega|\Psi) \geq 0$ for all possible ω, then either $\Im(O_W(\omega)) = 0$ for all ω or

$$\Im(O_W(\omega)) > 0 \,\forall\, \omega \in \Omega_+, \quad \Im(O_W(\omega)) < 0 \,\forall\, \omega \in \Omega_-. \tag{5.25}$$

That is, there is a subset of measurement results that correspond to an increase in shared entanglement and a subset corresponding to a decrease in entanglement. Thus, the selection criterion is equivalent to the existence of a measurement-based success condition. Consequently, in each run of the protocol, Bob makes the measurement on the ancilla and obtains result ω, after calculating its associated weak value, he classically communicates the result to Alice and they either keep or discard the state depending on the result.

Accordingly, in each fixed configuration we can calculate a success probability of the protocol. This is the probability of obtaining any $\omega \in \Omega_+$ and it can be obtained from the probability (or probability density if the measurement results form a continuum) of obtaining a particular post-selected state $|\omega\rangle$. We can derive an expression for this probability (or probability density) from

$$\rho(\omega) = \mathrm{Tr}\left\{\left(\hat{I}_A \otimes |\omega\rangle\langle\omega|\right) e^{-i\kappa_T \hat{n}_B \hat{O}_C} |\zeta(\lambda), \Psi\rangle\langle\zeta(\lambda), \Psi| e^{i\kappa_T \hat{n}_B \hat{O}_C}\right\}. \tag{5.26}$$

Where $|\Phi\rangle$ is the pre-selected state, i.e. the initially prepared state of the ancilla. Expanding the above exponentials gives

$$\rho(\omega) = \sum_{k,m=0}^{\infty} \frac{(-i\kappa_T)^m (i\kappa_T)^k}{m!k!} \langle\omega|\hat{O}_C^m|\Psi\rangle\langle\Psi|\hat{O}_C^k|\omega\rangle \mathrm{Tr}\left(\hat{n}_C^m |\zeta(\lambda)\rangle\langle\zeta(\lambda)|\hat{n}_C^k\right), \tag{5.27}$$

and assuming the usual weakness conditions means that

$$\rho(\omega) \approx P(\omega|\Psi)\mathrm{Tr}\left(e^{-i\kappa_T \hat{n}_B O_W(\omega)} |\zeta(\lambda)\rangle\langle\zeta(\lambda)| e^{i\kappa_T \hat{n}_B O_W^*(\omega)}\right), \tag{5.28}$$

and since the initial probe state is $|\zeta(\lambda)\rangle = \sqrt{1-\lambda^2}\sum_{n=0}^{\infty} \lambda^n |n, n\rangle$, then the probability (or probability density) is

$$\rho(\omega) = \frac{P(\omega|\Psi)(1-\lambda^2)}{1 - \lambda^2 e^{2\kappa_T \Im(O_W(\omega))}}. \tag{5.29}$$

The probability of success in a single run i.e. imprinting a weak value that will increase the shared entanglement is

$$P_S = \sum_{\omega \in \Omega_+} \rho(\omega), \tag{5.30}$$

and the corresponding probability of failure is then $P_F = 1 - P_S$. Consequently, we can expect different working configurations to have different probabilities of success. However, the maximum probability of success is limited by general theorems concerning the conditional transformation of bipartite entangled states [73].

Ultimately, this weak measurement model encodes all of the characteristic features of the entanglement concentration scheme in chapter 3. Moreover, it allows the explanation of all of these features without fixing the physical implementation of the ancillary system. Firstly, the Gaussian preserving aspect is a general feature of weak coupling between the entangled state and the ancilla. This is directly required to imprint the weak value of the ancilla onto the entangled state and thereby change its mean photon number and squeezing. Secondly, the reason that only selected ancillary configurations change the entanglement content of the TMSV is because each configuration has a different O_W and gives rise to a different back-action. Finally, the measurement based success condition, which allow Alice and Bob to determine the success of the protocol, occur as a result of the fundamental properties of weak values. The real power of the weak measurement formalism in this problem is the extent of its applicability - it allows one to consider the protocol for all possible ancilla systems regardless of their physical implementation.

5.2.4 Measuring the efficiency of the protocol

Finally, we note that the weak measurement formalism also provides the means to determine the efficiency of the entanglement concentration protocol for each working configuration. The efficiency of the protocol can be gauged by considering a number of different quantities provided by the model.

Firstly, we quantify the accuracy of the weak measurement formalism to describe the action of the protocol by summing over all the weakness conditions for different

Fock numbers:

$$\epsilon(\Phi_1, \Phi_2, \kappa_T, \lambda) = \left| \sum_{n=0}^{\infty} \lambda^n \left(\frac{\langle \Phi_2 | e^{-i\kappa_T n \hat{O}} | \Phi_1 \rangle}{\langle \Phi_2 | \Phi_1 \rangle} - e^{-i\kappa_T n O_W} \right) \right|. \tag{5.31}$$

This allows us to measure the accuracy of the weak regime in a single number which aids its numerical simulation. Furthermore, due to the complexity of the first term in (5.31), this quantity must be truncated at a very large finite n in the absence of a analytical expression for the infinite series. Alternatively, we can also use the fidelity between the final probe state in the weak regime compared to the final state predicted in general to measure the accuracy of our weak measurement model. Thus, we consider the fidelity $\mathcal{F} = |\langle \psi_f^W | \psi_f^G \rangle|^2$ with

$$|\psi_f^W\rangle = \sqrt{1 - \lambda^2 e^{2\kappa_T \Im(O_W)}} \sum_{n=0}^{\infty} \lambda^n e^{-i\kappa_T n O_W} |n, n\rangle, \tag{5.32}$$

and

$$|\psi_f^G\rangle = \frac{\sum_{n=0}^{\infty} \lambda^n \langle \Phi_2 | e^{-i\kappa_T n \hat{O}} | \Phi_1 \rangle |n, n\rangle}{\sqrt{\sum_{n=0}^{\infty} \lambda^{2n} |\langle \Phi_2 | e^{-i\kappa_T n \hat{O}} | \Phi_1 \rangle|^2}}, \tag{5.33}$$

given by

$$\mathcal{F}(\Phi_1, \Phi_2) = \frac{1 - \lambda^2 e^{2\kappa_T \Im(O_W)}}{\sum_{n=0}^{\infty} \lambda^{2n} |\langle \Phi_2 | e^{-i\kappa_T n \hat{O}} | \Phi_1 \rangle|^2} \left| \sum_{n=0}^{\infty} \lambda^{2n} e^{i\kappa_T n O_W^*} \langle \Phi_2 | e^{-i\kappa_T n \hat{O}} | \Phi_1 \rangle \right|^2. \tag{5.34}$$

Secondly, we use the probability of success P_S and its associated probability density together with the relative increase in entanglement to quantify the efficiency of each configuration. The expression for the former quantity has been given previously while the latter is defined as the ratio of Von Neumann entropies of the reduced density matrices for the final and input states denoted by $\mathcal{S}_f$ and $\mathcal{S}_i$. The quantity $\Delta\mathcal{S} = \mathcal{S}_f / \mathcal{S}_i$ is given explicitly as

$$\Delta\mathcal{S} = \frac{(1-\lambda^2)\{2\lambda^2 e^{2\kappa_T \Im(O_W)} \ln(\lambda e^{\kappa_T \Im(O_W)}) + (1 - \lambda^2 e^{2\kappa_T \Im(O_W)}) \ln(1 - \lambda^2 e^{2\kappa_T \Im(O_W)})\}}{(1 - \lambda^2 e^{2\kappa_T \Im(O_W)})\{2\lambda^2 \ln \lambda + (1-\lambda^2) \ln(1-\lambda^2)\}}.$$

This quantity measures the relative change in entanglement as a result of imprinting the weak value O_W on the two mode squeezed vacuum.

5.2.5 Experimental verification

Ultimately, any theory stands or falls in the face of empirical testing and the weak measurement model suggested here is no different. Whether or not the entanglement content of a TMSV is modified as a result of encoding certain weak values can be verified by state tomography [27] of a sub-ensemble of output entangled states. That is, Alice and Bob repeatedly run the protocol on an ensemble of identical input TMSVs until they have a sub-ensemble of output states with the same weak value imprinted onto them. They then perform tomography on that sub-ensemble and attempt to identify whether the entanglement has been modified in accordance with the weak measurement model.

5.3 Optical examples with the cross-Kerr effect

5.3.1 Introduction

We now demonstrate that previously discovered protocols of this type can emerge as special examples of the general model advocated here. We will also calculate the associate weak values and demonstrate that the weakness condition is satisfied. The previous schemes [1] and [54] required Bob's half of the TMSV to be mixed with an ancillary coherent state $|\alpha\rangle$, where $\alpha \in \Re$ and $\alpha > 0$, in a non-linear medium exhibiting the cross-Kerr effect $\hat{H}_I = \hbar\kappa(t)\hat{n}_B\hat{n}_C$ before being subjected to a measurement and post-selection condition. Using the success condition (5.21), we can derive a constraint on the possible post-selected ancilla states which will allow us to select measurement strategies that lead to Gaussian-preserving entanglement concentration. Thus, we are interested in the weak values of the number operator $\hat{n}_C$:

$$n_W = \frac{\langle\Phi_2|\hat{n}_C|\alpha\rangle}{\langle\Phi_2|\alpha\rangle} = \frac{e^{-\alpha^2/2}\alpha\partial_\alpha\left(e^{\alpha^2/2}\langle\Phi_2|\alpha\rangle\right)}{\langle\Phi_2|\alpha\rangle}. \tag{5.35}$$

The second equality in (5.35) follows from $\alpha\partial_\alpha(\alpha^n) = n\alpha^n$. Furthermore, if we assume

$$\langle\Phi_2|\alpha\rangle = R(\alpha)e^{i\theta(\alpha)}, \tag{5.36}$$

where $R(\alpha)$ and $\theta(\alpha)$ are the magnitude and phase of the scalar product of $\langle\Phi_2|\alpha\rangle$, then after some algebra (5.35) can be written as

$$n_W = \alpha^2 + \frac{\alpha}{R(\alpha)}\frac{\partial R}{\partial \alpha} + i\alpha\frac{\partial \theta}{\partial \alpha}. \tag{5.37}$$

Consequently, the success condition requires that

$$\Im(n_W) > 0 \Leftrightarrow \alpha\frac{\partial\theta(\alpha)}{\partial\alpha} > 0. \tag{5.38}$$

Thus, the only variants of this family of protocols which achieve the desired effect are those where the phase of $\langle\Phi_2|\alpha\rangle$ is a monotonic increasing function of α. This prediction allows us to recover previously suggested protocols and uncover new variants.

5.3.2 Double homodyne scheme

In the scheme of *Fiurà̌sek, Mišta and Filip*, (2003) [54], the ancillary coherent state is projected onto $|\beta\rangle = ||\beta|e^{i\phi}\rangle$ via double homodyne detection. This example prevails due to the over-complete nature of coherent states

$$\langle\beta|\alpha\rangle = e^{-\alpha^2/2}e^{-|\beta|^2/2}e^{\alpha\beta^*}, \tag{5.39}$$

where $\beta = \beta_x + i\beta_y$ and it is clear that the phase of the above is a monotonic increasing function of α only if the imaginary part of β is negative. This also follows from

$$n_w = \alpha\beta^* \tag{5.40}$$

with the imaginary part of this weak value being

$$\Im(n_W) = \alpha\partial_\alpha\theta(\alpha) = -\alpha\beta_y. \tag{5.41}$$

Hence, the success condition for this protocol is given by $\beta_y < 0$ and only states post-selected with respect to this condition will allow the desired effect. Moreover, this result allows us to compensate for a weak non-linearity κ_T by employing a large α. Thus, even though the coupling between probe and signal must be weak, the encoded weak value can be very large meaning that

$$\lambda \to \lambda e^{-\kappa_T\alpha\beta_y} \tag{5.42}$$

can still lead to a non-negligible modification of entanglement. Of course, the size of the weak value is ultimately constrained along with the coupling κ_T and the squeezing λ in the initial entangled state by the weakness conditions. These are given as

$$\lambda^n \left(\frac{\langle \beta | e^{-i\kappa_T n \hat{n}_C} | \alpha \rangle}{\langle \beta | \alpha \rangle} - e^{-i\kappa_T n \alpha \beta^*} \right) \approx 0 \ \ \forall n \in [0, \infty). \tag{5.43}$$

Using the identity [25]

$$\exp\left(\sigma \hat{a}^\dagger \hat{a}\right) =: \exp\left(\{e^\sigma - 1\} \hat{a}^\dagger \hat{a}\right) :, \tag{5.44}$$

where the notation $: \hat{A} :$ means the normal ordered version of $\hat{A}$ with all the annihilation operators gathered on the right, we can write (5.43) as

$$\lambda^n \left(e^{(e^{-i\kappa_T n} - 1)\beta^* \alpha} - e^{-i\kappa_T n \beta^* \alpha} \right) \approx 0 \ \ \forall n \in [0, \infty). \tag{5.45}$$

The above is true if $\kappa_T << 1$ such that $e^{-i\kappa_t n} \approx 1 - i\kappa_T n$, which only holds for sufficiently small n. Thus, for small values of n, (5.45) is satisfied. However, for large values of n where $e^{-i\kappa_t n} \neq 1 - i\kappa_T n$, (5.45) still holds because $\lambda < 1$ and hence $\lambda^n \to 0$ for progressively larger n. Thus, the weakness condition requires a balancing act between the non-linear coupling and the squeezing of the input TMSV. The authors of [54] arrive at the same conclusion.

The efficiencies of this protocol can be explored in physically realistic regime by numerical simulation of the relevant quantities. Here, we simulate a number of related quantities for this scheme. We take the ancilla coherent state to have an average photon number of 10^8 and so $\alpha = 10^4$. The phase shift per photon induced by the cross-Kerr effect is taken to be $\kappa_T = 2 \times 10^{-5}$ rad per photon, which is experimentally realistic for a cross-Kerr manifest in atomic vapors [113–115]. In addition, we assume that the initial squeezing shared between Alice and Bob is 4.5dB, which is a realistic value of squeezing and translates to $\lambda = 0.5$ [14]. The first quantity of interest is the total magnitude of the weakness conditions i.e. the total amount of deviation between the output state as predicted by the weak measurement formalism and what is expected in general. This quantity is precisely,

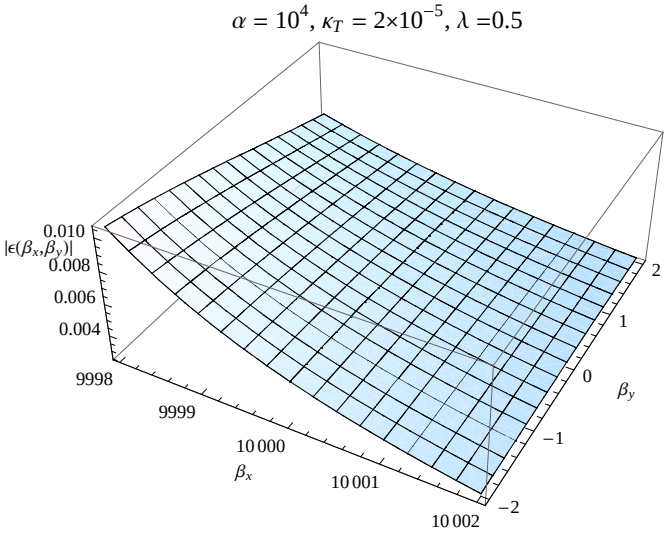

Figure 5.2: *Numerical simulation of the sum of the weakness conditions. This gives a quantitative measure of the deviation between the final state predicted by the weak measurement formalism and the final result expected in general.*

in this case, expressed as

$$\epsilon(\alpha,\beta,\kappa_T,\lambda) = \left|\sum_{n=0}^{\infty}\lambda^n\left(e^{(e^{-i\kappa_T n}-1)\beta^*\alpha} - e^{-i\kappa_T n\beta^*\alpha}\right)\right|. \tag{5.46}$$

Numerically we will truncate this sum for a very large integer. This deviation is plotted in Fig.5.2, where we note that the largest deviation occurs in the region where entanglement concentration occurs. In particular, for the selected parameters, the deviation is of the order of 0.01 in the region where $\beta_y \approx -2$ and $\beta_x \approx 9998$. The corresponding probability density of obtaining a particular complex number $\beta = \beta_x + i\beta_y$ in the weak regime is

$$\rho(\beta_x,\beta_y) = \frac{e^{-|\alpha-\beta|^2}(1-\lambda^2)}{\pi(1-\lambda^2\exp(-2\kappa_T\alpha\beta_y))}. \tag{5.47}$$

We plot this probability density in Fig.5.3 with the aforementioned parameter values and we note from Fig.5.3 that the height of the probability density around the region $\beta_y \approx -2$ and $\beta_x \approx 9998$ is negligible. This means that it is highly unlikely to obtain a weak value in this regime and so the weak measurement description remains a very good approximation to the final probe state. Furthermore, the

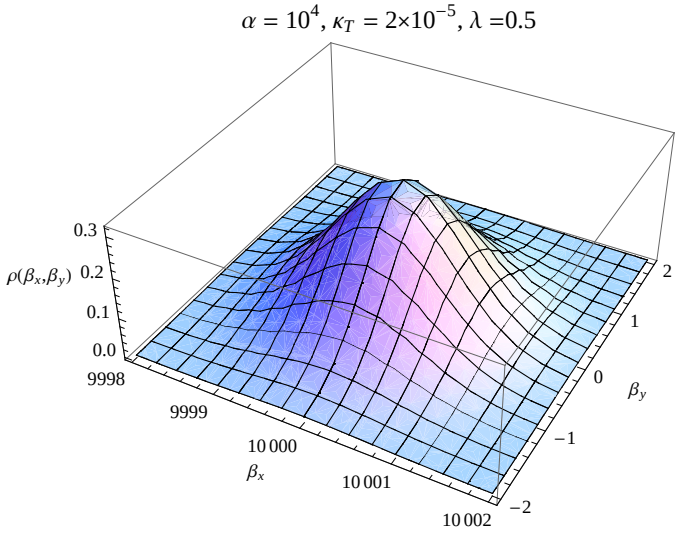

Figure 5.3: *The probability density of achieving a particular $\beta = \beta_x + i\beta_y$ is approximately Gaussian and thus, there is a very low probability density of obtaining values that accompany large deviation in the weakness conditions.*

almost Gaussian nature of the probability density means that the probability of success is approximately 50%

$$\int_{-\infty}^{\infty} d\beta_x \int_{-\infty}^{0} d\beta_y \, \rho(\beta_x, \beta_y) \approx 0.50. \tag{5.48}$$

Next, we consider the fidelity between the final probe state in the weak regime and what occurs in general given as

$$\mathcal{F}(\beta_x, \beta_y) = \left| \frac{\sqrt{1-\lambda^2 e^{-2\kappa_T \alpha \beta_y}} \sum_{n=0}^{\infty} \lambda^{2n} e^{in\kappa_T \alpha \beta^*} \exp\left(\alpha\beta^*(e^{-in\kappa_T} - 1)\right)}{\sqrt{\sum_{n=0}^{\infty} \lambda^{2n} |\exp\left(\alpha\beta^*(e^{-in\kappa_T} - 1)\right)|^2}} \right|^2. \tag{5.49}$$

Finally we have the relative increase in entanglement as a result of the weak measurement. This is given as the ratio of the Von Neumann entropies of the initial and final reduced density matrices of the probe. In this case, the increased entanglement is given by

$$\Delta\mathcal{S}(\beta_y) = \frac{(1-\lambda^2)\{2\lambda^2 e^{-2\kappa_T \alpha \beta_y} \ln(\lambda e^{-\kappa_T \alpha \beta_y}) + (1-\lambda^2 e^{-2\kappa_T \alpha \beta_y}) \ln(1-\lambda^2 e^{-2\kappa_T \alpha \beta_y})\}}{(1-\lambda^2 e^{-2\kappa_T \alpha \beta_y})\{2\lambda^2 \ln\lambda + (1-\lambda^2)\ln(1-\lambda^2)\}}.$$

The performance of this weak measurement configuration for physically realistic parameters $\alpha = 10^4$ and $\kappa_T = 2 \times 10^{-5}$ is best summarized in Fig.5.4, where the

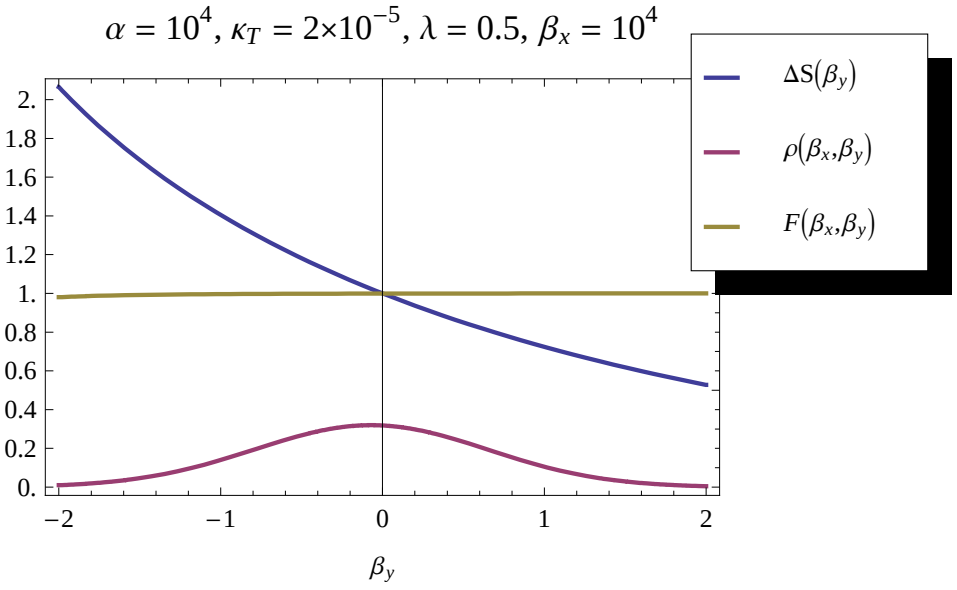

Figure 5.4: *The performance of the double-homodyne weak measurement configuration for* $\alpha = 10^4$ *and* $\kappa_T = 2 \times 10^{-5}$.

fidelity, relative entanglement and probability density are plotted when $\beta_x = 10^4$ is obtained. This reveals a number of interesting features. Firstly, the fidelity is approximately unity across the range of possible values of β_y meaning that the weak measurement description is a very good approximation. Secondly, we note that the most probable outcome of the double homodyne measurement is the imprinting of $\Im(n_W) = 0$ meaning that entanglement content is unchanged. Furthermore, outcomes which correspond to increasing or decreasing the shared entanglement by ever larger factors have ever small probability densities. Thus, the most probable imprinted weak values are those close to $\Im(n_W) = 0$. However, in spite of this behaviour, this protocol can still produce modest entanglement increases with a non-negligible probability density. For example, a 30% improvement of entanglement occurs with a probability density of $\rho(10^4, -0.8) \approx 0.15$.

5.3.3 Balanced homodyne scheme

In the scheme by us, *Menzies and Korolkova* (2006) [1], balanced Homodyne detection is employed by Bob, in other words, the post-selected state of the an-

cilla is the quadrature eigenstate $|x_\phi\rangle = |\Phi_2\rangle$ where $\hat{x}_\phi|x_\phi\rangle = x_\phi|x_\phi\rangle$ and $\hat{x}_\phi = 2^{-1/2}(e^{i\phi}\hat{a}^\dagger + e^{-i\phi}\hat{a})$. Once again, this protocol works because of the nature of the overlap between the pre- and post-selected states. In this case, we have [25]

$$\langle x_\phi|\alpha\rangle = \pi^{-1/4}\exp\left(-\frac{x_\phi^2}{2} + \sqrt{2}e^{-i\phi}x_\phi\alpha - \frac{e^{-2i\phi}\alpha^2}{2} - \frac{\alpha^2}{2}\right), \tag{5.50}$$

and so the weak value can be calculated to be

$$n_W = \sqrt{2}\alpha x_\phi\cos\phi + \alpha^2(\cos 2\phi - 1) - i(\sqrt{2}\alpha x_\phi\sin\phi - \alpha^2\sin 2\phi), \tag{5.51}$$

then the imaginary part of the weak value is

$$\Im(n_W) = \alpha\partial_\alpha\theta = -\sqrt{2}\alpha\sin\phi x_\phi + \alpha^2\sin(2\phi), \tag{5.52}$$

Hence, this means that only the measurement of certain quadrature observables are capable of inducing entanglement concentration since their eigenstates do not lead to an non-zero $\Im(n_W)$. This follows since different quadrature operators are labeled by the phase ϕ of the local oscillator in the homodyne measurement. The above condition allows us to determine which quadrature measurements which have the potential to allow entanglement concentration by restricting the possible values of ϕ. For example, any quadrature $\hat{x}_\phi$ specified by $\phi = (0, \pi, 2\pi)$ will not modify the entanglement as $\Im(n_W) = 0$. In particular, we note that choosing to measure the position quadrature $\hat{x}_0 = \hat{q}$ will only modify the phase of the TMSV and not the entanglement content. For those quadratures which do lead to a non-zero imaginary weak value, the selection criterion (5.21) translates to

$$\Im(n_W) > 0 \Leftrightarrow x_\phi < \sqrt{2}\alpha\cos\phi. \tag{5.53}$$

The fact that a number of quadrature operators satisfy the selection criterion immediately motivates the question of which one is optimal over the others. Our answer to this question is that the optimal quadrature measurement is the one which obtains a particular increase in entanglement with the highest probability density. In other words, for $\Delta\mathcal{S} = \mu$ with $\mu > 1$, what is the optimal ϕ which maximizes the probability density of achieving that increase? To calculate this, we first need the

probability density of obtaining a particular x_ϕ, from a measurement of $\hat{x}_\phi$ which is

$$\rho(x_\phi) = \frac{\exp\{-(x_\phi - \sqrt{2}\alpha\cos\phi)^2\}(1-\lambda^2)}{\sqrt{\pi}(1-\lambda^2 e^{2\kappa_T \Im(n_W)})} \tag{5.54}$$

meaning that for each configuration, the probability of success is approximately 50% as

$$\int_{-\infty}^{\sqrt{2}\alpha\cos\phi} dx_\phi\, \rho(x_\phi) \approx 0.5. \tag{5.55}$$

The relative increase in entanglement as a result of obtaining a result x_ϕ is then

$$\Delta\mathcal{S} = \frac{(1-\lambda^2)}{(1-\lambda^2 e^{2\kappa_T \Im(n_W)})} \times \left(\frac{2\lambda^2 e^{2\kappa_T \Im(n_W)} \ln(\lambda e^{\kappa_T \Im(n_W)}) + (1-\lambda^2 e^{2\kappa_T \Im(n_W)}) \ln(1-\lambda^2 e^{2\kappa_T \Im(n_W)})}{2\lambda^2 \ln\lambda + (1-\lambda^2)\ln(1-\lambda^2)}\right). \tag{5.56}$$

To proceed we need to solve the above for x_ϕ as a function of μ. Unfortunately, this is algebraically non-trivial. However, to over come this obstacle, we use a different, but equivalent entanglement measure derived from the linear entropy. The linear entropy is defined as

$$S_L(\hat{\rho}) = \mathrm{Tr}\left(\hat{\rho} - \hat{\rho}^2\right) = 1 - \mathrm{Tr}(\hat{\rho}^2), \tag{5.57}$$

and it is reasonably straight-forward to verify that this is also an entanglement measure. Indeed, the linear entropy is also used to quantify the disorder in a given density matrix $\hat{\rho}$ and can be consider as a linearized version of the Von Neumann entropy [9]. As a measure of entanglement, $\mathcal{R}(|\Psi\rangle\langle\Psi|) = (\mathcal{S}_L \circ \mathrm{Tr}_j)\,|\Psi\rangle\langle\Psi|$, it ranges between

$$0 \leq \mathcal{R}(|\Psi\rangle\langle\Psi|) \leq \left(1 - \frac{1}{K^2}\right), \tag{5.58}$$

where K is the dimension of the tensor product space and the lower bound occurs when $|\Psi\rangle$ is separable and the upper bound when $|\Psi\rangle$ is maximally entangled. Thus, for Gaussian continuous-variable states the bounds are $0 \leq \mathcal{R} \leq 1$. Furthermore, it is also a member of Shur's convex and preserves the majorization order [69]. We use it here since it has the advantage of being a polynomial in $\hat{\rho}$ rather than a logarithmic function and, hence, allows for an algebraic solution of our problem.

Thus, in this case we need to calculate $\Delta\mathcal{R} = \mathcal{R}_f/\mathcal{R}_i = \mu$ where

$$\mathcal{R}_i = 1 - \frac{(1-\lambda^2)^2}{1-\lambda^4}, \quad \mathcal{R}_f = 1 - \frac{(1-\lambda^2 e^{2\kappa_T \Im\{n_W(x_\phi)\}})^2}{(1-\lambda^4 e^{4\kappa_T \Im\{n_W(x_\phi)\}})} \tag{5.59}$$

and then solve $\Delta\mathcal{R} = \mu$ for x_ϕ, which, after some algebra, yields

$$x_\phi(\mu) = \sqrt{2}\alpha\cos\phi - \frac{\ln\left(\frac{\mu}{1+\lambda^2(1-\mu)}\right)}{2\sqrt{2}\alpha\kappa_T \sin\phi}. \tag{5.60}$$

The above equation describes the required measurement result that will give a μ factor improvement of the entanglement of the input state. The height of the probability density at $x_\phi(\mu)$ is then

$$\rho(x_\phi(\mu)) = \frac{(1-\lambda^2\mu+\lambda^4\mu-\lambda^4)}{\sqrt{\pi}(1-\lambda^2(2\mu-1))} \times \exp\left(-\frac{\ln\left(\frac{\mu}{1+\lambda^2(1-\mu)}\right)^2}{8\alpha^2\kappa_T^2\sin^2\phi}\right). \tag{5.61}$$

Thus, if all other parameters except ϕ are fixed then the optimal quadrature observable is the one which maximises the height of the probability density. It is immediately obvious from (5.61) that the optimal quadrature is $\phi = \pi/2$ or odd integer multiples of this and so, the quadrature measurements which obey $\phi = \pi/2$ are considered optimal.

The weakness conditions for this protocol is given as

$$\lambda^n\left(\frac{\langle x_\phi|e^{-i\kappa_T n\hat{n}_C}|\alpha\rangle}{\langle x_\phi|\alpha\rangle} - e^{-i\kappa_T n n_W}\right) \approx 0, \forall n \in [0,\infty). \tag{5.62}$$

This can be re-expressed as ($\forall\, n \in [0,\infty)$):

$$\lambda^n\left[\exp\left(\sqrt{2}\alpha x_\phi e^{-i\phi}(e^{-i\kappa_T n}-1) - \alpha^2 e^{-2i\phi}\frac{(e^{-2i\kappa_T n}-1)}{2}\right) - \exp\left(-i\kappa_T n\left\{\sqrt{2}x_\phi\alpha e^{-i\phi} - \alpha^2 e^{-2i\phi}\right\}\right)\right] \approx 0.$$

So, just as for the previous example, we see that (5.62) is equivalent to (5.45). Thus, both schemes require the balancing between the initial *Schmidt* coefficients and the magnitude of the non-linear coupling. To give a quantitative measure of the weakness conditions, we can numerically simulate the magnitude of their sum for physically realistic parameter values of $\alpha = 10^4$ and $\kappa_T = 2\times10^{-5}$. This magnitude

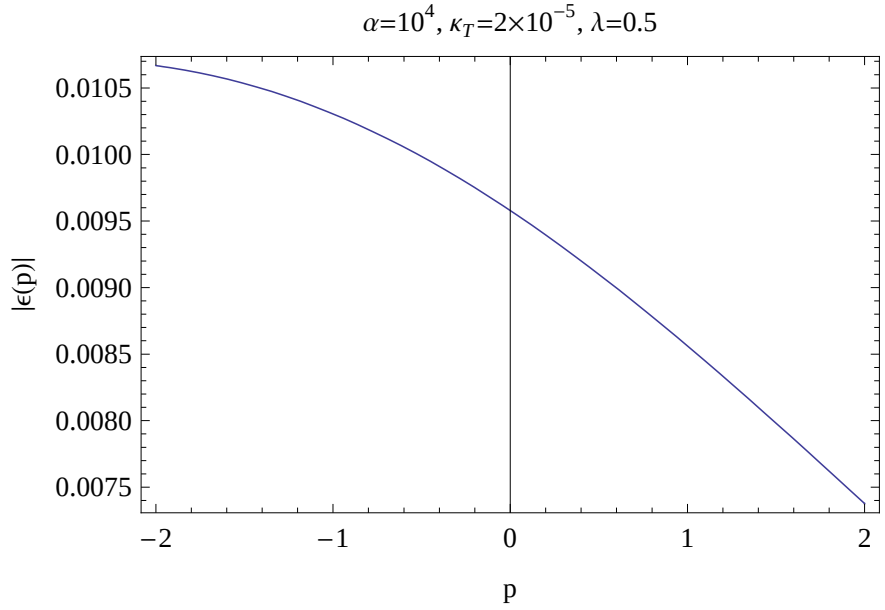

Figure 5.5: *Numerical simulation of the relevant quantities for the weak measurement where post-selection is provided by balanced homodyne detection with the phase quadrature selected.*

is defined as

$$\epsilon(x_\phi) = \left| \sum_{n=0}^{\infty} \lambda^n \left[\exp\left(\sqrt{2}\alpha x_\phi e^{-i\phi}(e^{-i\kappa_T n} - 1) - \alpha^2 e^{-2i\phi} \frac{(e^{-2i\kappa_T n} - 1)}{2} \right) \right. \right. \\ \left. \left. - \exp\left(-i\kappa_T n \left\{ \sqrt{2} x_\phi \alpha e^{-i\phi} - \alpha^2 e^{-2i\phi} \right\} \right) \right] \right|^2 \tag{5.63}$$

and is plotted in Fig. 5.5 for the case where the optimal phase quadrature $\hat{p}$ is measured. Examining Fig. 5.5, we note that the greatest value of this magnitude and, hence, the greatest deviation occurs in the region where $p \approx -2$. However, it is still a small number. Consequently, we can be assured that the weak measurement description of the protocol is a very good approximation.

The performance of the protocol for the optimal quadrature measurement can be gauged by numerically simulating the characteristic quantities that describe the protocol for physically realistic parameter values quoted above. In this case, we need to simulate the relative increase in entanglement defined by

$$\Delta\mathcal{S}(p) = \frac{(1-\lambda^2)}{(1-\lambda^2 e^{-2\sqrt{2}\kappa_T \alpha p})}$$

$$\times \left(\frac{2\lambda^2 e^{-2\sqrt{2}\kappa_T \alpha p} \ln(\lambda e^{-\sqrt{2}\kappa_T \alpha p}) + (1-\lambda^2 e^{-2\sqrt{2}\kappa_T \alpha p}) \ln(1-\lambda^2 e^{-2\sqrt{2}\kappa_T \alpha p})}{2\lambda^2 \ln \lambda + (1-\lambda^2)\ln(1-\lambda^2)} \right). \quad (5.64)$$

The fidelity between the final probe state in the weak regime and the final state produced in general is

$$\mathcal{F}(p) = \frac{(1-\lambda^2 e^{-2\sqrt{2}\kappa_T \alpha p})}{\sum_{n=0}^{\infty} \lambda^{2n} \left| e^{-i\sqrt{2}p\alpha(e^{-in\kappa_T}-1)+\frac{\alpha^2}{2}(e^{-2in\kappa_T}-1)} \right|^2}$$

$$\times \left| \sum_{n=0}^{\infty} \lambda^{2n} e^{in\kappa_T \alpha^2 - \sqrt{2}n\kappa_T \alpha p} \exp\left(-i\sqrt{2}p\alpha(e^{-in\kappa_T}-1) + \frac{\alpha^2}{2}(e^{-2in\kappa_T}-1) \right) \right|^2. \quad (5.65)$$

In Fig.5.6 we plot these quantities along with the probability density for obtaining p from the phase quadrature measurement

$$\rho(p, \kappa_T, \alpha) = \frac{e^{-p^2}(1-\lambda^2)}{\sqrt{\pi}(1-\lambda^2 e^{-2\sqrt{2}\kappa_T \alpha p})}. \quad (5.66)$$

Once again, we note the typical feature where the measurement outcomes that

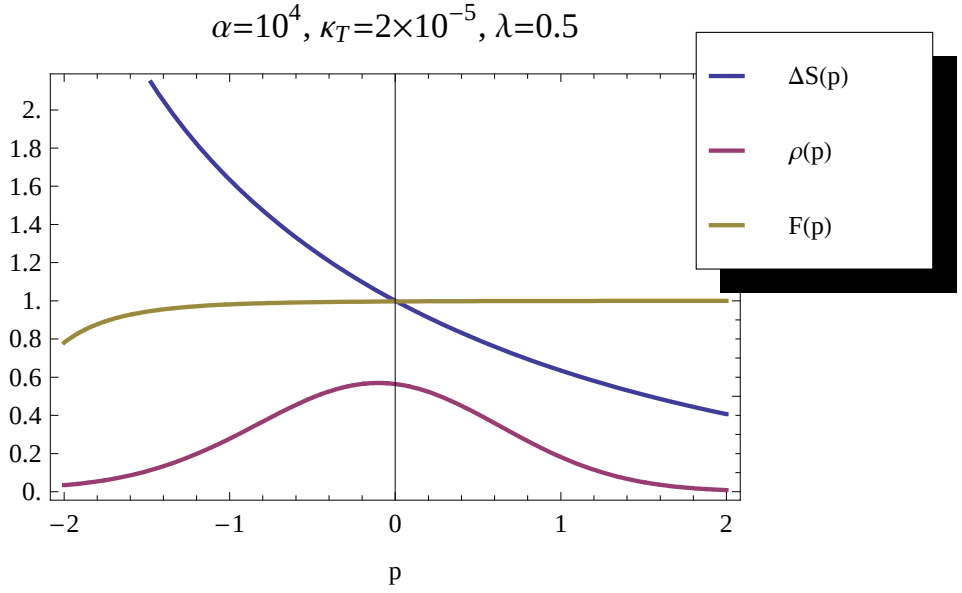

Figure 5.6: *Numerical simulation of the relevant quantities for the weak measurement where post-selection is provided by balanced homodyne detection with the phase quadrature selected.*

generate the greatest increase or decrease in the shared entanglement are the less probable than smaller increases or decreases. Thus, the probability distribution is

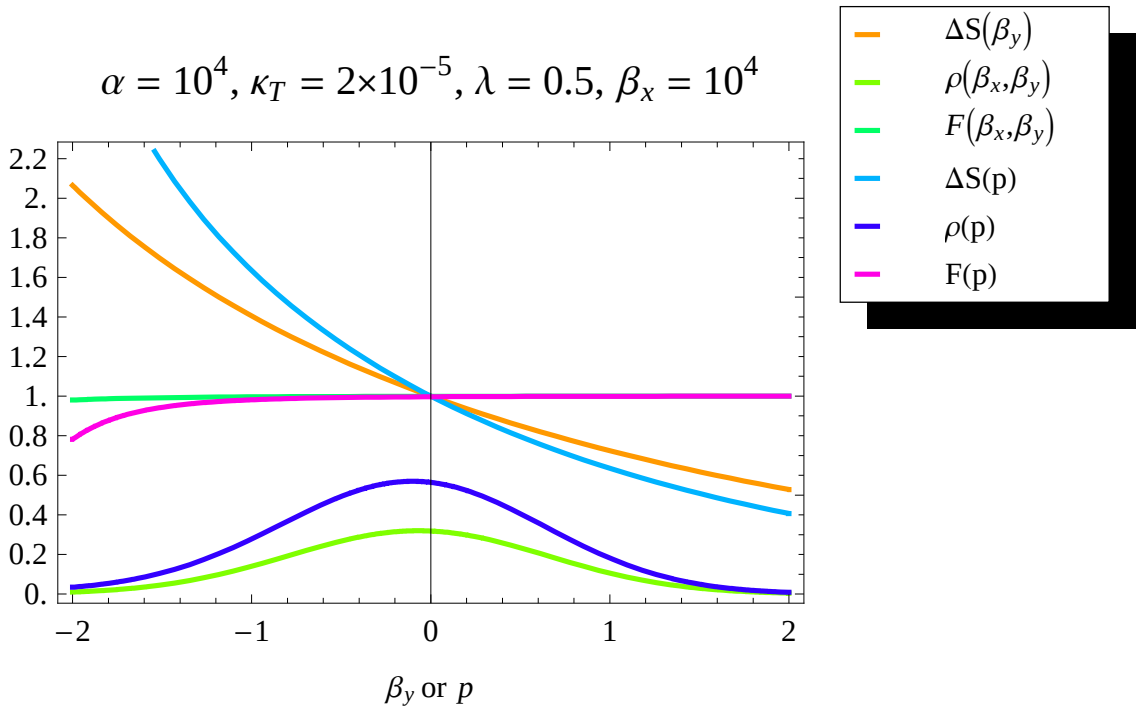

Figure 5.7: *A comparison between the performance of the double homodyne (solid lines) and balanced homodyne (measuring $\hat{p}$, dashed lines) working configurations. The fidelities, entanglement increases and probability densities are numerically compared for $\alpha = 10^4$ and $\kappa_T = 2 \times 10^{-5}$.*

symmetric around the origin i.e. around imprinting of a weak value with $\Im(n_W) = 0$. We also note that the fidelity is at its smallest when we are near the point $p = -2$ which suggests that the accuracy of the weak measurement formalism is reduced for huge increases in entanglement. This, however, is to be expected since the ultimate source of the increased entanglement is supplied by the interaction that couples the TMSV to the ancilla mode. Nevertheless, we note that we can obtain a 60% increase in the shared entanglement of $\lambda = 0.5$ if we encode the weak value labeled by $p = -1$. This outcome has a probability density of $\rho(-1) \approx 0.25$, meaning that 25% of the total runs of this protocol will result in the aforementioned increase.

It is interesting to compare the performance of this configuration with the earlier example. On a purely experimental note, we observe that the measurement of a

single quadrature in balanced homodyne as opposed to measuring two incompatible ones the double homodyne is more simple. However, the real comparison resides in the relative increase in entanglement for a particular probability density. This is the subject of Fig.5.7, where we compare the fidelities, entanglement increases and probability densities for each of these schemes assuming $\alpha = 10^4$ and $\kappa_T = 2 \times 10^5$. Note that we fix $\beta_x = 10^4$ in the former scheme since this is the most probable outcome related to the real part of the weak value and measure the phase quadrature in the latter since it proved to be optimal. It is clear from Fig.5.7 that the configuration involving the balanced homodyne measurement is superior to that of the double homodyne measurement since it is able to achieve larger relative increases in entanglement for equal or larger values of the probability density.

5.3.4 Squeezed vacuum post-selection scheme

To generate further examples, we simply need to identify further quantum optical states that satisfy $\partial_\alpha \theta(\alpha) > 0$. An immediate and obvious choice is given by selecting the post-selected state as a single mode squeezed vacuum $|\Phi_2\rangle = |re^{i\phi}\rangle$ since [25]

$$\langle re^{i\phi}|\alpha\rangle = \sqrt{\text{sech}r}\exp\left(-\frac{\alpha^2}{2}\{1 + e^{-i\phi}\tanh r\}\right). \tag{5.67}$$

In practice, we could realize such a post-selection by first anti-squeezing the signal state (following its interaction with the probe) by the desired amount and then subjecting the mode to a binary photo-detector. The post-selection is successful when the detector does not click and the POVM element corresponding to this post-selection is $\hat{\Pi}(re^{i\phi}) = \hat{S}(re^{i\phi})\hat{\Pi}_{noclick}\hat{S}^\dagger(re^{i\phi})$. In the event that this occurs the weak value, that is imprinted on the entangled state, is

$$n_W = -\alpha^2 \tanh r \cos\phi + i\alpha^2 \tanh r \sin\phi = -\alpha^2 e^{-i\phi}\tanh r. \tag{5.68}$$

Hence, in this example, the success condition (5.21) is

$$\Im(n_W) = \alpha^2 \tanh r \sin\phi > 0 \Leftrightarrow 0 < \phi < \pi/2. \tag{5.69}$$

In this case, since we can select the desired squeezing deterministically, the probability of success depends on the action of the binary photo-detector. That is, this

protocol will achieve entanglement concentration only when the detector doesn't click. This happens with a probability

$$P_S(r,\phi) = \frac{|\langle re^{i\phi}|\alpha\rangle|^2(1-\lambda^2)}{(1-\lambda^2 e^{2\kappa_T\alpha^2\sinh r\sin\phi})} = \frac{\mathrm{sech}r\; e^{-\alpha^2(1+\cos\phi\tanh r)}(1-\lambda^2)}{(1-\lambda^2 e^{2\kappa_T\alpha^2\sinh r\sin\phi})}. \tag{5.70}$$

This equation is enough to demonstrate that this particular configuration has a very poor efficiency. This fact is evident since a large α is required to compensate for a weak coupling κ_T to ensure a non-negligible modification factor $\exp(\kappa_T\alpha^2\sinh r\sin\phi)$, since $\sin\phi\tanh r < 1$ for all squeezed vacuum post-selections. However, having a large α in the pre-selected state $|\alpha\rangle$ means that the post-selection on $|re^{i\phi}\rangle$ only occurs with a very small probability. Ultimately, this is because the larger α the less likely that the binary photo-detector will not detect the presence of photons. Thus, this protocol requires a much larger coupling than the previous examples. This will be evident in the following numerical simulations.

The weak condition is expressed as

$$\lambda^n\left(\frac{\langle re^{i\phi}|e^{-i\kappa_T n\hat{n}_C}|\alpha\rangle}{\langle re^{i\phi}|\alpha\rangle} - e^{-i\kappa_T n n_W}\right) \approx 0, \quad \forall n\in[0,\infty), \tag{5.71}$$

where the first term on the LHS is $\exp\left(-\frac{\alpha^2}{2}\{e^{-2in\kappa_T}-1\}e^{-i\phi}\tanh r\right)$ and the second is $\exp\left(i\kappa_T n\alpha^2 e^{-i\phi}\tanh r\right)$. Clearly (5.71) can only be satisfied if $\kappa_T n << 1$. Note that for large n, (5.71) holds because $\lambda^n \to 1$. Once again we can probe this numerically by first considering the magnitude of the sum of the weak conditions

$$\epsilon(r,\phi) = \left|\lambda^n\left\{\exp\left(-\frac{\alpha^2}{2}\{e^{-2in\kappa_T}-1\}e^{-i\phi}\tanh r\right) - e^{i\kappa_T n\alpha^2 e^{-i\phi}\tanh r}\right\}\right|^2 \tag{5.72}$$

and the fidelity for this configuration is then

$$\begin{aligned}\mathcal{F}(r,\phi) = {} & \frac{1-\lambda^2 e^{2\kappa_T\alpha^2\tanh r\sin\phi}}{\sum_{n=0}^{\infty}\lambda^{2n}|\exp\left(-\frac{\alpha^2}{2}\{e^{-2in\kappa_T}-1\}e^{-i\phi}\tanh r\right)|^2} \\ \times & \left|\sum_{n=0}^{\infty}\lambda^{2n}e^{-i\kappa_T n\alpha^2 e^{i\phi}\tanh r}\exp\left(-\frac{\alpha^2}{2}\{e^{-2in\kappa_T}-1\}e^{-i\phi}\tanh r\right)\right|^2.\end{aligned} \tag{5.73}$$

In addition, the relative increase in entanglement is then given by

$$\begin{aligned}\Delta\mathcal{S}(r,\phi) = {} & \frac{(1-\lambda^2)}{(1-\lambda^2 e^{2\kappa_T\alpha^2\tanh r\sin\phi})}\frac{2\lambda^2 e^{2\kappa_T\alpha^2\tanh r\sin\phi}\ln(\lambda e^{\kappa_T\alpha^2\tanh r\sin\phi})}{(2\lambda^2\ln\lambda+(1-\lambda^2)\ln(1-\lambda^2))} \\ & + \frac{(1-\lambda^2)\ln(1-\lambda^2 e^{2\kappa_T\alpha^2\tanh r\sin\phi}))}{(2\lambda^2\ln\lambda+(1-\lambda^2)\ln(1-\lambda^2))},\end{aligned} \tag{5.74}$$

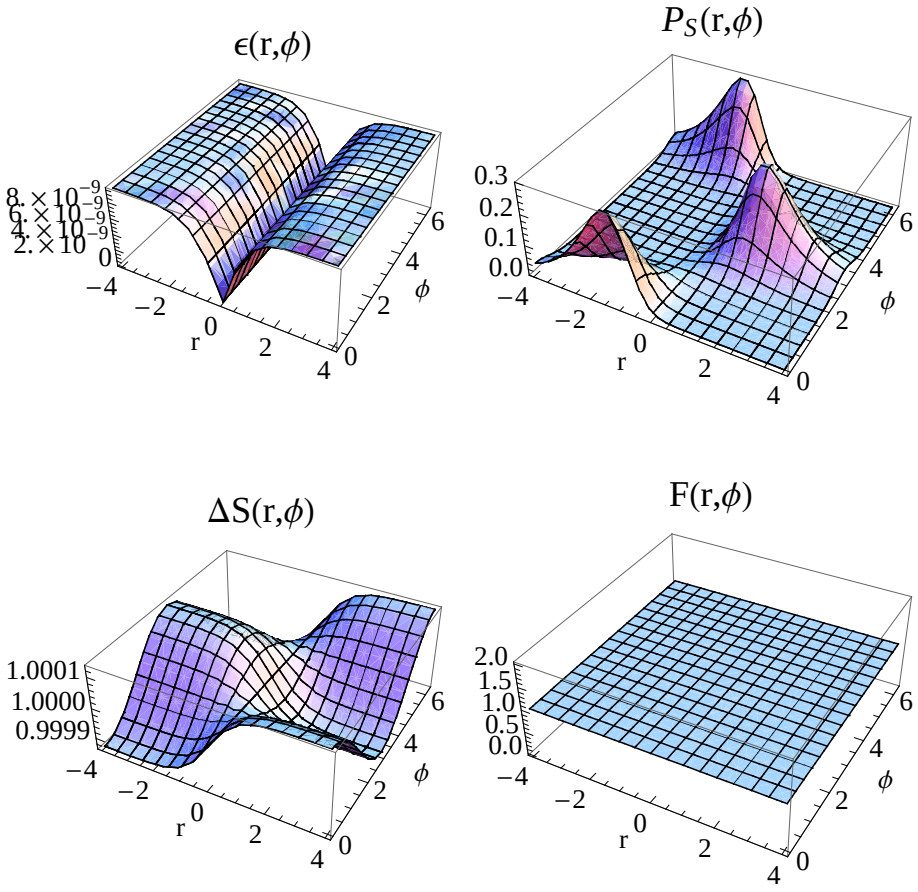

Figure 5.8: *The performance of the squeezed vacuum post-selection configuration can be determined by considering the magnitude of the weakness conditions, the probability of success of the protocol, the relative entanglement increase and the fidelity between the possible output states. The figures are plotted from the parameter values* $\alpha = 2$, $\lambda = 0.5$ *and* $\kappa_T = 2 \times 10^{-5}$.

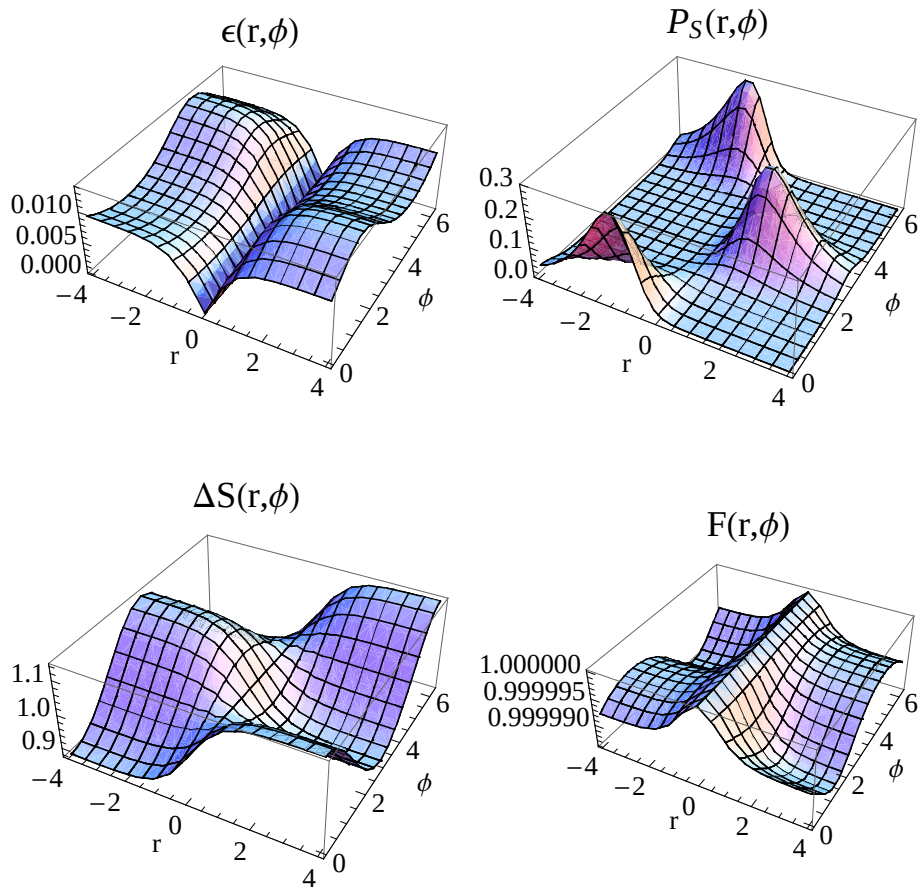

Figure 5.9: *The performance of the squeezed vacuum post-selection configuration can be determined by considering the magnitude of the weakness conditions, the probability of success of the protocol, the relative entanglement increase and the fidelity between the possible output states. The figures are plotted from the parameter values* $\alpha = 2$, $\lambda = 0.5$ *and* $\kappa_T = 2 \times 10^{-2}$.

All of these quantities are plotted in Fig.5.8 and Fig.5.9 for the parameter values $\alpha = 2$, $\lambda = 0.5$ and $\kappa_T = 2\times10^{-5}$ and $\alpha = 2$, $\lambda = 0.5$ and $\kappa_T = 2\times10^{-2}$, respectively. Fig.5.8 illustrates the point that the performance of this protocol is very poor for very weak coupling κ_T, since α can only be increased at the expense of the probability of success. Moreover, we note that in the regions where there is an increase in entanglement, the probability of success is zero. Clearly, the performance of this protocol forbids it from being a serious contender for entanglement concentration. From Fig.5.9, we can observe a more desirable increase in entanglement when the coupling is $\kappa_T = 2\times10^{-2}$, however, once again this occurs with a very low probability.

5.3.5 Experimental feasibility of all optical schemes

The experimental feasibility of these optical weak measurement schemes is primarily constrained by the magnitude of the coupling constant κ_T. Ultimately, this is because generating the cross-Kerr effect between two radiation modes even weakly is an extremely challenging prospect. For example, if we used 1 m of a micro-structured fibre to provide the non-linear interaction together with a $10fs$ pulsed coherent beam with average power 1mW and repetition rate 80 μHz for the ancillary state, then it is possible, in principle, to achieve $\kappa_T \approx 10^{-9}$ rad per photon [116]. To compensate for this tiny nonlinear coupling would require an ancilla with $\alpha \approx 10^8$ to achieve the previous mentioned performances shown in Fig.5.7. However, preparing the ancilla with $\alpha \approx 10^8$ is completely unrealistic with current technology and would likely damage the non-linear medium.

Alternatively, one could use the large cross-Kerr effect manifest in atomic Rubidium [113, 114], which can yield the $\kappa_T \approx 10^{-5}$ rad per photon required by our simulations. While achieving this coupling could prove feasible, one must also consider the various sources of decoherence that can spoil the entanglement. These include absorption by the atomic medium and a scrambling of the phase reference of the interacting light fields. Moreover, such effects have only been experimentally demonstrated for classical light fields and not for quantum states and there

is some debate whether even a weak cross-Kerr effect suitable for quantum information protocols can be achieved [51, 117–119]. Thus, a more realistic version of this entanglement concentration model could be done by taking these sources of decoherence in account and including sources of decoherence in the measurement strategies employed in each configuration.

5.4 Concluding remarks and open problems

In this chapter, we have highlighted the utility of adopting an operational viewpoint of weak values and demonstrated how this viewpoint can be used to understand a family of entanglement concentration protocols. However, there remain a number of open problems and future lines of investigation to explore. Firstly, in the case of entanglement concentration of the TMSV, it would be interesting to know how we select the optimal weak measurement configuration out of all the working possibilities. Our work only allows the identification of working configurations, but leaves the question of optimization unanswered. This could prove to be challenging since different operators and pre and post-selected states could generate the same weak value. Thus, a weak value may not correspond to an unique set of ingredients.

A second interesting question resides in the observation that the mechanism underlying this weak measurement induced entanglement concentration is the noiseless amplification of photon number. Thus, the average number of photons in shared entangled state is either increased or decreased depending on the weak value encoded on the state. In particular, it is interesting that the number of photons is amplified without changing the purity of the entangled state i.e. without inducing noise onto the state. It is therefore an intriguing question to determine whether this mechanism can be put to use on other continuous-variable quantum optical information protocols. Finally, it is equally interesting to understand whether the connection between weak measurements and entanglement concentration extends beyond Gaussian entangled states to arbitrary pure bipartite entangled states. In particular, is there a deeper connection between weak measurements and entanglement? We consider

these issues in the following chapter.

Chapter 6

Weak measurements and state engineering

In this chapter we build on the utility of weak measurements by demonstrating that they have applications beyond Gaussian entanglement concentration. In particular, we show how they can be used to realize noiseless amplification of photon number on a set of quantum states that satisfy the associated weakness conditions. In addition, we uncover a deeper connection between weak measurements and Procrustean entanglement concentration, where we show that a weak measurement on an entangled probe can lead to an entanglement concentration effect.

6.1 Weak noiseless amplification

6.1.1 Non-physical nature of noiseless amplification

The previous weak measurement entanglement concentration protocol can actually be regarded as an example of a weak measurement allowing the probabilistic noiseless amplification of photon number. Being able to implement such an operation, albeit on a subset of states, has a number of possible applications in state engineering and quantum information in general. Our work here can be considered as an alternative means of achieving noiseless amplification to the method suggested in [120].

Noiseless amplification of the photon number in a given state $\hat{\rho}$ is performed via the abstract operation $\hat{\Gamma}(r) = c\, r^{\hat{n}}$, where $r > 1$ and c is a constant related to the probability of occurrence. Such an operation does not preserve probabilities $\langle\psi|\psi\rangle \neq \langle\psi|\hat{\Gamma}^{\dagger}(r)\hat{\Gamma}(r)|\psi\rangle$ and cannot be achieved by a local unitary transformation [121]. In particular, as shown in [120], assuming that noiseless amplification can be achieved by an unitary transformation leads to a contradiction as the commutation relation between the mode operators is not preserved. In addition, we now provide a novel argument that demonstrates that this operation cannot be performed by a generalised measurement as described by a POVM measurement. To do this we recall the definition of a POVM as a set of operators $\{\hat{\Pi}_{\omega}\}_{\omega\in\Omega}$ that obey

$$\sum_{\omega\in\Omega}\hat{\Pi}_{\omega} = \hat{I}, \;\; \langle\hat{\Pi}_{\omega}\rangle \geq 0, \;\; \hat{\Pi}_{\omega}^{\dagger} = \hat{\Pi}_{\omega}. \tag{6.1}$$

where Ω is the set of all possible distinguishable outcomes of the measurement with each outcome labeled by ω, which can be either a discrete or continuous index. If the latter is true then we need to replace all the summations with integrals. The probability of obtaining the ω outcome on a state $\hat{\rho}$ is given by $P_{\omega} = \mathrm{Tr}(\hat{\Pi}_{\omega}\hat{\rho})$. To define the state transformation law that accompanies each outcome requires the introduction of the associated Kraus operators for each POVM element [9]. These are defined by $\hat{\Pi}_{\omega} = \hat{A}_{\omega}^{\dagger}\hat{A}_{\omega}$ and consequently, the projection postulate for a pure state $|\psi\rangle$ when ω is measured is [9]

$$|\psi\rangle \rightarrow \frac{\hat{A}_{\omega}|\psi\rangle}{\sqrt{\langle\psi|\hat{A}_{\omega}^{\dagger}\hat{A}_{\omega}|\psi\rangle}}, \tag{6.2}$$

and the corresponding equation for a general state $\hat{\rho}$ is [9]

$$\hat{\rho} \rightarrow \frac{\hat{A}_{\omega}\hat{\rho}\hat{A}_{\omega}^{\dagger}}{\mathrm{Tr}(\hat{\rho}\hat{A}_{\omega}^{\dagger}\hat{A}_{\omega})}. \tag{6.3}$$

To demonstrate that noiseless amplification cannot be achieved even by a POVM measurement requires framing the $\hat{\Gamma}(r)$ operation in the language of POVMs. Firstly, we identify $\hat{A}_1(r) = c\, r^{\hat{n}}$ and $\hat{A}_2(r) = (\hat{I} - c\, r^{2\hat{n}})^{-1/2}$ as the Kraus operators for the set of operators $\mathbf{\Pi}_z = \{\hat{\Pi}_1, \hat{\Pi}_2\}$ where

$$\hat{\Pi}_1 = \hat{A}_1^{\dagger}(r)\hat{A}_1(r) = |c|^2 r^{2\hat{n}}, \quad \hat{\Pi}_2 = \hat{A}_2^{\dagger}(r)\hat{A}_2(r) = \hat{I} - |c|^2 r^{2\hat{n}}. \tag{6.4}$$

Where c is an arbitrary constant related to the probability of applying the $\hat{A}_1(r)$. Clearly, these measurement operators obey the resolution of the identity with

$$\hat{\Pi}_1 + \hat{\Pi}_2 = |c|^2 r^{2\hat{n}} + \hat{I} - |c|^2 r^{2\hat{n}} = \hat{I}, \tag{6.5}$$

and they are also obviously Hermitian. However, for $r > 1$ as required for amplification, they do not obey the positivity requirement since for arbitrary $|\psi\rangle = \sum_{n=0}^{\infty} \psi_n |n\rangle$ we get

$$\langle\psi|\hat{\Pi}_1|\psi\rangle = |c|^2 \sum_{n=0}^{\infty} |\psi_n|^2 r^{2n} \geq 0, \quad r > 1. \tag{6.6}$$

However,

$$\langle\psi|\hat{\Pi}_2|\psi\rangle = \sum_{n=0}^{\infty} (1^n - |c|^2 r^{2n}) |\psi_n|^2, \tag{6.7}$$

Thus, the above is only positive if $(1^n - |c|^2 r^{2n})|\psi_n|^2 > 0$ for all $n \in [0, \infty)$, i.e. $|c|^2 < r^{-2n}$ for all $n \in [0, \infty)$. Consequently, the only way this constraint can be satisfied for arbitrary states is if $|c|^2 = 0$, i.e. it can only occur in the trivial case of vanishing probability of success. Thus, noiseless amplification only obeys the axioms of a POVM in the trivial case but is otherwise nonphysical because it leads to the possibility of negative probabilities.

Given this general argument against the probabilistic realisation of noiseless amplification, why can it be achieved via either weak measurements is demonstrated in the previous chapter or in the alternative scheme suggested in [120]? In the first case, the latter scheme is consistent because it only approximates $\hat{\Pi}_1$ by introducing a high-energy cut off. This means that they generate the operator $\hat{\Pi}_1(N) = |c|^2 \sum_{n=0}^{N} r^{2n} |n\rangle\langle n|$ which allows amplification since the previous constraint becomes $|c|^2 < r^{-2n}$ for all $n \in [0, N]$, which is satisfied by selecting $|c|^2 < r^{-2N}$. Consequently, they truncate their input state before performing noiseless amplification on this subspace to approximate their desired amplified output. The weak measurement model is also consistent with this constraint since it doesn't hold for arbitrary input states instead it is only valid for a certain subset of states. These states are ones with negligible support for very large photon numbers n and thus behave as though they are effectively truncated. Thus, the weak measurement induced

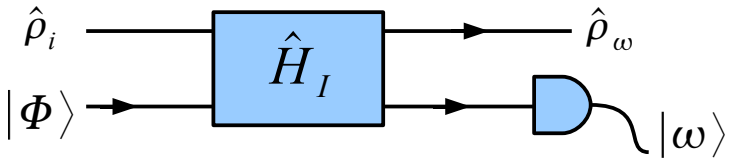

Figure 6.1: *The probe system (at the top) is used to encode the weak value of the pre and post-selected system. Each individual run corresponds to imprinting a different weak value since the each measurement results in a different post-selected state.*

noiseless amplification satisfies the POVM axioms on a reduced set of states that obey the weakness conditions and not on arbitrary states. We explore this next.

6.1.2 Weak probabilistic noiseless amplification

Our weak measurement model is based on the following configuration where, as depicted in Fig.6.1, the probe state in mode A is coupled to an ancilla state in mode B by means of a unitary evolution between A and B. The requirements of noiseless amplification dictate that the interaction Hamiltonian describing this process must be of the form $\hat{H}_I = \hbar\kappa(t)\hat{n}\hat{O}$. Assuming the interaction persists for T seconds, then the corresponding unitary evolution operator is $\hat{U} = e^{-i\int_0^T \kappa(t)\hat{n}\hat{O}} = e^{-i\kappa_T\hat{n}\hat{O}}$, where $\kappa_T = \kappa(T) - \kappa(0)$.

Consequently, following the evolution the ancilla is subjected to a measurement with outcome ω corresponding to a projection of $|\omega\rangle\langle\omega|$. Thus, the final state is

$$\hat{\rho}_\omega \propto \mathrm{Tr}_B\left(\{\hat{I}_A \otimes |\omega\rangle\langle\omega|\}e^{-i\kappa_T\hat{n}\hat{O}}(\hat{\rho}_i \otimes |\Phi\rangle\langle\Phi|)e^{i\kappa_T\hat{n}\hat{O}}\right),$$

and so $\hat{\rho}_\omega \propto \langle\omega|e^{-i\kappa_T\hat{n}\hat{O}}|\Phi\rangle\hat{\rho}_i\langle\Phi|e^{i\kappa_T\hat{n}\hat{O}}|\omega\rangle/|\langle\Phi|\omega\rangle|^2$. Expanding the exponential yields

$$\hat{\rho}_\omega \propto \sum_{m=0}^{\infty}\sum_{\ell=0}^{\infty}\frac{(-i\kappa_T)^m}{m!}\frac{(i\kappa_T)^\ell}{\ell!}\frac{\langle\omega|\hat{O}^m|\Phi\rangle}{\langle\omega|\Phi\rangle}\frac{\langle\Phi|\hat{O}^\ell|\omega\rangle}{\langle\Phi|\omega\rangle}\hat{n}^m\hat{\rho}_i\hat{n}^\ell.$$

This can then be rewritten as

$$\hat{\rho}_\omega = \mathcal{N}\left(e^{-i\kappa_T O_W(\omega)\hat{n}} + \hat{\epsilon}\right)\hat{\rho}_i\left(e^{i\kappa_T O_W^*(\omega)\hat{n}} + \hat{\epsilon}^\dagger\right), \tag{6.8}$$

where the weak value $O_W(\omega) = \langle\omega|\hat{O}|\Phi\rangle/\langle\omega|\Phi\rangle$ is imprinted on the probe provided $\hat{\epsilon}\hat{\rho}_i \approx 0 \cdot \hat{A}$ with $\hat{A}$ arbitrary, i.e.

$$\hat{\epsilon}\hat{\rho}_i = \left(\frac{\langle\omega|e^{-i\kappa_T \hat{n}\hat{O}}|\Phi\rangle}{\langle\omega|\Phi\rangle} - e^{-i\kappa_T O_W(\omega)\hat{n}} \right) \hat{\rho}_i \approx 0 \cdot \hat{A}. \tag{6.9}$$

Furthermore, by expanding $\hat{\rho}_i = \sum_k p_k |\psi_k\rangle\langle\psi_k|$ we note that (6.9) is equivalent to

$$\sum_{m=0}^{\infty} \sum_k p_k \left(\frac{\langle\omega|e^{-i\kappa_T m\hat{O}}|\Phi\rangle}{\langle\omega|\Phi\rangle} - e^{-i\kappa_T O_W(\omega)m} \right) \langle m|\psi_k\rangle|m\rangle \approx 0 \cdot |\phi\rangle, \tag{6.10}$$

for an arbitrary vector $|\phi\rangle$. The linear independence of the Fock basis allows (6.10) to be expressed as an infinite set of equations

$$\sum_k p_k \left(\frac{\langle\omega|e^{-i\kappa_T m\hat{O}}|\Phi\rangle}{\langle\omega|\Phi\rangle} - e^{-i\kappa_T O_W(\omega)m} \right) \langle m|\psi_k\rangle \approx 0, \tag{6.11}$$

$\forall m \in [0, \infty)$ are the weakness conditions. Satisfying these conditions for small m is automatic provided that the coupling between signal and probe is weak $\kappa_T << 1$. These conditions can still be satisfied provided $\sum_k p_k \langle m|\psi_k\rangle \approx 0$ for large or intermediate m. Thus, the imprinting of the weak value $O_W(\omega)$ on the probe is only valid in the limit of weak coupling and for certain probe states.

Assuming such conditions are approximately true assumes that we are operating in the weak regime and the post measurement probe state becomes

$$\hat{\rho}_\omega = \frac{e^{-i\kappa_T O_W(\omega)\hat{n}} \hat{\rho}_i e^{i\kappa_T O_W^*(\omega)\hat{n}}}{\mathrm{Tr}(e^{2\kappa_T \Im\{O_W(\omega)\}} \hat{\rho}_i)}. \tag{6.12}$$

This transformation has two components corresponding to imprinting different parts of the weak value $O_W(\omega)$ onto the probe state. On the one hand, the imprinting of $\Re\{O_W(\omega)\}$ is done by a unitary transformation $e^{-i\kappa_T \Re\{O_W(\omega)\}\hat{n}}$ imparting a phase shift on the probe state. On the other, the imprinting of $\Im\{O_W(\omega)\}$ is done via the operator $e^{\kappa_T \Im\{O_W(\omega)\}\hat{n}}$. It is this transformation that allows the conditional realisation of noiseless amplification on the state with $r = e^{\kappa_T \Im\{O_W(\omega)\}}$. Consequently, noiseless amplification occurs when $r > 1 \implies \Im\{O_W(\omega)\} > 0$. Thus, the imprinting of a positive imaginary part of a weak value will lead to an increase in the average number of photons and, hence, achieve a noiseless amplification effect.

The condition $\Im\{O_W(\omega)\} > 0$ can be used as a selection criterion to pick out particular ancilla configurations including the pre-selected state $|\Phi\rangle$, interaction Hamiltonian $\hat{H}_I = \kappa\hbar\hat{n}\hat{O}$, and measurement strategy that projects onto different $|\omega\rangle\langle\omega|$. It is this universality that is the true power of the weak measurement approach; It allows this amplification effect to occur for a wide range of physical ancilla systems and interactions. Ultimately, this effect is probabilistic since only a subset of all measurement outcomes ω company a weak value such that $\Im\{O_W(\omega)\} > 0$. Accordingly, this protocol has a measurement based success condition which tells us whether a weak value with a positive imaginary component has been encoded on the probe state. This condition follows from the earlier identical argument in chapter 5. Thus, there are two possibilities either $\Im\{O_W(\omega)\} = 0$ for all $\omega \in \Omega$, which is trivial or $\exists\omega \in \Omega^+$ such that $\Im\{O_W(\omega)\} > 0$ and $\exists\omega \in \Omega^-$ such that $\Im\{O_W(\omega)\} < 0$.

This latter possibility demonstrates the manifestation of a measurement based success condition linking the measurement outcome on the ancilla with the properties of the imaginary part of the imprinted weak value. Consequently, one can formulate a probability of success with this protocol that is directly related to the probability of obtaining a particular ω. This probability emerges from

$$P(\omega) = \mathrm{Tr}\left(\{\hat{I}_A \otimes |\omega\rangle\langle\omega|\}e^{-i\kappa_T\hat{n}\hat{O}}(\hat{\rho}_i \otimes |\Phi\rangle\langle\Phi|)e^{i\kappa_T\hat{n}\hat{O}}\right),$$

which becomes in the weak regime

$$P(\omega) = |\langle\omega|\Phi\rangle|^2\mathrm{Tr}\left(e^{2\kappa_T\Im\{O_W(\omega)\}\hat{n}}\hat{\rho}_i\right), \tag{6.13}$$

and so the probability of success of the noiseless amplification is

$$P_S = \sum_{\omega\in\Omega^+} P(\omega), \tag{6.14}$$

and the probability of failure $P_F = 1 - P_S = \sum_{\omega\in\Omega^-} P(\omega)$. Accordingly, any attempt to optimize the amplification will need to consider the optimization of (6.14).

We are still faced with the question of accuracy of our model, i.e. for a given initial probe state how accurate is the weak measurement model when compared to the general predictions of quantum mechanics. We propose to measure this accuracy

via the fidelity of the two final probe states, one in the weak regime and the other as the general output state predicted by quantum mechanics. That is, we consider the fidelity between $\hat{\rho}_\omega$ as defined in (6.12) and the final probe state in general given by

$$\hat{\rho}_\omega^{(G)} = \frac{\langle\omega|e^{-i\kappa_T\hat{n}\hat{O}}|\Phi\rangle\hat{\rho}_i\langle\Phi|e^{i\kappa_T\hat{n}\hat{O}}|\omega\rangle}{\mathrm{Tr}\left(\langle\omega|e^{-i\kappa_T\hat{n}\hat{O}}|\Phi\rangle\hat{\rho}_i\langle\Phi|e^{i\kappa_T\hat{n}\hat{O}}|\omega\rangle\right)}. \tag{6.15}$$

Thus, we use the fidelity $\mathcal{F}(\hat{\rho}_\omega, \hat{\rho}_\omega^{(G)}) = (\mathrm{Tr}\sqrt{\hat{\rho}_\omega^{1/2}\hat{\rho}_\omega^{(G)}\hat{\rho}_\omega^{1/2}})^2$ as measuring the accuracy of the predictions from the weak measurement model for a particular state $\hat{\rho}_i$ and coupling strength κ_T. Consequently, this can be interpreted as measuring the degree of violation of the aforementioned weakness conditions: the greater the deviation then the smaller the fidelity.

Finally, we can show that this weak measurement obeys the axioms of a POVM only for states which satisfy the weakness conditions derived above. With this in mind we identify the $\hat{A}_\omega = \langle\omega|\Phi\rangle e^{-i\kappa_T O_W(\omega)\hat{n}}$ as the associated Kraus operators and

$$\hat{\Pi}(\omega) = \hat{A}_\omega^\dagger\hat{A}_\omega = |\langle\omega|\Phi\rangle|^2 e^{2\kappa_T\Im(O_W(\omega))\hat{n}} \tag{6.16}$$

as the corresponding POVM elements. However, these can only be regarded as POVM elements on the set of states which obey the weakness conditions. Thus, let $\hat{\rho}$ be such a state then by definition, the $\hat{\Pi}_\omega$ are Hermitian and the resolution of the identity follows from the substitution of the weakness relations:

$$\sum_\omega \hat{\Pi}_\omega\hat{\rho} = \sum_\omega |\langle\omega|\Phi\rangle|^2 e^{2\kappa_T\Im(O_W(\omega))\hat{n}}\hat{\rho} \approx \sum_\omega \langle\omega|e^{-i\kappa_T\hat{O}\hat{n}}|\Phi\rangle\langle\Phi|e^{i\kappa_T\hat{O}\hat{n}}|\omega\rangle\hat{\rho} = \hat{I}\hat{\rho}.$$

While the positivity of the POVM elements is satisfied in

$$\mathrm{Tr}\left(|\langle\omega|\Phi\rangle|^2 e^{2\kappa_T\Im(O_W(\omega))\hat{n}}\hat{\rho}\right) \approx \sum_{n=0}^{\infty}\left|\langle\omega|e^{-i\kappa_T\hat{O}n}|\Phi\rangle\right|^2\rho_{nn} \geq 0, \quad \forall\omega\in\Omega, \tag{6.17}$$

which follows since $|\langle\omega|e^{-i\kappa_T\hat{O}n}|\Phi\rangle|^2$ is positive for all measurement outcomes ω. Thus, the weak measurement is a POVM on a subset of states that approximately satisfy the weakness conditions.

6.1.3 Applications

Our weak measurement model of a probabilistic noiseless photon number amplifier has a number of potential uses in a diverse range of quantum information protocols. This is in spite of the restrictions that need to be observed to grant the weak regime validity. We now consider a number of applications of this model beginning with the previously known application to entanglement concentration.

Gaussian entanglement concentration

This result was explicitly considered in [2] and in the last chapter for the two-mode squeezed vacuum state $|\zeta(\lambda)\rangle = \sqrt{1-\lambda^2}\sum_{n=0}^{\infty}\lambda^n|n,n\rangle$ where the weak measurement allowed the probabilistic transformation

$$\lambda \to \lambda e^{i\kappa_T \Re\{O_W(\omega)\}} e^{\kappa_T \Im\{O_W(\omega)\}}. \tag{6.18}$$

Consequently, the imprinting of $\Im\{O_W(\omega)\}$ leads to Gaussian-preserving entanglement concentration provided $\Im\{O_W(\omega)\} > 0$. The probability of obtaining a particular ω is given by

$$P(\omega) = \frac{(1-\lambda^2)|\langle\omega|\Phi\rangle|^2}{1-\lambda^2 e^{2\kappa_T \Im\{O_W(\omega)\}}}, \tag{6.19}$$

and the efficiency of this protocol can be measured by comparing the probabilities $P(\omega)$ with respect to a particular increase in entanglement $\Delta\mathcal{S}$.

Growing Schrödinger kittens

Noiseless amplification is also useful for amplifying Schrödinger cat states with $|\alpha| < 1$, i.e. the so-called Schrödinger kitten states [59]. Consider the case where the probe state is the kitten state $|\psi_+(\beta)\rangle = \mathcal{N}(|\beta\rangle + |-\beta\rangle)$, then the weak measurement induces the transformation $\beta \to \beta e^{-i\kappa_T O_W}$ meaning that the final probe state is $|\psi_+(\beta e^{-i\kappa_T O_W})\rangle \propto |\beta e^{-i\kappa_T O_W}\rangle + |-\beta e^{-i\kappa_T O_W}\rangle$. The probe state is rotated in an amount depending on the real part of the weak value and is amplified by an amount dependant on the imaginary part. Thus, the size of the cat state is increased if $\Im(O_W) > 0$. The probability (or probability density) of obtaining a particular ω

with a corresponding weak value $O_W(\omega)$ is

$$P(\omega) = \frac{|\langle\omega|\Phi\rangle|^2 \cosh\left(|\beta|^2 e^{2\kappa_T \Im(O_W(\omega))}\right)}{\cosh|\beta|^2}, \tag{6.20}$$

and the amplitude factor $g = e^{\kappa_T \Im(O_W(\omega))}$ can be used as a figure of merit and the accuracy can be measured by the fidelity $\mathcal{F}$ between the general result and the weak measurement result.

Following the analysis in [2] and in the previous chapter, we consider the efficiency of this protocol in an all optical setting configuration using the cross-Kerr effect $\hat{H}_I = \kappa\hbar\hat{n}_A\hat{n}_B$ with an ancilla coherent state $|\alpha \in \Re\rangle$ followed by a measurement strategy that projects onto $|\omega\rangle$. In this case, as noted in [2], we are interested in the weak values of the number operator $\hat{n}_B$ which can be written as

$$n_W = \frac{\langle\omega|\hat{n}|\alpha\rangle}{\langle\omega|\alpha\rangle} = \alpha^2 + \frac{\alpha}{R_\omega(\alpha)}\frac{\partial R_\omega}{\partial\alpha} + i\alpha\frac{\partial\theta_\omega}{\partial\alpha}, \tag{6.21}$$

with $\langle\omega|\alpha\rangle = R_\omega(\alpha)e^{i\theta_\omega(\alpha)}$ [2]. Thus, only measurement strategies that allow

$$\alpha\frac{\partial\theta_\omega(\alpha)}{\partial\alpha} > 0, \tag{6.22}$$

for a subset of possible values $\omega \in \Omega_+$, have the potential to achieve the desired effect. Such a measurement basis was identified in [2] as the phase quadrature $\hat{p}$ basis $|p\rangle$ with $\langle p|\alpha\rangle = \pi^{-1/4}e^{-p^2/2-i\sqrt{2}\alpha p}$ and so $\Im(n_W(p)) = -\sqrt{2}\alpha p$ meaning that any measurement outcome $p < 0$ leads to noiseless amplification. We plot the relevant quantities for the parameter values $\kappa_T = 4 \times 10^{-5}$ rad per photon and $\alpha = 10^4$ and $\beta = 0.2$, including the probability density

$$\rho(p) = \frac{e^{-p^2}\cosh\left(|\beta|^2 e^{-2\sqrt{2}\kappa_T\alpha p}\right)}{\sqrt{\pi}\cosh|\beta|^2}, \tag{6.23}$$

the amplification factor $g = e^{-\sqrt{2}\alpha p\kappa_T}$ and the fidelity $\mathcal{F}(p) = |\langle\psi_f^{(G)}(p)|\psi_f(p)\rangle|^2$ given by

$$\mathcal{F} = \frac{\left|\sum_{n=0}^{\infty}\frac{|\beta|^{2n}}{(2n)!}e^{i2n\kappa_T\alpha^2-\sqrt{2}2n\kappa_T\alpha p}\exp\left(-i\sqrt{2}p\alpha(e^{-i2n\kappa_T}-1)+\frac{\alpha^2}{2}(e^{-4in\kappa_T}-1)\right)\right|^2}{\sum_{n=0}^{\infty}\frac{|\beta|^{2n}}{(2n)!}|e^{-i\sqrt{2}p\alpha(e^{-i2n\kappa_T}-1)+\frac{\alpha^2}{2}(e^{-4in\kappa_T}-1)}|^2\cosh(|\beta|^2e^{-2\sqrt{2}\alpha\kappa_T p})},$$

in Fig.6.2. From Fig.6.2, we note that the probability density $\rho(p)$ is approximately Gaussian and so the probability of success of the protocol $P_S = \int_{-\infty}^{0} dp\,\rho(p) \approx 0.5$.

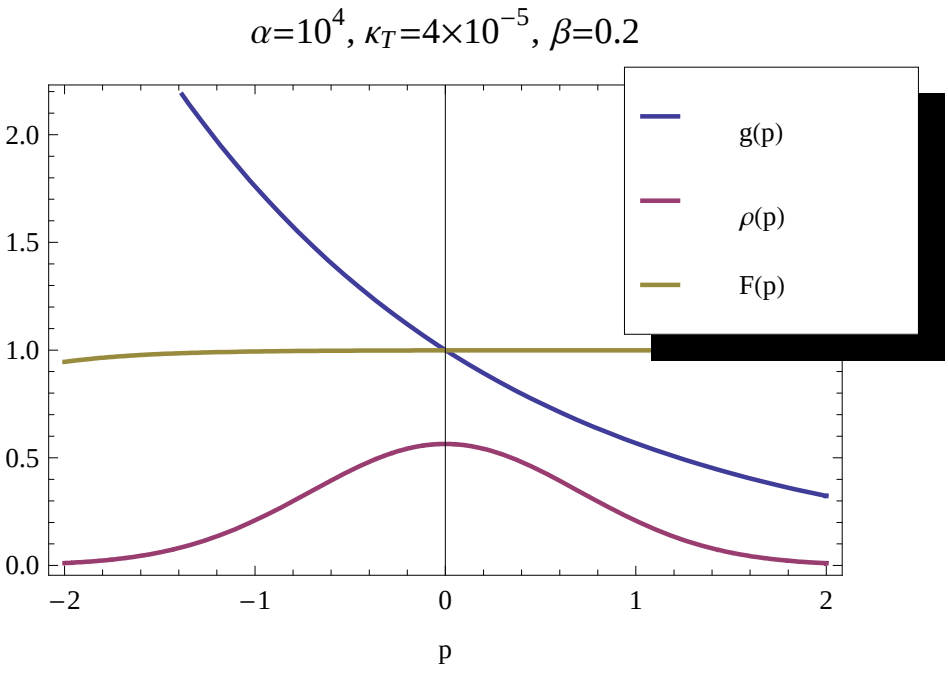

Figure 6.2: *The efficiency of the noiseless amplification of cats. Here we consider the probability density $\rho(p)$, the amplification factor $g(p)$ and the fidelity $F(p)$ between the final probe state as given by the weak formalism and what we get in general. The numerical values are $\kappa_T = 4 \times 10^{-5}$, $\alpha = 10^4$ and $\beta = 0.2$.*

Furthermore, we also note that it is possible to achieve an amplification factor of $g = 2$ when the outcome is $p_2 = -(5\ln 2)/(2\sqrt{2})$ with a probability density of $\rho(p_2) \approx 0.12$. In particular, the probability of achieving an amplification effect $g \geq 1.5$ is $\int_{-\infty}^{-0.72} dp\, \rho(p) \approx 0.15$, i.e. 15% and we also note that the fidelity is very close to unity for all measurement results in the range $p \in [-2, 2]$.

Weak coherent state cloning

It is well known that the probabilistic cloning of coherent states can be achieved using a noiseless amplifier in combination with a $50-50$ beam splitter [28]. This follows from the behaviour of coherent states incident on a noiseless beam splitter

$$\hat{U}_{BS}|\alpha, \beta\rangle = |\sqrt{T}\alpha + e^{i\theta}\sqrt{R}\beta, \sqrt{T}\beta - \sqrt{R}e^{-i\theta}\alpha\rangle. \tag{6.24}$$

The beam splitter will not entangle coherent states and the output modes are generated by constructive and destructive interference. Hence, it is possible to clone an unknown coherent state $|\alpha\rangle$ if it is noiselessly amplified to $|\sqrt{2}\alpha\rangle$ before splitting it on a $50-50$ beam splitter with the vacuum. The output is then $|\alpha, -\alpha\rangle$ and a π phase shift on the copy gives $|\alpha, \alpha\rangle$.

In general, the noiseless amplification is impossible for the reasons outlined previously, however, if the unknown coherent state to be copied is weak then our weak measurement model allows cloning to be achieved conditionally. Again this follows since it is able to induce the transformation $\alpha \rightarrow \alpha \exp(-i\kappa_T O_W(\omega))$ and so the success of the protocol is achieved when $\exp(\kappa_T \Im\{O_W(\omega)\}) \geq \sqrt{2}$. The probability of obtaining a particular ω is once again given by (6.13), where as the probability of success for the cloning is given by

$$\sum_{\omega \in \Omega_C} P(\omega) = P_S, \tag{6.25}$$

where Ω_C is defined as

$$\Omega_C = \left(\omega \in \Omega : \Im\{O_W(\omega)\} \geq \frac{\ln 2}{2\kappa_T}\right), \tag{6.26}$$

i.e. any measurement result which leads to a $\Im\{O_W(\omega)\}$ that induces a back-action greater than or equal to $\sqrt{2}$. This result has important implications in weak coherent

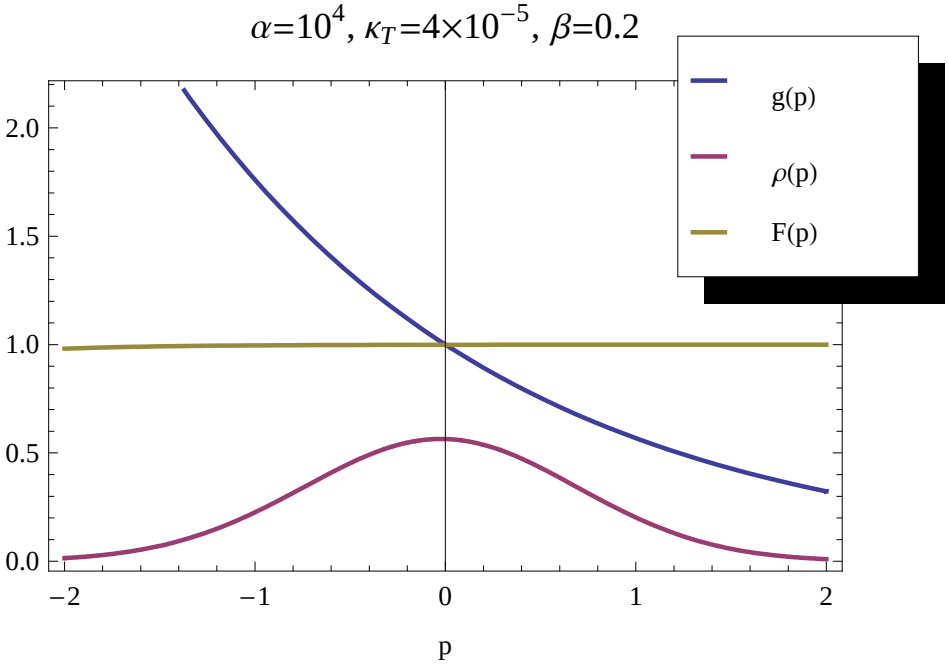

Figure 6.3: *The efficiency of the cloning of weak coherent states. Here we consider the probability density $\rho(p)$, the amplification factor $g(p)$ and the fidelity $F(p)$ between the final probe state as given by the weak formalism and what we get in general. The numerical values are $\kappa_T = 4 \times 10^{-5}$, $\alpha = 10^4$ and $\beta = 0.2$.*

state quantum key distribution [12] since our model can be regarded as a non-Gaussian attack by Eve on the channel shared by Alice and Bob. That is, Eve can conditionally copy the states exchanged between Alice and Bob and use it to infer the shared key without Alice and Bob's knowledge.

We consider the efficiency of this protocol in the case where we want to clone $|\beta \in \Re\rangle$ using an all optical configuration with the cross-Kerr effect $\hat{H}_I = \kappa\hbar\hat{n}_A\hat{n}_B$ and an ancilla coherent state $|\alpha\rangle$ that is subjected to a measurement of the phase quadrature $\hat{p}$ in balanced homodyne detection. In Fig.6.3 we plot the probability density for p

$$\rho(p) = \pi^{-1/2} \exp\left(-p^2 + e^{-2\sqrt{2}\alpha p\kappa_T}\beta^2 - \beta^2\right), \tag{6.27}$$

the amplification factor $g = e^{-\sqrt{2}\alpha p \kappa_T}$ and the fidelity

$$\mathcal{F} = \frac{\left|\sum_{n=0}^{\infty} \frac{|\beta|^{2n}}{n!} e^{in\kappa_T\alpha^2 - \sqrt{2}n\kappa_T\alpha p} \exp\left(-i\sqrt{2}p\alpha(e^{-in\kappa_T}-1) + \frac{\alpha^2}{2}(e^{-2in\kappa_T}-1)\right)\right|^2}{\sum_{n=0}^{\infty} \frac{|\beta|^{2n}}{n!} |e^{-i\sqrt{2}p\alpha(e^{-in\kappa_T}-1)+\frac{\alpha^2}{2}(e^{-2in\kappa_T}-1)}|^2 \sum_{n=0}^{\infty} \frac{|\beta|^{2n}}{n} e^{-2\sqrt{2}\alpha\kappa_T np}}$$

for physically realistic parameter values of $\kappa_T = 4 \times 10^{-5}$, $\alpha = 10^4$ and $\beta = 0.2$. From Fig.6.3, we note that the threshold for cloning is ≈ -0.8 and so the probability of success of this protocol is $\int_{-\infty}^{-0.8} dp\, \rho(p) \approx 0.20$ i.e. approximately 20% in a single run.

6.2 Weak values with entangled probes

As noted previously, it is an intriguing question whether the connection between weak values and Procrustean entanglement concentration can be extended to a larger class of pure bipartite entangled states. We shall answer this question in the positive with our weak measurement model in this section.

6.2.1 Output state

The success of the weak measurement induced continuous-variable entanglement concentration encourages an investigation in to its applicability on other bipartite pure states. Hence, the central question here is whether weak measurements can, in general, lead to a Procrustean entanglement concentration effect. To set the scene, we assume a general configuration illustrated in Fig.6.4. The probe is initially prepared in an entangled state $|\psi_i\rangle \in \mathcal{H}^{\otimes 2}$ with *Schmidt* decomposition:

$$|\psi_i\rangle = \sum_{k=1}^{K} s_k |a_k\rangle |a_k\rangle. \tag{6.28}$$

The usual properties are assumed with $\{s_k\}_{k=1}^K$ obeying $\sum_{k=1}^K s_k^2 = 1$, $s_k \geq 0 \; \forall \, k \in [1, K]$ and $\langle a_k | a_j \rangle = \delta_{jk}$. One subsystem of the probe interacts with the system initially prepared in $|i\rangle$. This mixing is provided by the interaction Hamiltonian

$$\hat{H}_I = \hbar\kappa \hat{K} \otimes \hat{O}, \tag{6.29}$$

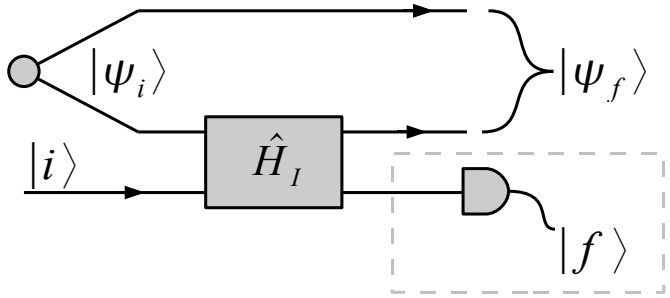

Figure 6.4: *Mixing one of the entangled sub-systems of $|\psi_i\rangle$ with an ancilla system initially prepared in $|i\rangle$, before post-selecting the ancilla in the state $|f\rangle$.*

with, for simplicity, $\kappa = \text{const}$. In addition, it is assumed that all of the systems have vanishing free Hamiltonians. This can be done without loss of generality, provided we note that all results are unique up to a suitable unitary transformation. Furthermore, the observable $\hat{K}$ is required to admit the *Schmidt* basis as an eigenbasis with $\hat{K}|a_k\rangle = \lambda_k|a_k\rangle$. Consequently, the appropriate unitary evolution operator generated by (6.29) is

$$\hat{U}_{BC} = \exp\left(-\frac{i}{\hbar}\int_0^T dt\hat{H}_I\right) = e^{-i\kappa_T \hat{K}\otimes\hat{O}}. \tag{6.30}$$

Following the interaction, the observable $\hat{F}$ is measured which results in the system being post-selected in a particular eigenstate $|f\rangle$ and so the final probe state is

$$|\psi_f\rangle \propto \langle f|\left(\hat{I}\otimes\hat{U}\right)|\psi_i\rangle|i\rangle. \tag{6.31}$$

The critical feature of weak measurements is the "weakness" of the coupling between probe and system, thus it is assumed that $\kappa_T << 1$, meaning that only linear terms are kept:

$$|\psi_f\rangle \approx \mathcal{N}\left(\langle f|i\rangle\hat{I} - i\kappa_T\,\langle f|\hat{O}|i\rangle(\hat{I}\otimes\hat{K})\right)|\psi_i\rangle. \tag{6.32}$$

This approximation is more strict than the previously used approximations. Ultimately, this is because the result has to be applicable to any bipartite pure state and so the Schmidt coefficients of an arbitrary state may not have a simple analytical relationship like the Schmidt coefficients of the TMSV. The weak value of $\hat{O}$ is

$$O_W = \frac{\langle f|\hat{O}|i\rangle}{\langle f|i\rangle} \tag{6.33}$$

and noting that $\tilde{\mathcal{N}} = \mathcal{N}\langle f|i\rangle$ allows (6.32) to be given as

$$|\psi_f\rangle = \tilde{\mathcal{N}}\left(\hat{I}_{AB} - i\kappa_T\, O_W(\hat{I}\otimes\hat{K})\right)|\psi_i\rangle. \tag{6.34}$$

The normalisation constant $\tilde{\mathcal{N}}$ is

$$\tilde{\mathcal{N}} \approx \frac{e^{i\phi}}{\sqrt{1 + 2\kappa_T\,\Im(O_W)\langle\psi_i|(\hat{I}\otimes\hat{K})|\psi_i\rangle}}, \tag{6.35}$$

where $e^{i\phi}$ is an arbitrary global phase that can be set to $\phi = 0$ without loss of generality. Consequently, the final entangled state is

$$|\psi_f\rangle = \frac{\left(\hat{I} - i\kappa_T\, O_W(\hat{I}\otimes\hat{K})\right)|\psi_i\rangle}{\sqrt{1 + 2\kappa_T\,\Im(O_W)\langle\psi_i|(\hat{I}\otimes\hat{K})|\psi_i\rangle}}. \tag{6.36}$$

6.2.2 Modification of entanglement

From (6.36) it is clear that both the real and imaginary parts of the weak value contribute towards the transformation of the state. However, only the latter induces a non-unitary effect that is responsible for the modification of the entanglement content of (6.28). The verification of this effect requires the demonstration of a quantitative change in the entanglement content of the state. For bipartite pure states, we use the entanglement measure derived from the *Von Neumann* entropy [65, 9]:

$$\mathcal{E}(|\Psi\rangle) = \{\mathcal{S}\circ \mathrm{Tr}_j\}|\Psi\rangle\langle\Psi| = -\mathrm{Tr}\left(\hat{\rho}_j \ln\hat{\rho}_j\right). \tag{6.37}$$

Denoting $\hat{\rho}_i = |\psi_i\rangle\langle\psi_i|$ and $\hat{\rho}_f = |\psi_f\rangle\langle\psi_f|$, the reduced density matrices are $\hat{\sigma}_i = \mathrm{Tr}_1(\hat{\rho}_i)$ and $\hat{\sigma}_f = \mathrm{Tr}_1(\hat{\rho}_f)$. Accordingly, our starting point is the global density matrix

$$\hat{\rho}_f = \frac{\hat{\rho}_i + 2\kappa_T\,\Im(O_W)\hat{K}\hat{\rho}_i}{1 + 2\kappa_T\,\Im(O_W)\mathrm{Tr}(\hat{K}\hat{\sigma}_i)}, \tag{6.38}$$

which leads to the reduced density matrix

$$\hat{\sigma}_f = \frac{\hat{\sigma}_i + 2\kappa_T\,\Im(O_W)\hat{K}\hat{\sigma}_i}{1 + 2\kappa_T\,\Im(O_W)\mathrm{Tr}(\hat{K}\hat{\sigma}_i)}. \tag{6.39}$$

Moreover,

$$\begin{aligned}\ln(\hat{\sigma}_f) &= \ln(\hat{\sigma}_i + 2\kappa_T\,\Im(O_W)\hat{K}\hat{\sigma}_i) - \ln(1 + 2\kappa_T\,\Im(O_W)\mathrm{Tr}(\hat{K}\hat{\sigma}_i)) \\ &\approx \ln(\hat{\sigma}_i) + 2\kappa_T\,\Im(O_W)(\delta\hat{K}),\end{aligned} \tag{6.40}$$

where $\delta\hat{K} = \hat{K} - \mathrm{Tr}(\hat{K}\hat{\sigma}_i)$ and the second line follows from keeping only linear terms in κ_T. Hence

$$\hat{\sigma}_f \ln \hat{\sigma}_f \approx \frac{\hat{\sigma}_i \ln(\hat{\sigma}_i) + 2\kappa_T \, \Im(O_W)(\delta\hat{K}\sigma_i + \hat{K}\hat{\sigma}_i \ln \hat{\sigma}_i)}{1 + 2\kappa_T \, \Im(O_W)\mathrm{Tr}(\hat{K}\hat{\sigma}_i)}, \tag{6.41}$$

and so

$$\mathcal{S}(\hat{\sigma}_f) = \frac{\mathcal{S}(\hat{\sigma}_i) - 2\kappa_T \Im(O_W) \, \mathrm{Tr}(\hat{K}\hat{\sigma}_i \ln \hat{\sigma}_i)}{1 + 2\kappa_T \, \Im(O_W)\mathrm{Tr}(\hat{K}\hat{\sigma}_i)}. \tag{6.42}$$

Finally, if we note that $\hat{\omega} = -\hat{\sigma}_i \ln \hat{\sigma}_i / \mathcal{S}(\hat{\sigma}_i)$ can be formally identified as a density matrix in its own right, then (6.42) becomes

$$\frac{\mathcal{S}(\hat{\sigma}_f)}{\mathcal{S}(\hat{\sigma}_i)} = \frac{1 + 2\kappa_T \, \Im(O_W)\mathrm{Tr}(\hat{K}\hat{\omega})}{1 + 2\kappa_T \, \Im(O_W)\mathrm{Tr}(\hat{K}\hat{\sigma}_i)}. \tag{6.43}$$

The entanglement content of the probe is altered if and only if $\mathcal{S}_f \neq \mathcal{S}_i$ and so $\mathcal{S}_f/\mathcal{S}_i \neq 1$, which is true if both $\Im(O_W)$ and $\mathrm{Tr}(\hat{K}(\hat{\sigma}_i - \hat{\omega}))$ (since $\mathrm{Tr}(\hat{K}\hat{\sigma}_i) \neq \mathrm{Tr}(\hat{K}\hat{\sigma}_i)$) cannot be zero. The requirement that $\Im(O_W) \neq 0$ is obvious from (6.36) as it accompanies a non-unitary transformation of the probe state. This follows from the properties of entanglement measures which are designed to be non-increasing under local unitary operations [65].

On the other hand, the second simultaneous requirement that $\mathrm{Tr}(\hat{K}(\hat{\sigma}_i - \hat{\omega})) \neq 0$ is the precise meaning to the claim that $\hat{K}$ must be able to distinguish states of different entropies given earlier. This is because the entropy of $\hat{\sigma}_i$ is identical to that of $\hat{\omega}$ only when the global probe state is either separable or maximally entangled. Essentially, the probe observable $\hat{K}$ must be able to witness the difference between the states $\hat{\sigma}_i$ and ω. It is instructive to compare this requirement on $\hat{K}$ with the definition of an entanglement-witness [13, 65] used in the discussion of mixed state entanglement. Such a witness is a self-adjoint operator $\hat{W}$ that can distinguish between the set of separable states $\mathcal{S}$ and a particular entangled state $\hat{\rho}_E$ via $\mathrm{Tr}(\hat{W}\hat{\rho}) \geq 0 \; \forall \hat{\rho} \in \mathcal{S}, \;\; \mathrm{Tr}(\hat{W}\hat{\rho}_E) < 0$. The essential difference between this and the role played by $\hat{K}$ is that the latter need only distinguish between two states.

6.2.3 Application to entanglement concentration

It is now widely acknowledged that the counter-intuitive features of quantum states can also be interpreted as information theoretic resources. This realization has provided ample motivation for quantum state engineering, with the aim of manufacturing, enhancing or repairing the desired non-classical features of a particular quantum state. Entanglement concentration protocols are designed to augment the entanglement content of a particular entangled state. From a state-engineering viewpoint, the weak measurement with an entangled probe can be interpreted as an entanglement concentration protocol. Essentially, by mixing a subsystem with an ancilla which is both pre and post-selected can augment the initial entanglement available in the global shared state. In particular, this association can be a calculational aid for *Procrustean* entanglement concentration protocols which modify the *Schmidt* coefficients. In our case, the output coefficients are a function of the weak value of the ancilla $t_k = f(s_k, \kappa_T, O_W)$. When viewed in this manner, we can use (6.44) to determine the requisite conditions on $\{|i\rangle, \hat{O}, |f\rangle, \hat{K}\}$ that will collectively allow an entanglement concentration effect. Entanglement concentration of the shared state (previously known as the probe state) is given if $\mathcal{S}_f/\mathcal{S}_i > 1$ and hence

$$\Im(O_W)\mathrm{Tr}(\hat{K}(\hat{\omega} - \hat{\sigma}_i)) > 0, \tag{6.44}$$

Thus, the weak value formalism can be used in a quantum information context to single out individual examples of entanglement concentration protocols. Consequently, one can view $\Im(O_W)$ as a calculational aid allowing one to pick out suitable ancilla ingredients. Furthermore, in conjunction with condition on $\hat{K}$, we find the required properties of the interaction Hamiltonian to allow the desired effect.

6.3 Future open problems

In this chapter, we have detailed our original contributions that showcase the ability of weak measurements to allow for noiseless probabilistic photon number amplification and modification of the entanglement content of an arbitrary bipartite pure

entangled probe states. These results motivate further investigation into weak values. Three immediate questions surface:

1. Can weak values be considered a quantum resource for state engineering? In particular can one establish a rigorous resource theory related to weak values and measurements in a similar vein to that of entanglement?

2. If weak values are a resource, can entanglement be sacrificed to increase this resource?

3. Can weak measurements be used to modify other non-classical features of probe states?

Answering the first issue is likely to be challenging since one would need a clear idea of the particular processing tasks that weak values could aid. To understand this, remember that the resource interpretation of entanglement follows from our inability to perform certain tasks if we are limited to local operations and classical communication. From this very general restriction, the notion of entanglement as resource can be developed [122, 123]. In contrast, our work only highlights a particular application of weak measurements in state engineering and does not identify the essential restriction weak measurements resolve.

Nevertheless, issues two and three are potentially easier to solve since previous work has been done to identify the non-classicality associated to the real part of the weak values themselves [124, 125]. The thrust of these works is that for any observable $\hat{O}$, its eigen-value spectrum and its expectation value provide a relative definition of classicality which the real part of weak values can violate. For example, for a continuous-variable bosonic system, the number operator $\hat{n} = \hat{a}^\dagger \hat{a}$ has a completely positive countable spectrum and its expectation values are positive or zero. Thus, any choice of pre and post-selection contrary to this behaviour can be regarded as a signature of non-classicality i.e. $\Re(n_W) < 0$. While this analysis is restricted only to examining the real part of the weak value, a simple modification allows this idea to include the imaginary parts of weak values. In particular, non-classical pre and post-selections for the self-adjoint operator $\hat{A}$ are those such that

$\Im(A_W) \neq 0$. This is precisely the condition required for entanglement concentration derived earlier. Thus, point two could be investigated by determining if entangled states can be used to increase this non-classicality or not. Point three can be addressed by demonstrating that a weak measurement could modify a non-classical feature of a probe state as measured by some non-classical measure. Some work has already been done in this direction in the context of super-conducting qubits and the Leggett inequality [126].

Chapter 7

Gaussian optimized preparation of non-Gaussian states

Non-Gaussian states are highly sought-after resources in continuous-variable quantum optical information processing protocols. In this chapter, we outline our novel method for the optimized preparation of any pure non-Gaussian state to a desired accuracy. Our proposal arises from two connected concepts. Firstly, we define the operational cost of a desired state as the largest Fock state required for its approximate preparation. Secondly, we suggest this non-Gaussian operational cost can be reduced by judicial application of optimized Gaussian operations. In particular, we identify a minimal core non-Gaussian state for any target pure state, which is related to the core state by Gaussian operations alone. We will demonstrate this method for the Schrödinger cat states.

7.1 Resource cost function for non-Gaussian states

7.1.1 Resource interpretation of non-Gaussian states

Non-classical features of quantum states are now interpreted as potential resources ready for exploitation in various quantum information processing tasks. This modern viewpoint is particularly acute in the realm of optical continuous-variable quan-

tum information, where there is a clear distinction between different types of resource. On the one hand, we have the Gaussian states and operations which are readily available and relatively easy to prepare. On the other, Gaussian resources alone are not enough for some key tasks and they must be augmented by non-Gaussian resources, with universal quantum computation [19, 20] being a crucial example of this. Moreover, during the last three decades, a diverse range of non-Gaussian states of light have been successfully generated, namely, sub-Poissonian states [127], Fock states [128, 129], superposition of Fock states [130], superposition of coherent states [61, 131], single-photon subtracted states [44, 61, 132, 133], single-photon added states [48] and squeezed two-photon states [77]. In addition, two-mode non-Gaussian states are now understood as potentially useful resources for the enhancement of entanglement and continuous-variable teleportation [134–137], the improvement of non-local correlations [138, 139] and the demonstration of the violation of Bell's inequalities with homodyne detectors [140–143]. The first experimental demonstration of this two-photon non-Gaussian state was recently reported in [77]. So the interest in non-Gaussian states and operations is of a fundamental and operational character. However, these necessary states and operations are notoriously difficult to prepare or execute. While this point is widely acknowledged, the question whether Gaussian operations can aid in the construction of non-Gaussian states has been neglected.

In this chapter, we are interested in the potential application of Gaussian operations to reduce the complexity of non-Gaussian pure state preparation. We consider this question in the context of experimentally realistic state preparation schemes utilizing photon subtraction [46, 61, 132, 133] and addition [48, 49] techniques. In addition, feasible schemes for multi-photon subtracted states were suggested in [144–146]. To be concrete, in the absence of a suitable Hamiltonian, arbitrary non-Gaussian quantum optical states can be approximately constructed using finite high order non-classical resources via experimentally feasible photon subtraction [46, 147] or photon addition [47, 49] methods. These schemes allow the construction of arbitrary finite superpositions of Fock states $\sum_{n=0}^{N} c_n|n\rangle$. For example, in [46] such

a superposition can be conditionally prepared from a squeezed state subjected to a sequence of $N+1$ displacements interspaced with N photon subtractions before a final anti-squeezing. Similarly, in [49], such a state can be probabilistically prepared from a supply of N single photon states.

The non-Gaussian resources required in the idealized noiseless execution of these schemes is N, i.e. the number of photon subtractions or the number of single photon states required to prepare $\sum_{n=0}^{N} c_n|n\rangle$. Consequently, we can identify the minimum non-Gaussian resource cost as the minimum number of successive photon subtractions/additions to produce this state. This logic can also be applied to continuous-variable states like $|\psi\rangle = \sum_{n=0}^{\infty} c_n|n\rangle$ with a caveat that the desired state can only be produced approximately by $|\psi^N\rangle = \mathcal{N}\sum_{n=0}^{N} c_n|n\rangle$ where $\mathcal{N}$ is a normalisation factor. Thus, in this case, the minimum number of photon subtractions/additions required to prepare our desired state to a *sufficient* accuracy, determined by the fidelity $\mathcal{F}(\psi,\psi^N) = |\langle\psi|\psi^N\rangle|^2$, is the operational cost for that state. It should be stressed, that this operational cost is not a measure, but a useful ruler for gauging the difficulty of preparing the state. Our method is, therefore, in contrast to approaches which attempt to quantitatively measure the degree of non-classicality [33–35, 148–151] or non-Gaussianity possessed by a particular state [152, 153].

7.1.2 Example of state preparation

Crucial to our idea in this chapter is the notion of the conditional preparation of arbitrary finite superpositions of Fock states as the means of approximating desired non-Gaussian pure states. It is therefore worthwhile to briefly discuss the protocols which allow the construction of such states. In this section we consider the protocol advanced by Dakna *et. al.* [49], where the state $\sum_{n=0}^{N} c_n|n\rangle$ is conditionally manufactured from a N single photon states introduced into an array of beam splitters interspaced by $N+1$ consecutive displacements as shown in Fig.7.1. This protocol is build from two simple techniques: displacement and photon addition. The former is achieved by requiring that each of the beam splitters used to displace the state are highly transmitting with $T > 99\%$. This is chosen in order to avoid the generation

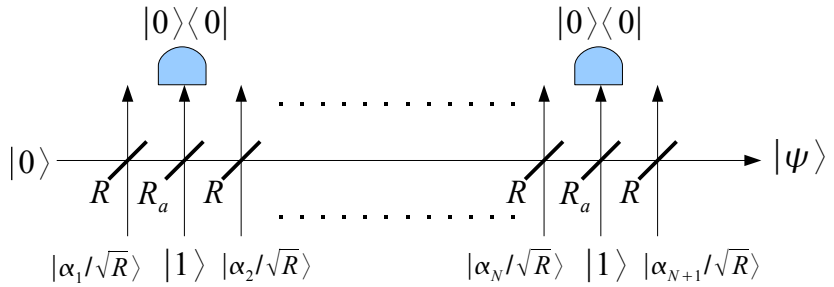

Figure 7.1: *One can conditionally prepare a N dimensional arbitrary finite superposition of Fock states by a sequence of N photon additions interspaced by $N+1$ displacements.*

of entanglement between the ancilla coherent state $|\alpha/\sqrt{R}\rangle$ and the input state $|\phi\rangle$. For example, consider the case where $|\phi\rangle$ is the input state mixed with $|\alpha\rangle$ on a highly unbalanced beam splitter modeled by $\hat{U}$ with $T \approx 1$ then

$$\hat{U}|\phi,\alpha\rangle = \hat{U}\left(\hat{I}\otimes\hat{D}(\alpha)\right)\hat{U}^{\dagger}\hat{U}|\psi,0\rangle, \tag{7.1}$$

with $\hat{U}\left(\hat{I}\otimes\hat{D}(\alpha)\right)\hat{U}^{\dagger} = \hat{D}(\sqrt{R}\alpha)\otimes\hat{D}(\sqrt{T}\alpha)$ and

$$\hat{U}|\phi,0\rangle = \sum_{n=0}^{\infty}\frac{\phi_n(\sqrt{T}\hat{a}^{\dagger}-\sqrt{R}\hat{a})^n}{\sqrt{n!}}|0,0\rangle. \tag{7.2}$$

Given that $T \approx 1$ then the final state approximates to

$$\hat{U}|\phi,\alpha\rangle \approx \hat{D}(\sqrt{R}\alpha)\otimes\hat{D}(\sqrt{T}\alpha)\sum_{n=0}^{\infty}\frac{\phi_n(\hat{a}^{\dagger})^n}{\sqrt{n!}}|0,0\rangle = \hat{D}(\sqrt{R}\alpha)\otimes\hat{D}(\sqrt{T}\alpha)|\phi,0\rangle, \tag{7.3}$$

and so we are able to displace the original state to a good approximation with a final state $\hat{D}(\sqrt{R}\alpha)|\phi\rangle$. In the present scheme, the transformation for the jth displacement is $|\phi\rangle \rightarrow \hat{D}(\alpha_j)|\phi\rangle$. The photon addition technique is achieved as described in chapter two, by mixing the single photon with the signal on a beam splitter before projecting onto the vacuum at the output. This vacuum projection can be performed either with the binary photo-detector or a double homodyne detector. When the addition is successful, then the signal state is transformed as $|\phi\rangle \rightarrow \sqrt{R}\sqrt{T}^{\hat{n}}\hat{a}^{\dagger}|\phi\rangle$.

Consequently, after the N successful additions and $N+1$ displacements the final state is

$$|\psi\rangle \propto \hat{D}(\alpha_{N+1})\sqrt{T}^{\hat{n}}\hat{a}^\dagger\hat{D}(\alpha_N)\ldots\hat{D}(\alpha_2)\sqrt{T}^{\hat{n}}\hat{a}^\dagger\hat{D}(\alpha_1)|0\rangle. \tag{7.4}$$

Then we write $\sqrt{T}^{\hat{n}}\hat{D}(\alpha_k) = \hat{D}(\alpha_k)\left\{\hat{D}^\dagger(\alpha_k)\sqrt{T}^{\hat{n}}\hat{D}(\alpha_k)\right\}$ and propagate these expressions through to the right [49]. After some algebra [49], the final result can be shown to be

$$|\psi\rangle = \hat{D}^\dagger(\beta_N)\hat{a}^\dagger\hat{D}(\beta_N)\hat{D}^\dagger(\beta_{N-1})\hat{a}^\dagger\ldots\hat{D}(\beta_1)\hat{a}^\dagger\hat{D}(\beta_1)|0\rangle, \tag{7.5}$$

where the β_j are defined from

$$\alpha_1 = -\sum_{\ell=1}^{N}\sqrt{T}^{-\ell}\alpha_{\ell+1}, \tag{7.6}$$

$$\alpha_k = \sqrt{T}^{N-k+1}(\beta_{k-1}-\beta_k), \quad k = 2,3,\ldots N, \tag{7.7}$$

$$\alpha_{N+1} = \beta_N. \tag{7.8}$$

Finally, we note that (7.5) is equivalent to

$$|\psi\rangle = (\hat{a}^\dagger-\beta_N^*)(\hat{a}^\dagger-\beta_{N-1}^*)\ldots(\hat{a}^\dagger-\beta_1^*)|0\rangle, \tag{7.9}$$

which is identical to

$$|\psi\rangle = \sum_{n=0}^{N}\psi_n|n\rangle, \tag{7.10}$$

provided that $(\beta_1^*,\beta_2^*,\ldots,\beta_N^*)$ are the complex roots of the characteristic polynomial [49]

$$\sum_{n=0}^{N}\frac{\psi_n}{\sqrt{n!}}(\beta^*)^n = 0. \tag{7.11}$$

Thus, to build a desired state $|\psi\rangle$, we must first calculate the $(\beta_1^*,\beta_2^*,\ldots,\beta_N^*)$ and use them to calculate the required $(\alpha_1,\alpha_2,\ldots,\alpha_{N+1})$ displacements. The photon-subtraction scheme [46] works in a similar manner. In both of these schemes, it is the number of subtractions or additions which determine the length of the manufactured superposition. In our view, this number provides an insight into the non-Gaussian off-line resource required to produce a desired state.

7.1.3 Reducing the non-Gaussian resource

Our inspiration for the work present here resides two simple questions. In the first instance, can unitary Gaussian operations applied to the prepared finite dimensional state increase the fidelity with the desired continuous-variable target state? In the second, can the applied unitary Gaussian operations help to reduce the number of photon subtractions/additions to reach desired fidelity? These questions are motivated by a desire to prepare non-Gaussian states in a manner which minimizes the non-Gaussian resource overhead. If we restrict ourselves to directly preparing truncated versions of $|\psi\rangle$ then we have no freedom in reducing the non-Gaussian resources. This follows from the fact that the fidelity between $|\psi\rangle$ and a truncated approximation scales with largest Fock state in the latter. Thus, a greater accuracy requires a ever greater number of subtractions or an ever larger Fock state preparation. Here we suggest an alternative approach to the approximate preparation of $|\psi\rangle$. Instead of directly constructing a truncated version of the target, we advocate the identification and preparation of a minimum core state. This core state will minimize the non-Gaussian resources required to prepare a sufficiently accurate approximation to the target. Moreover, each core is related to the desired target through Gaussian operations alone. Consequently, we are motivated to understand whether Gaussian operations can reduce the accumulative cost of employing ever elaborate non-Gaussian operations. To this end we formulate a criterion to answer this and then use it to optimize the parameters of the associated non-Gaussian operations.

7.2 Gaussian optimized preparation

7.2.1 Identification of core states

Our central problem is this: we want to prepare a very good approximation to the continuous-variable non-Gaussian pure state $|\psi(\lambda)\rangle = \sum_{n=0}^{\infty} \psi_n(\lambda)|n\rangle$, where the parameters $\lambda = (\lambda_1, \ldots, \lambda_M)$ specify a particular state from a family of like states.

For example, α labels each possible even parity Schrödinger cat state $|\psi(\alpha)\rangle = \mathcal{N}(|\alpha\rangle + |-\alpha\rangle)$, where $\mathcal{N}$ is a normalization factor. To prepare the state, we restrict ourselves to Gaussian operations supplemented by photon subtractions or a supply of Fock states. The implementation of the former is considerably easier than the latter; Minimization of the non-Gaussian resource is our key priority. Thus, for a given $|\psi(\lambda)\rangle$ we wish to identify the optimal Gaussian parameters that correspond to the smallest number of photon subtractions. To this end, we introduce a family of single-mode core states $|\lambda, r, \alpha, \theta\rangle$ related to the target via

$$|\psi(\lambda)\rangle = \hat{U}(\theta)\hat{D}(\alpha)\hat{S}(r)|\lambda, r, \alpha, \theta\rangle. \tag{7.12}$$

Where $\hat{D}(\alpha)$ and $\hat{S}(r)$ are the single-mode unitary displacement and squeezing operators [27], $\hat{D}(\alpha) = \exp\left(\alpha\hat{a}^\dagger - \alpha^*\hat{a}\right)$ and $\hat{S}(r) = \exp\left(\frac{r}{2}\{(\hat{a}^\dagger)^2 - \hat{a}^2\}\right)$ and $\hat{U}(\theta) = e^{i\theta\hat{n}}$ is the phase operator. Conversely, each core state is given by the inverse on the target

$$|\lambda, r, \alpha, \theta\rangle = \hat{S}(-r)\hat{D}(-\alpha^*)\hat{U}(-\theta)|\psi(\lambda)\rangle. \tag{7.13}$$

This definition of a corresponding core state allows us to distinguish between two classes of continuous-variable non-Gaussian pure state. The first class are those with a finite dimensional core

$$|\psi(\lambda)\rangle = \hat{U}(\theta)\hat{D}(\alpha)\hat{S}(r)\left(\sum_{n=0}^{N} c_n(\lambda)|n\rangle\right), \tag{7.14}$$

which can be prepared with perfect fidelity by first preparing the finite core before applying the unitary Gaussian operations. Examples of such states include the photon added coherent state [154]

$$|\psi\rangle = \frac{\hat{a}^\dagger|\alpha\rangle}{\sqrt{1+|\alpha|^2}} = \hat{D}(\alpha)\left(\frac{\alpha^*|0\rangle + |1\rangle}{\sqrt{1+|\alpha|^2}}\right), \tag{7.15}$$

which can be prepared with unit fidelity by first preparing $c_0|0\rangle + c_1|1\rangle$ and displacing the result. The second, more general class of pure non-Gaussian states are those with corresponding continuous-variable core states

$$|\psi(\lambda)\rangle = \hat{U}(\theta)\hat{D}(\alpha)\hat{S}(r)\left(\sum_{n=0}^{\infty} c_n(\lambda)|n\rangle\right). \tag{7.16}$$

In contrast to the previous class, such targets cannot be perfectly prepared by either the photon subtraction or addition techniques as they would require infinite non-Gaussian resources. Of course, these states are typically generated from a suitable Hamiltonian by a time evolution. Consequently, such states can only be prepared approximately as

$$|\psi_C^N(\lambda)\rangle = \hat{U}(\theta)\hat{D}(\alpha)\hat{S}(r)\left(\frac{\sum_{n=0}^{N} c_n(\lambda)|n\rangle}{\sqrt{\sum_{n=0}^{N}|c_n(\lambda)|^2}}\right), \tag{7.17}$$

to an accuracy determined by the fidelity with the target

$$\mathcal{F}_C = |\langle\psi(\lambda)|\psi_C^N(\lambda)\rangle|^2. \tag{7.18}$$

A little algebra reveals that the fidelity is a function of the Gaussian parameters (r, α, θ) and the non-Gaussian resource cost N. This follows since the truncated core is given by

$$|\lambda, r, \alpha, \theta; N\rangle = \frac{\hat{\Pi}_N|\lambda, r, \alpha, \theta\rangle}{\sqrt{\langle\lambda, r, \alpha, \theta|\hat{\Pi}_N|\lambda, r, \alpha, \theta\rangle}}, \tag{7.19}$$

where $\hat{\Pi}_N = \sum_{n=0}^{N}|n\rangle\langle n|$ projects onto an N dimensional subspace. Thus, the approximate target state from a truncate core is then

$$|\psi_C^N(\lambda)\rangle = \hat{U}(\theta)\hat{D}(\alpha)\hat{S}(r)|\lambda, r, \alpha, \theta; N\rangle, \tag{7.20}$$

and so

$$\langle\psi(\lambda)|\psi_C^N(\lambda)\rangle = \langle\lambda, r, \alpha, \theta|\lambda, r, \alpha, \theta; N\rangle \tag{7.21}$$

by virtue of unitarity of the Gaussian operations. Accordingly

$$\langle\psi(\lambda)|\psi_C^N(\lambda)\rangle = \frac{\langle\lambda, r, \alpha, \theta|\hat{\Pi}_N|\lambda, r, \alpha, \theta\rangle}{\sqrt{\langle\lambda, r, \alpha, \theta|\hat{\Pi}_N|\lambda, r, \alpha, \theta\rangle}}, \tag{7.22}$$

which leads to the conclusion

$$\mathcal{F}_C(\lambda, r, \alpha, \theta, N) = \langle\lambda, r, \alpha, \theta|\hat{\Pi}_N|\lambda, r, \alpha, \theta\rangle. \tag{7.23}$$

For this latter class of states, we first fix λ and N and then we optimize the phase θ, squeezing r and displacement α to maximize the fidelity and, hence, obtain the

optimal agreement between $|\psi(\lambda)\rangle$ and $|\psi_C^N(\lambda)\rangle$. This optimization process unifies several issues related to the state preparation of non-Gaussian pure states. Firstly, it identifies the essential non-Gaussian operational cost that underlies each non-Gaussian pure state. Secondly, it highlights the possible tradeoffs between Gaussian and non-Gaussian operations in this form of state preparation. In general, this optimization must be performed numerically due to the non-trivial nature of Fock state decomposition for each core. This is given by

$$|\lambda, r, \alpha, \theta\rangle = \sum_{n,m,k=0}^{\infty} e^{-i\theta k} S_{nm}(-r) D_{mk}(-\alpha^*) \psi_k(\lambda)|n\rangle = \sum_{n=0}^{\infty} c_n |n\rangle,$$

where the displacement matrix elements are given by [31] $\langle m|\hat{D}(\beta)|k\rangle = D_{mk}(\beta)$ with

$$D_{mk}(\beta) = (m!/k!)^{-1/2} e^{-|\beta|^2/2} (-\beta^*)^{k-m} L_m^{k-m}(|\beta|^2),$$

for $m \leq k$ and

$$D_{mk}(\beta) = (k!/m!)^{-1/2} e^{-|\beta|^2/2} \beta^{m-k} L_k^{m-k}(|\beta|^2), \tag{7.24}$$

for $m \geq k$. Note that the $L_k^{m-k}(|\beta|^2)$ are the generalized *Laguerre* Polynomials. The matrix coefficients for the squeezing operator [155] are $\langle n|\hat{S}(r)|m\rangle = S_{nm}(r)$. When both m and n are even integers then

$$S_{nm}(r) = \frac{(-1)^{m/2}}{(m/2)!(n/2)!} \sqrt{\frac{n!m!}{\cosh r}} \left(\frac{\tanh r}{2}\right)^{(n+m)/2} \times {}_2F_1\left(-\frac{m}{2}, -\frac{n}{2}; \frac{1}{2}; -\frac{1}{\sinh^2 r}\right), \tag{7.25}$$

but when both m and n are odd then

$$S_{nm}(r) = \frac{(-1)^{\frac{m-1}{2}}}{(\frac{m-1}{2})!(\frac{n-1}{2})!} \sqrt{\frac{n!m!}{\cosh^3 r}} \left(\frac{\tanh r}{2}\right)^{\frac{(n+m)}{2}-1} \times {}_2F_1\left(-\frac{(m-1)}{2}, -\frac{(n-1)}{2}; \frac{3}{2}; -\frac{1}{\sinh^2 r}\right), \tag{7.26}$$

and $S_{nm}(r)$ vanish for all other possibilities. Note that ${}_2F_1$ are Gauss Hypergeometric Polynomials [155].

7.2.2 The utility of unitary Gaussian operations

The main inspiration of this work was whether Gaussian unitary operations can reduce the non-Gaussian cost, with respect to photon subtraction/addition schemes, involved in preparing a desired non-Gaussian target. The extent to which this is true is revealed by comparing the non-Gaussian resources required to prepare a direct truncation of $|\psi(\lambda)\rangle$ with that required for the minimum core state. Essentially, we determine the utility of Gaussian operations by considering the approximate preparation of $|\psi(\lambda)\rangle$ with and without them. This can be done by comparing the fidelities of the states produced by each method. These fidelities are defined as

$$\mathcal{F}_{DT}(\lambda, N) = |\langle\psi(\lambda)|\psi_{DT}^{N}(\lambda)\rangle|^2, \tag{7.27}$$

with

$$\mathcal{F}_{DT}(\lambda, N) = \langle\psi(\lambda)|\hat{\Pi}_N|\psi(\lambda)\rangle = \sum_{n=0}^{N} |\psi_n(\lambda)|^2, \tag{7.28}$$

where $\psi_n(\lambda) = \langle n|\psi(\lambda)\rangle$, for the direct truncation method and

$$\mathcal{F}_C = \langle\lambda, r, \alpha, \theta|\hat{\Pi}_N|\lambda, r, \alpha, \theta\rangle = \sum_{n=0}^{N} |c_n|^2, \tag{7.29}$$

for the core state method. The superiority of the core state method can be established on two levels corresponding to the two questions asked in the introduction. Firstly, the core state method is better than the direct truncation method using the same non-Gaussian resources if

$$\langle\lambda, r, \alpha, \theta|\hat{\Pi}_N|\lambda, r, \alpha, \theta\rangle > \langle\psi(\lambda)|\hat{\Pi}_N|\psi(\lambda)\rangle. \tag{7.30}$$

The second condition, if true, that would demonstrate the superiority of the core method using *less* non-Gaussian resources over the direct truncation method is

$$\langle\lambda, r, \alpha, \theta|\hat{\Pi}_M|\lambda, r, \alpha, \theta\rangle \geq \langle\psi(\lambda)|\hat{\Pi}_N|\psi(\lambda)\rangle, \tag{7.31}$$

for $M < N$. That is, we would expect that one can better the fidelity with the target by our approach with potentially *less* non-Gaussian resources than simply building a truncated target. For the first class of states with finite dimensional cores, this is

obviously true. This is because we can perfectly prepare the state by preparing the core first and then applying unitary Gaussian operations

$$\mathcal{F}_C(N) = \sum_{n=0}^{N} |c_n|^2 = 1. \tag{7.32}$$

In contrast, the direct truncation method yields

$$\mathcal{F}_{DT}(N) = \sum_{n=0}^{N} |\psi_n(\lambda)| \leq 1, \tag{7.33}$$

because $|\psi(\lambda)\rangle$ is, in general, an infinite dimensional state and is only reproduced with unity fidelity as $N \to \infty$ and so

$$\lim_{N\to\infty} (\mathcal{F}_{DT}(N)) = \mathcal{F}_C(N) = 1. \tag{7.34}$$

Thus, we would need infinite non-Gaussian resources to perfectly prepare the target by the direct truncation method. The reason for this is because in the direct truncation method the non-Gaussian subtractions/additions also contribute to building the Gaussian envelope of the state in addition to its non-Gaussian core. In contrast, in the core method all of the non-Gaussian resources are concentrated into preparing the non-Gaussian part of the state. Thus, for the example of the photon added coherent state (7.15), the core method is superior since none of the non-Gaussian subtractions/additions contribute to the construction of the displacement operator. In contrast, in the direct truncation method, each subtraction/addition contributes to building both the core and the displacement operator.

For the second class of states with infinite dimensional cores, the situation is more subtle since both converge to unit fidelity as $N \to \infty$. However, proving the optimal nature of the core state method to a direct truncation method for arbitrary pure target states is a non-trivial task and will not be tackled here. Ultimately, this is because the core state method is a complicated optimization process that is dependant on the both the non-Gaussian resource N and the desired fidelity. We can, nevertheless, gain a limited insight into the superiority of the core state method over the direct truncation method from the following phase space argument. In particular, we note that the core method can only be con-

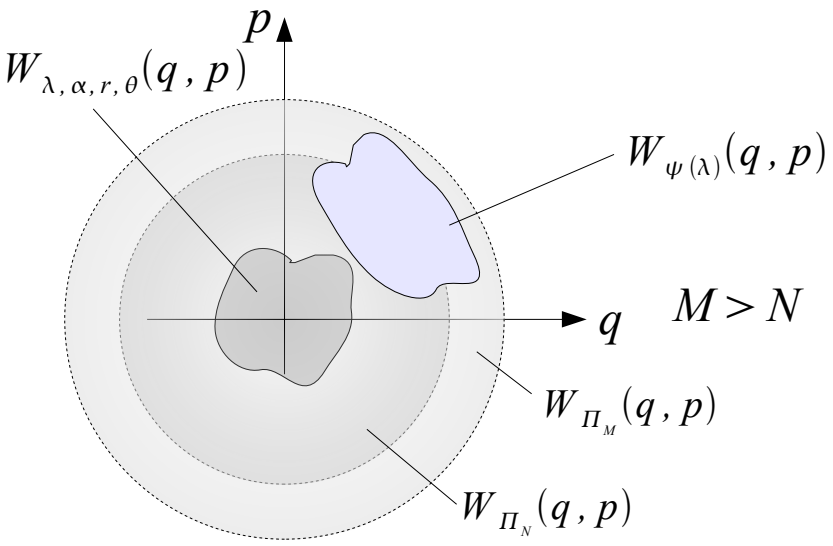

Figure 7.2: *The superiority of the core state method as compared to the direct truncation method is evident from this phase space diagram. By applying Gaussian operations to the target's Wigner function $W_{\psi(\lambda)}(q,p)$ we can generate the core state's Wigner function $W_{\lambda,\alpha,r,\theta}(q,p)$. This latter quasi-distribution is closer to the origin of phase space and has a more symmetric quadrature noise profile. This transformation achieves two simultaneous feats. One the one hand, the first and second order moments of the core can be tuned to resemble the first and second order moments of $W_{\Pi_N}(q,p)$ and so increase its fidelity with $W_{\Pi_N}(q,p)$. Such tuning cannot be performed in the direct truncation method. On the other hand, the core, as a result of this tuning, is closer to $W_{\Pi_N}(q,p)$ than $W_{\Pi_M}(q,p)$ for $M > N$ since it is located near the origin while being symmetric.*

sidered as advantageous if transforming the first and second moments of the target concentrate the state on a smaller finite dimensional subspace as depicted in Fig.7.2. This follows since the Gaussian operations can only effect the first and second order moments $W_{\lambda,\alpha,r,\theta}(q,p) = W_{\psi(\lambda)}(Q(q,p,\alpha,r,\theta),P(q,p,\alpha,r,\theta))$, where $Q(q,p,\alpha,r,\theta)$ and $P(q,p,\alpha,r,\theta)$ are linear functions of q and p. For example, if we restrict ourselves to only squeezing and displacing the target then the core is given by $W_{\lambda,\alpha,r}(q,p) = W_{\psi(\lambda)}(e^r(q-\sqrt{2}\Re(\alpha)),e^{-r}(p-\sqrt{2}\Im(\alpha)))$. Thus, the core

state method is only better in the first sense (i.e. increasing the fidelity over the direct truncation method with the same resource) if $W_{\lambda,\alpha,r,\theta}(q,p)$ enjoys a better overlap with $W_{\Pi_N}(q,p) = \sum_{n=0}^{N} W_n(q,p)$ than the original $W_{\psi(\lambda)}(q,p)$. This can only happen if the first and second order moments of $W_{\lambda,\alpha,r,\theta}(q,p)$ can be tuned to be more like the first and second order moments of $W_{\Pi_N}(q,p)$. Essentially, provided that the Gaussian parameters of the core can be tuned so that the Wigner function $W_{\lambda,\alpha,r,\theta}(q,p)$ is located at the origin and has a symmetric quadrature noise profile, as is the case with $W_{\Pi_N}(q,p)$, then it is an improvement over the direct truncation method. This is because the direct truncation method does not allow us to modify these moments to increase the resemblance with $W_{\Pi_N}(q,p)$. Of course, if $W_{\psi(\lambda)}(q,p)$ is already located at the origin with a symmetric quadrature noise profile then unitary Gaussian operations cannot improve on its overlap with $W_{\Pi_N}(q,p)$.

In addition, this argument can also answer the second question whether the core state method could offer an equal or better fidelity to the target for less non-Gaussian resources. This is also evident from Fig.7.2 since the ability to tune the Gaussian parameters of the core offers the possibility of being able to make the first and second moments of the core more like $W_{\Pi_N}(q,p)$ than $W_{\Pi_M}(q,p)$. That is, by tuning the first and second moments of the core to be close to the origin and symmetric means that the vacuum has a larger contribution to the core state than in the target. While this argument does not capture the full complexity of the core state method it does allow an simplified picture that suggests the advantageous nature of the core state method. We can build on this sentiment by providing some examples of states for which the core method is indeed superior to direct truncation. Specifically, in the next section, we consider the Schrödinger cat states and demonstrate that they support our case.

7.3 Example: Schrödinger cat states

The odd parity superposition of coherent states $|\psi(\alpha)\rangle = \mathcal{N}(|\alpha\rangle - |-\alpha\rangle)$ (where, for simplicity, we assume $\alpha \in \Re$) is a well known non-Gaussian state and is the

subject of numerous theoretical quantum information protocols [21, 59]. The characteristic feature of this state, from a photon number point of view, is the exclusion of all even Fock states $|\psi(\alpha)\rangle = \mathcal{N}' \sum_{n=0}^{\infty} \alpha^{2n+1}/\sqrt{(2n+1)!}|2n+1\rangle$. Consequently, each core state $|\alpha, r, \beta, \theta\rangle$, where $\beta \in \Re$, has the following Fock decomposition

$$\begin{aligned}|\alpha, r, \beta, \theta\rangle \propto & \sum_{n,m,k=0}^{\infty} (\alpha e^{-i\theta})^{2k+1} \\ & \times \left(\frac{S_{2n,2m}(-r) D_{2m,2k+1}(-\beta)}{\sqrt{(2k+1)!}} |2n\rangle \right. \\ & \left. + \frac{S_{2n+1,2m+1}(-r) D_{2m+1,2k+1}(-\beta)}{\sqrt{(2k+1)!}} |2n+1\rangle \right).\end{aligned}$$

Thus, displacement acts to destroy the parity of the state since it destroys the symmetry of the state around the origin of phase space. Consequently, there is good reason to regard the optimal displacement for the cat is zero. Moreover, the optimal phase is also zero since we assumed $\alpha \in \Re$. This is also evident from our numerical simulations and so we will restrict or attention to core states related to the target via squeezing alone. Accordingly, the core states are of the form

$$|\alpha, r\rangle = \mathcal{N}' \sum_{n,k=0}^{\infty} \frac{\alpha^{2k+1} S_{2n+1,2k+1}(-r)}{\sqrt{(2k+1)!}} |2n+1\rangle, \tag{7.35}$$

where $\mathcal{N}'$ is a normalization factor, and so, the photon number probability distribution of a core state is a function of the squeezing parameter r. This behaviour is readily illustrated in Fig.7.3, where it can be observed that for $\alpha = 1.5$, each core exhibits a different photon number probability distribution. The most important point to be gained from this is that different cores will require different number of minimum subtractions to approximately prepare the desired target state.

Each core state, when truncated, yields an approximation to the initial target state $|\psi(\alpha)\rangle$. These approximate target states are given by

$$|\psi_C^N(\alpha)\rangle = \mathcal{N}'' \sum_{m,k=0}^{\infty} \frac{\alpha^{2k+1} A_{2m+1,2k+1}^N}{\sqrt{(2k+1)!}} |2m+1\rangle, \tag{7.36}$$

where $A_{2m+1,2k+1}^N = \sum_{n=0}^{N} S_{2m+1,2n+1}(r) S_{2n+1,2k+1}(-r)$, i.e. $|\psi^N(\alpha)\rangle \propto \hat{S}(r)\hat{\Pi}_N|\alpha, r\rangle$ with $\mathcal{N}''$ as a normalization factor. The fidelity between the actual desired target

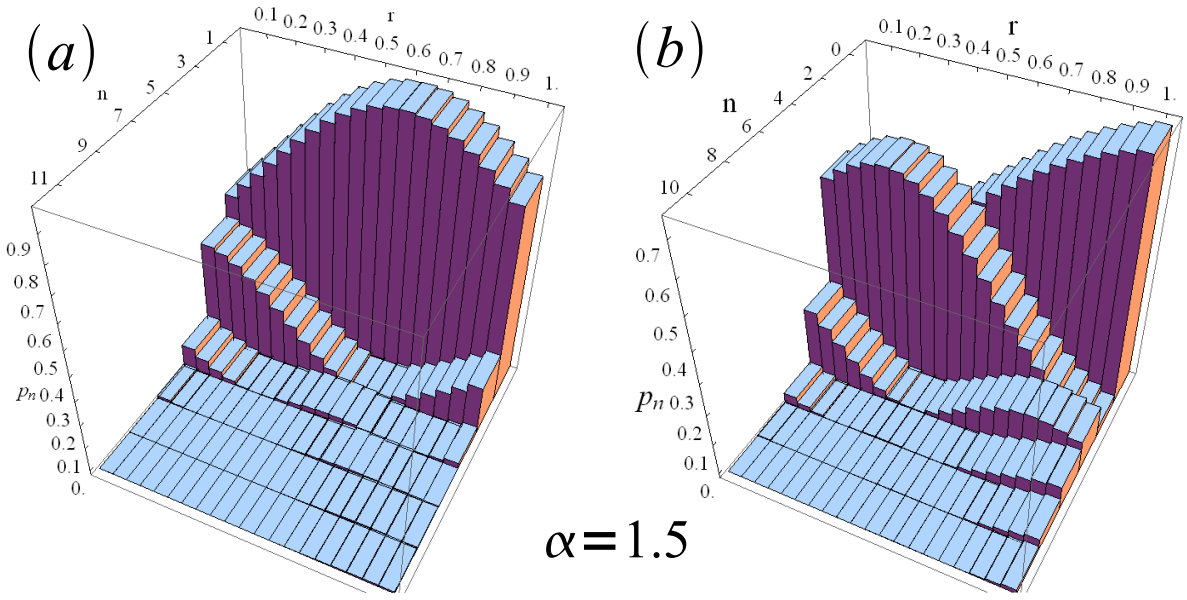

Figure 7.3: *Each core state, for the odd and even cats,* $|\alpha = 1.5, r\rangle$ *are labeled by a different squeezing and possess a diverse range of photon number probability distributions.*

state $|\psi(\alpha)\rangle$ and each of the approximate targets is then defined as

$$\mathcal{F}_C(\alpha, r, N) = \sum_{n=0}^{N} \left| \mathcal{N}'' \sum_{k=0}^{\infty} \frac{\alpha^{2k+1} S_{2n+1,2k+1}(-r)}{\sqrt{(2k+1)!}} \right|^2 , \tag{7.37}$$

and the optimal core state for a given N is obtained by maximizing this quantity. This optimization is performed numerically due to its complexity, but we can still gain an insight into the relationship between α and r for constant values of the above fidelity. For example, when $\alpha = 1.5$, numerical optimization of the fidelity yields $F = 0.96$ for $r = 0.597$ and $N = 1$ and $F = 0.999505$ for $r = 0.263$ and $N = 3$. This is precisely the content of Fig.7.4(a) and Fig.7.4(b), which show the relation between α and r for fixed non-Gaussian resources of $N = 1, 3$, respectively. In addition to this, it is important to show that the preparation of the target state $|\psi(\alpha)\rangle$ via the optimal core and Gaussian operations is more economical than a direct production of a truncated version of the target from non-Gaussian operations only.

To demonstrate that this is indeed the case, we show that the core method can produce a cat to an equal or better accuracy for smaller number of photon subtrac-

tions. This is shown in Fig.7.4(c), where we compare the fidelities $\langle\alpha, r|\hat{\Pi}_N|\alpha, r\rangle$ and $\langle\psi(\alpha)|\hat{\Pi}_M|\psi(\alpha)\rangle$ for $N < M$ and reveal the instances where our core preparation method is more economical. In particular, we note that the fidelity using the core with $N = 1$ is better than that of the truncated version of the target for both $M = 1$ and $M = 3$. Thus, instead of attempting to successfully perform three successive subtractions to approximately prepare $|\psi(\alpha)\rangle$ for $0 < \alpha < 2$, we need only perform a single subtraction and then squeeze the state accordingly.

Finally, it is important to compare the photon number distributions of the approximate targets $(|\psi_C^1(\alpha)\rangle, |\psi_C^3(\alpha)\rangle, |\psi_C^5(\alpha)\rangle)$ with the actual target $|\psi(\alpha)\rangle$. This is illustrated in Fig.7.4(d) for $\alpha = 1.5$, where it is clear that the latter two approximate targets provide an excellent approximation to $|\psi(1.5)\rangle$. Thus, for $\alpha = 1.5$, the squeezed single photon state as the core lacks a sufficient accuracy. This fact is also readily evident when one consults the contour plot in Fig.7.4(a) as there are no contours that satisfy $\mathcal{F}_C(1.5, r, 1) \geq 0.96$. This particular example provides a concrete understanding of our proposal and illustrates the main features of it.

An identical analysis can be performed on the even parity cat state $|\phi(\alpha)\rangle = \mathcal{M}(|\alpha\rangle + |-\alpha\rangle)$ with $\alpha \in \Re$. In this case, we find that all the essential points of the previous example are repeated. Firstly, the even symmetry of this state $|\phi(\alpha)\rangle \propto \sum_{n=0}^{\infty} \alpha^{2n}/(\sqrt{(2n)!})|2n\rangle$, means that the optimal displacement and phase are both zero. Consequently, each core state is labeled by the corrective squeezing

$$|\alpha, r\rangle = \mathcal{M}' \sum_{k,n=0}^{\infty} \frac{S_{2n,2k}(-r)\alpha^{2k}}{\cosh \alpha^2 (2k)!}|2n\rangle, \tag{7.38}$$

also shown in Fig.7.3(b). Again, the reason that the external squeezing is useful is because it preserves the symmetry of the state. Furthermore, each core state, when truncated, yields an approximation to the even parity cat. These approximate target states are given by

$$|\phi_C^N(\alpha)\rangle = \mathcal{M}'' \sum_{m,k=0}^{\infty} \frac{\alpha^{2k} B_{2m,2k}^N}{\sqrt{(2k!)}}|2m\rangle, \tag{7.39}$$

where $B_{2m,2k}^N = \sum_{n=0}^{N} S_{2m,2n}(r) S_{2n,2k}(-r)$ and $\mathcal{M}''$ is a normalization factor. The fidelity between the actual desired target state $|\psi(\alpha)\rangle$ and each of the approximate

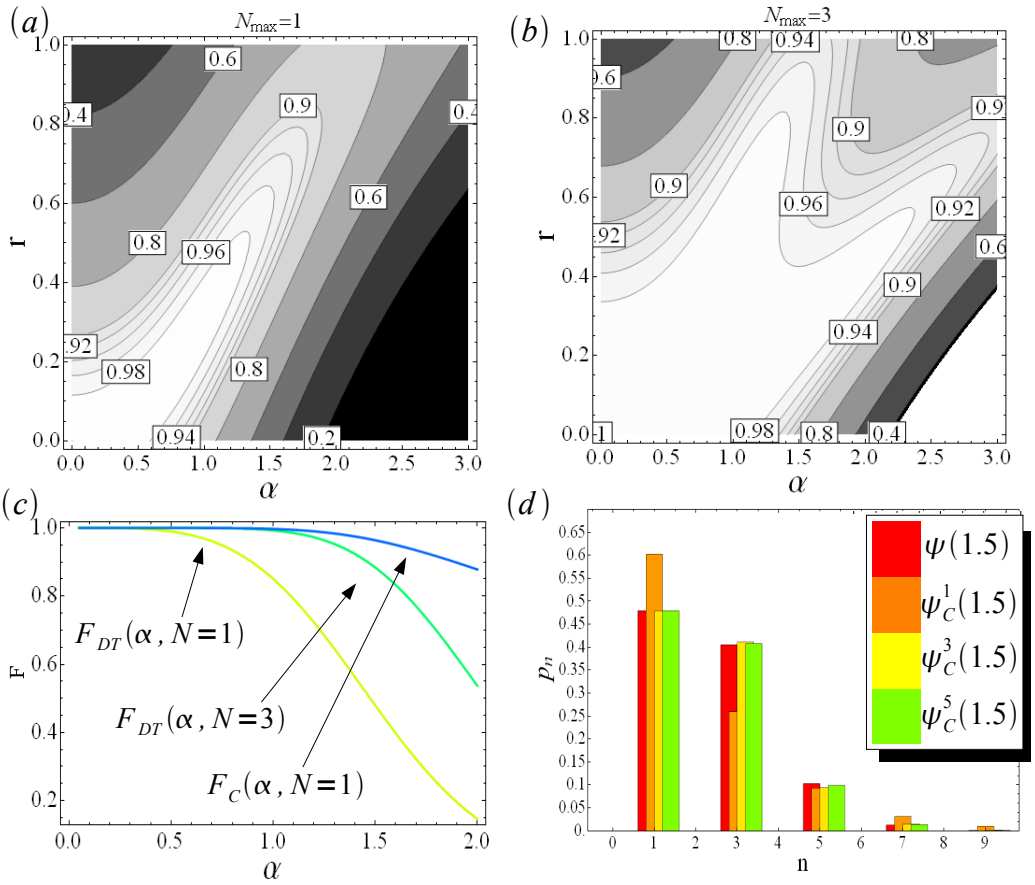

Figure 7.4: *(a) Displays the relation between* α *and* r *for different constant values of the fidelity* $\mathcal{F}_C(\alpha, r, N = 1)$ *for one photon subtraction. (b) Shows the same information, i.e.* $\mathcal{F}_C(\alpha, r, N = 3)$*. (c) Displays a comparison of the fidelities between the target state and states from our core method and direct truncation. Finally, (d) compares the photon number distributions of the approximate targets with the actual target* $|\psi(\alpha)\rangle$ *for* $\alpha = 1.5$ *with* $N = 1, 3, 5$*. The optimal squeezing for these cores are* $r = (0.597, 0.263, 0.157)$ *giving fidelities* $\mathcal{F}_C = (0.9638, 0.9995, 0.9999)$*.*

targets is then defined as

$$\mathcal{F}_C(\alpha, r, N) = \sum_{n=0}^{N} \left| \mathcal{M}'' \sum_{k=0}^{\infty} \frac{\alpha^{2k} S_{2n,2k}(-r)}{\sqrt{(2k)!}} \right|^2 , \tag{7.40}$$

and the optimal core state for a given N is obtained by maximizing this quantity. Just as in the previous case for the odd parity cat, we consider this fidelity for $\alpha = 1.5$ in the case of $N = 2$ and $N = 4$. Already, one can consider the preparation of the even parity cat state more complicated than the odd one since the most basic even cat will require two photon subtractions rather than one. All of this is is shown in Fig.7.5. Firstly, in Fig.7.5(a) and Fig.7.5(b), we plot the $\mathcal{F}_C(\alpha, r, N)$ for $N = 2, 4$ where we once again see the non-trivial and non-unique relationship between α and the optimal squeezing. In Fig.7.5(c), we once again demonstrate that employing Gaussian operations is to our advantage since it allows an improvement in the accuracy of approximating $|\phi(\alpha)\rangle$ for less photon subtractions than required for the direct truncation method. Finally, Fig.7.5(d) shows how the states prepared by the core method approximate the desired target $|\phi(\alpha = 1.5)\rangle$. These examples are particularly elegant due to their inherent symmetry. In principle, this method could provide key insights into other desirable non-Gaussian pure states and their approximate preparation.

7.4 Discussion and concluding remarks

In summary, we have proposed that Gaussian operations can reduce the required non-Gaussian resources for pure state preparation. It is a non-trivial problem to establish the exact nature of this trade-off and ascertain whether it applies to all non-Gaussian pure states. Instead, we are limited to analyzing the properties of each desired target non-Gaussian state to determine if Gaussian operations are advantageous. Unfortunately, being able to demonstrate that this is true in general for arbitrary pure non-Gaussian states is a non-trivial task.

It remains an open question as to the application of this method to mixed states [156–158], which is likely to be a challenging problem. An insight into

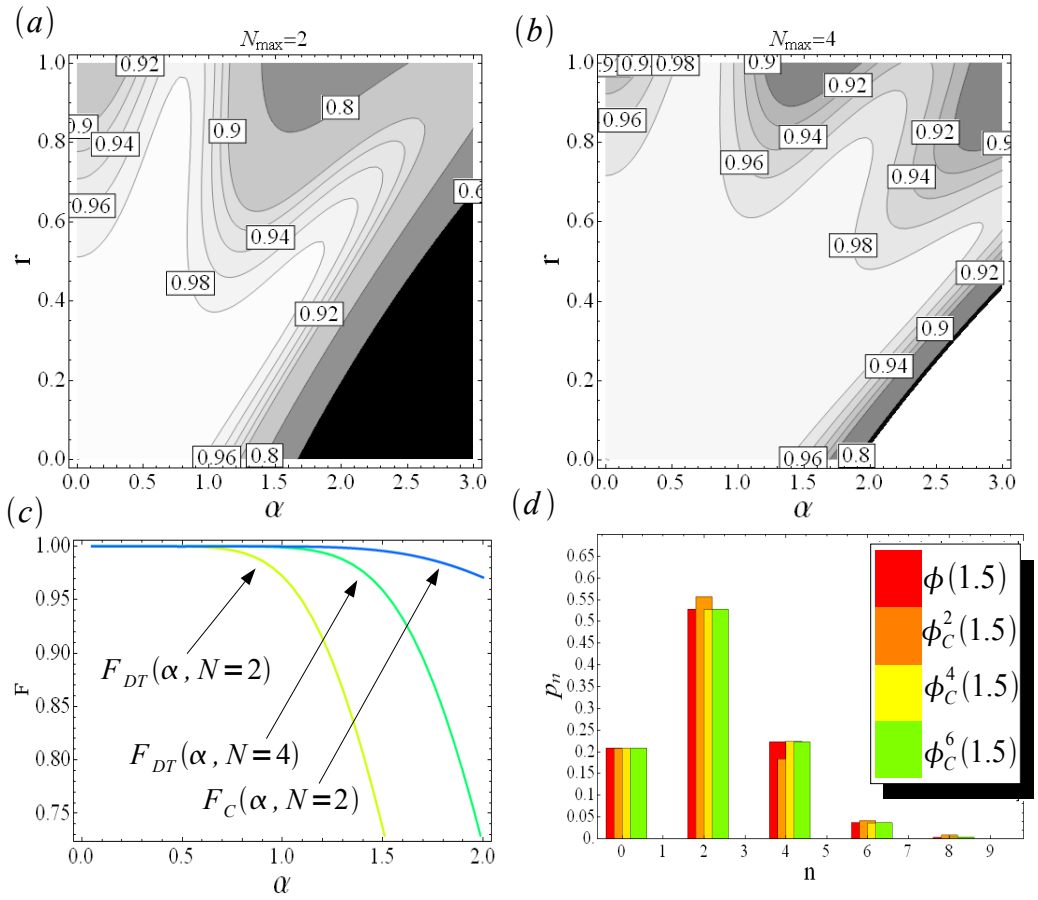

Figure 7.5: *(a) Displays the relation between* α *and* r *for different constant values of the fidelity* $\mathcal{F}_C(\alpha, r, N = 2)$ *for two photon subtractions. (b) Shows the same information, i.e.* $\mathcal{F}_C(\alpha, r, N = 4)$*. (c) Displays a comparison of the fidelities between the target state and states from our core method and direct truncation. Finally, (d) compares the photon number distributions of the approximate targets with the actual target* $|\phi(\alpha)\rangle$ *for* $\alpha = 1.5$ *with* $N = 2, 4, 6$*. The optimal squeezing for these cores are* $r = (0.376, 0.198, 0.272)$ *giving fidelities* $\mathcal{F}_C = (0.9958, 0.9999, 0.9999)$.

this can be gained by considering the attenuated version of the state $|\psi(\alpha)\rangle$ as the target state characterized by a transmission η. The target can be written as $p|\psi(\eta\alpha)\rangle\langle\psi(\eta\alpha)| + (1-p)/2(|\eta\alpha\rangle\langle\eta\alpha| + |-\eta\alpha\rangle\langle-\eta\alpha|)$, where $p = p(\alpha, \eta)$. Thus, it is enough to prepare the pure state $|\psi(\eta\alpha)\rangle$ and obtain the target by applying additional random operations which add the mixture of two coherent states. It follows, to find the core state, we have to subtract the non-Gaussian noise contribution from the target state. However, identifying this non-Gaussian noise remains an open problem. On the other hand, majority of the desired non-Gaussian states are pure, therefore our result is sufficient for all practical purposes. Another outstanding issue raised by our work is the assumption of perfect photon subtraction techniques. If we relax this assumption to consider noisy detectors then both the number of photon subtractions and the purity of each implemented subtraction could be advanced as a cost function for state preparation. This generalization would be an interesting problem to pursue. Moreover, our work here provides motivation to further investigate potential benefits of Gaussian operations on manipulations of non-Gaussian states including transmission through noisy channels, measurement induced nonlinearity schemes and in the preparation of non-Gaussian entangled states. In this way, we will come closer to understanding the subtle interplay between Gaussian and non-Gaussian structure of non-classical resources in quantum information.

Chapter 8

Conclusion

In this thesis, we have demonstrated the applicability of the weak measurement paradigm in a novel operational manner and highlighted the power of such an interpretation in certain state engineering protocols. The power of the weak measurement is that it allows the interaction between a probe and signal system, in which the signal is prepared and then measured in particular quantum states can be described via a single number, the weak value, in the limit of weak coupling. We have demonstrated its application in Gaussian entanglement concentration protocols, cloning of weak coherent states and in general bipartite pure Procrustean entanglement concentration protocols. We have found that the imaginary part of the weak value allows us to select particular configurations on the signal system that will allow the desired outcome of the protocol. We also found that this constraint generates a measurement-based success condition that allows the participating agents to decide when the protocol is successful. The weak measurement formalism is particularly elegant in this regard. Whilst the work in this thesis demonstrates the utility of exploring a weak measurement approach to these protocols, it is not an exhaustive analysis of the general applicability of weak measurements to quantum state engineering. The question whether such an analysis is even possible is left for future investigation.

In addition, we have also suggested and constructed an operational approach to the issue of non-Gaussian state preparation for quantum optical information. We

have shown that by specifying the method in which states are to be universally constructed allows a classification of non-Gaussian states in terms of the non-Gaussian resource cost with respect to that method. Furthermore, it also allows an investigation into whether the non-Gaussian resource overhead required for a desired state can be reduced by applying Gaussian unitary operations. We demonstrate this method on the Schrödinger cat states where we show that the single mode squeezing operation can be used to reduce the number of consecutive photon subtractions to sufficiently approximate the desired state. Much remains to be explored with this method and its wider applicability to non-Gaussian state engineering remains an open issue.

Bibliography

[1] D. Menzies and N. Korolkova. *Phys. Rev. A* **74**, *042315*, 2006.

[2] D. Menzies and N. Korolkova. *Phys. Rev. A* **76**, *062310*, 2007.

[3] D. Menzies and N. Korolkova. *Phys. Rev. A* **77**, *062105*, 2008.

[4] D. Menzies and R. Filip. *Phys. Rev. A* **79**, *012313*, 2009.

[5] D. Menzies and S. Croke. *e-print: arXiv:0903.4181v1*, 2009.

[6] C. Fuchs. *Journ. Mod. Opt.* **50**, *6-7, 987*, 2003.

[7] C. H. Bennett, G. Brassard, C. Crèpeau, R. Jozsa, A. Peres, and W. K. Wootters. *Phys. Rev. Lett.* **70**, *1895*, 1993.

[8] S. L. Braunstein and H. J. Kimble. *Phys. Rev. Lett.* **80**, *4, 869*, 1998.

[9] M. Nielsen and I. Chuang. *Quantum Computation and Quantum Information.* Cambridge University Press, 2000.

[10] M. Hirvensalo. *Quantum computing (Natural Computing Series).* Springer-Verlag (Berlin), 2003.

[11] A. Ekert. *Phys. Rev. Lett.* **67**, *661*, 1991.

[12] D. Brouwmeester, A. Ekert, and A. Zeilinger. *The physics of quantum information.* Springer-Verlag (Berlin), 2000.

[13] V. Vedral. *Introduction to Quantum Information Science.* Oxford University Press, 2006.

[14] H. A. Bachor and T. C. Ralph. *A Guide to Experiments in Quantum Optics*. Wiley-Vch, 2006.

[15] S. L. Braunstein and P. van Loock. *Rev. Mod. Phys.* **77**, *513*, 2003.

[16] G. Giedke and J.I. Cirac. *Phys. Rev. A* **66**, *032316*, 2002.

[17] S. Scheel J. Eisert and M. B. Plenio. *Phys. Rev. Lett.* **89**, *137903*, 2002.

[18] J. Fiurášek. *Phys. Rev. Lett.* **89**, *137904*, 2002.

[19] S. Lloyd and S. Braunstein. *Phys. Rev. Lett.* **82**, *1784*, 1999.

[20] A. Kitaev D. Gottesman and J. Preskill. *Phys. Rev. A.* **64**, *012310*, 2001.

[21] N. J. Cerf, G. Leuchs, and E. S. Polzik (Eds.). *Quantum Information with Continuous Variables of Atoms and Light*. Imperial College Press, 2007.

[22] R. Loudon. *The quantum theory of light*. Oxford University Press, 1973.

[23] D. Walls and G. Milburn. *Quantum Optics*. Spinger, 1995.

[24] L. Mandel and E. Wolf. *Optical Coherence and Quantum Optics*. Cambridge University Press, 1995.

[25] S. Barnett and P. Radmore. *Methods in Theoretical Quantum Optics*. Oxford science publications, 2002.

[26] M. O'Scully and M. Zubairy. *Quantum Optics*. Cambridge University Press, 1997.

[27] U. Leonhardt. *Measuring the Quantum State of Light*. Cambridge University Press, 1997.

[28] C. Gerry and P. Knight. *Introductory Quantum Optics*. Cambridge University Press, 2005.

[29] R. Y. Chiao J. C. Garrison. *Quantum Optics*. Oxford University Press, 2008.

[30] G. Auletta. *Foundations and Interpretations of Quantum Mechanics*. World Scientific, 2001.

[31] A. Ferraro, S. Olivares, and M. G. A. Paris. *Gaussian states in continuous variable quantum information*. Bibliopolis, (Napoli), 2005.

[32] E. P. Wigner. *Phys. Rev.* **40**, *749*, 1932.

[33] U. Titulaer and R. Glauber. *Phys. Rev.* **140**, *B676*, 1965.

[34] R. F. OConnell, M. O. Scully, and E. P. Wigner. *Phys. Reports* **106**, *121*, 1984.

[35] L. Mandel. *Phys. Scr. T12, 34*, 1986.

[36] A. Kenfack and K. Zyczkowski. *J. Opt. B: Quantum Semiclass. Opt.* **6**, *396*, 2004.

[37] U. Leonhardt. *Rep. Prog. Phys.* **66**, *1207*, 2003.

[38] F. Dell'anno, S. De Siena, and F. Illuminati. *Phys. Rep.* **428**, *2-3, 53*, 2006.

[39] N. Korolkova, G. Leuchs, R. Loudon, T. C. Ralph, and C. Silberhorn. *Phys. Rev. A.* **65**, *052306*, 2002.

[40] T. Tyc and B. C. Sanders. *Journ. Phys. A: Mat. Gen.* **37**, *7341*, 2004.

[41] S. L. Braunstein and H. J. Kimble. *Phys. Rev. A* **61**, *042302*, 2000.

[42] J. Eisert, D. Browne, S. Scheel, and M. B. Plenio. *Annals of Physics* **311**, *431*, 2004.

[43] S. Olivares and M. G. A. Paris. *Laser Phys.* **16**, *11, 1433*, 2006.

[44] S. Olivares and M. G. Paris. *Journ. Opt. B: Quantum Semiclass. Opt.* **7**, *S616*, 2005.

[45] E. Knill, R. Laflamme, and G. J. Milburn. *Nature* **409**, *46*, 2000.

[46] J. Fiurášek, R. García-Patrón, and N. J. Cerf. *Phys. Rev. A.* **72**, *033822*, 2005.

[47] M. Dakna, T. Anhut, T. Opatrný, L. Knöll, and D. G. Welsch. *Phys. Rev. A.* **55**, *3184*, 1997.

[48] A. Zavatta, S. Viciani, and M. Bellini. *Science* **306**, *660*, 2004.

[49] M. Dakna, J. Clausen, L. Knöll, and D. G. Welsch. *Phys. Rev. A.* **59**, *2, 1658*, 1999.

[50] S. Scheel, K. Nemoto, W. Munro, and P. Knight. *Phys. Rev. A* **68**, *032310*, 2003.

[51] W. J. Munro, K. Nemoto, R. G. Beausoleil, and T. P. Spiller. *Phys. Rev. A.* **71**, *033819*, 2005.

[52] G. J. Milburn. *Phys. Rev. Lett.* **62**, *18, 2124*, 1989.

[53] K. Nemoto and W. J. Munro. *Phys. Rev. Lett.* **93**, *250502*, 2004.

[54] J. Fiurášek, L. Mišta, and R. Filip. *Phys. Rev. A* **67**, *022304*, 2003.

[55] J. Clausen, L. Knöll, and D-G. Welsch. *J. Opt. B: Quantum Semiclass. Opt.* **4**, *155*, 2002.

[56] Z-M. Zhang, A. H. Khosa, M. Ikram, and M. S. Zubairy. *Journ. Phys. B: Mol. Opt. Phys.* **40**, *1917*, 2007.

[57] T. Tyc and N. V. Korolkova. *New Journ. Phys.* **10**, *023041*, 2008.

[58] T. C. Ralph, A. Gilchrist, G. J. Milburn, W. J. Munro, and S. Glancy. *Phys. Rev. A.* **68**, *042319*, 2003.

[59] T. C. Ralph. *Rep. Prog. Phys.* **69**, *853*, 2006.

[60] H. Jeong, M. S. Kim, T. C. Ralph, and B. S. Ham. *Phys. Rev. A.* **70**, *061801(R)*, 2004.

[61] A. Ourjoumtsev, R. Tualle-Brouri, J. Laurat, and Ph. Grangier. *Science* **312**, *83*, 2006.

[62] A. Einstein, B. Podolsky, and N. Rosen. *Phys. Rev.* **47**, *777*, 1935.

[63] J. Bell. *Speakable and unspeakable in Quantum Mechanics*. Cambridge University Press, 1987.

[64] A. Aspect, P. Grangier, and G. Roger. *Phys. Rev. Lett.* **48**, *460*, 1981.

[65] D. Bruss. *Journ. Math. Phys.* **43**, *4237*, 2002.

[66] S. Barnett and S. J. D. Phoenix. *Phys. Rev. A*. **40**, *5, 2404*, 1989.

[67] H. K. Lo, S. Popescu, and T. Spiller. *Introduction to quantum computation and information*. World Scientific, 2000.

[68] M. Hayashi. *Quantum Information, An Introduction*. Springer, 2006.

[69] K. Życzkowski and I. Bengtsson. *Ann. Phys.* **295**, *113*, 2002.

[70] C. H. Bennett, H. J. Bernstein, S. Popescu, and B. Schumacher. *Phys. Rev. A* **53**, *4, 2046*, 1996.

[71] M. A. Nielsen. *Phys. Rev. Lett.* **83**, *2, 436*, 1999.

[72] A. W. Marshall. *Inequalities: theory of majorization and its applications*. Academic Press, 1979.

[73] G. Vidal. *Phys. Rev. Lett.* **83**, *5, 1046*, 1999.

[74] D. Jonathan and M. B. Plenio. *Phys. Rev. Lett.* **83**, *7, 1455*, 1999.

[75] D. Jonathan and M. B. Plenio. *Phys. Rev. Lett.* **83**, *17, 3566*, 1999.

[76] M. Ban. *J. Opt. B: Quantum Semiclass. Opt.* **2**, *576*, 2000.

[77] A. Ourjoumtsev, A. Dantan, R. Tualle-Brouri, and P. Grangier. *Phys. Rev. Lett.* **98**, *030502*, 2007.

[78] L. M. Duan, G. Giedke, J. I. Cirac, and P. Zoller. *Phys. Rev. Lett.* **84**, *17, 4002*, 2000.

[79] L. M. Duan, G. Giedke, J. I. Cirac, and P. Zoller. *Journ. Mod. Opt.* **47**, *14 -15, 2529*, 2000.

[80] B. Hage, A. Franzen, J. DiGuglielmo, P. Marek, J. Fiurášek, and R. Schnabel. *New Journal of Physics* **9**, *227*, 2007.

[81] R. Dong, M. Lassen, J. Heersink, C. Marquardt, R. Filip, G. Leuchs, and U. L. Andersen. *Nature Physics* **4**, *12, 919*, 2008.

[82] B. Hage, A. Samblowski, J DiGuglielmo, A. Franzen, J. Fiurášek, and R. Schnabel. *Nature Physics* **4**, *12, 915*, 2008.

[83] Y. Aharonov and L. Vaidman. *Phys. Rev. A.* **41**, **1**, *11*, 1990.

[84] Y. Aharonov, D. Z. Albert, and L. Vaidman. *Phys. Rev. Lett.* **60**, **4**, *1351*, 1988.

[85] Y. Aharonov and D. Rohrlich. *Quantum Theory for the Perplexed*. Wiley-Vch, 2005.

[86] Y. Aharonov and A. Botero. *Phys. Rev. A.* **72**, *052111*, 2005.

[87] J. Von Neumann. *Mathematical Foundations of Quantum Mechanics*. Princeton Unversity Press, 1955.

[88] R. Jozsa. *Phys. Rev. A.* **76**, *0441031*, 2007.

[89] G. Mitchison, R. Jozsa, and S. Popescu. *Phys. Rev. A.* **76**, *062105*, 2007.

[90] G. Mitchison. *Phys. Rev. A* **77**, *052102*, 2008.

[91] J. G. Story, N. W. M. Richie, and R. G. Hulet. *Mod. Phys. Lett. B* **5**, **26**, *1713*, 1991.

[92] I. M. Duck, P. M. Stevenson, and E. C. G. Sudarshan. *Phys. Rev. D.* **40**, **6**, *2112*, 1989.

[93] D. R. Solli, C. F. McCormick, R. Y. Chiao, S. Popescu, and J. M. Hickmann. *Phys. Rev. Lett.* **92**, **4**, *043601*, 2004.

[94] Y. Aharonov, N. Erez, and B. Reznik. *Journ. Mod. Opt.* **50**, *6-7, 1139*, 2003.

[95] Y. Aharonov, N. Erez, and B. Reznik. *Phys. Rev. A.* **65**, *052124*, 2002.

[96] N. Brunner, A. Acín, D. Collins, N. Gisin, and V. Scarani. *Phys. Rev. Lett.* **91**, **18**, *180402*, 2003.

[97] R. Brout, S. Massar, R. Parentani, S. Popescu, and P. Spindel. *Phys. Rev. D.* **52**, **2**, *1120*, 1995.

[98] Y. Aharonov and L. Vaidman. *Journ. Phys. A: Math. Gen.* **24**, *2315*, 1991.

[99] B. Reznik and Y. Aharonov. *Phys. Rev. A.* **52**, **4**, *2538*, 1995.

[100] Y. Aharonov and L. Vaidman. *Physica Scripta* **T76**, *85*, 1998.

[101] Y. Aharonov and J. Tollaksen. *e-print: arXiv:0706.1232*, 2007.

[102] J. Tollaksen. *J. Phys. A. Math. Theor.* **40**, *9033*, 2007.

[103] A. Tanaka. *Phys. Lett. A.* **297**, *307*, 2002.

[104] A. Botero and B. Reznik. *Phys. Rev. A.* **61**, *050301*, 2000.

[105] E. Sjöqvist and J. Aberg. *Phys. Lett. A* **354**, *396*, 2006.

[106] A. D. Parks. *J. Phys. A: Math. Gen.* **33**, *2555*, 2000.

[107] G. J. Pryde, J. L. O'Brien, A. G. White, T. C. Ralph, and H. M. Wiseman. *Phys. Rev. Lett.* **94**, **22**, *220405*, 2005.

[108] T. C. Ralph, S. D. Bartlett, J. L. O'Brien, G. J. Pryde, and H. M. Wiseman. *Phys. Rev. A.* **73**, *012113*, 2006.

[109] G. S. Agarwal and P. K. Pathak. *Phys. Rev. A.* **75**, *032108*, 2007.

[110] O. Hosten and P. Kwiat. *Science* **319**, *787*, 2008.

[111] K. J. Resch. *Science* **319**, *733*, 2008.

[112] L. M. Johansen. *Phys. Rev. Lett.* **93**, **12**, *120402*, 2004.

[113] H. Kang and Y. Zhu. *Phys. Rev. Lett.* **91**, *9, 093601*, 2003.

[114] K-P. Marzlin Z-B. Wang and B. C. Sanders. *Phys. Rev. Lett.* **97**, *063901*, 2006.

[115] G. Sinclair and N. Korolkova. *Phys. Rev. A.* **76**, *033803*, 2007.

[116] G. Agrawal. *Nonlinear Fiber Optics.* Academic Press, 2001.

[117] J. H. Shapiro. *Phys. Rev. A.* **73**, *062305*, 2006.

[118] J. H. Shapiro and M. Razavi. *New Journ. Phys.* **9**, *16*, 2007.

[119] W. J. Munro, K. Nemoto, R. G. Beausoleil, and T. P. Spiller. *Phys. Rev. A.* **71**, *033819*, 2005.

[120] T. C. Ralph and A. P. Lund. *e-print: arXiv:0809.0326v1*, 2008.

[121] C. M. Caves. *Phys. Rev. D* **26**, *1817*, 1982.

[122] N. Schuch, F. Verstraete, and J. I. Cirac. *Phys. Rev. A.* **70**, *042310*, 2004.

[123] S. D. Bartlett, T Rudolph, and R. W. Spekkens. *Rev. Mod. Phys.* **79**, *555*, 2007.

[124] L. M. Johansen and A. Luis. *Phys. Rev. A* **70**, *052115*, 2004.

[125] L. M. Johansen. *Phys. Lett. A.* **329**, *184*, 2004.

[126] N. S. Williams and A. N. Jordan. *Phys. Rev. Lett.* **100**, *026804*, 2008.

[127] R. Short and L. Mandel. *Phys. Rev. Lett.* **51**, *384*, 1983.

[128] A. I. Lvovsky, H. Hansen, T. Aichele, O. Benson, J. Mlynek, and S. Schiller. *Phys. Rev. Lett.* **87**, *050402*, 2001.

[129] A. Ourjoumtsev, R. Tualle-Brouri, and Ph. Grangier. *Phys. Rev. Lett.* **96**, *213601*, 2006.

[130] A. I. Lvovsky and J. Mlynek. *Phys. Rev. Lett.* **88**, *250401*, 2002.

[131] A. Ourjoumtsev, H. Jeong, R. Tualle-Brouri, and Ph. Grangier. *Nature* **448**, *784*, 2007.

[132] J. Wenger, R. Tualle-Brouri, and Ph. Grangier. *Phys. Rev. Lett.* **92**, *153601*, 2004.

[133] J. S. Neergaard-Nielsen, B. Melholt Nielsen, C. Hettich, K. Moelmer, and E. S. Polzik. *Phys. Rev. Lett.* **97**, *083604*, 2006.

[134] T. Opatrny, G. Kurizki, and D. G. Welsch. *Phys. Rev. A* **61**, *032302*, 2000.

[135] S. Olivares, M. G. A. Paris, and R. Bonifacio. *Phys. Rev. A* **67**, *032314*, 2003.

[136] A. Kitagawa, M. Takeoka, M. Sasaki, and A. Chefles. *Phys. Rev. A.* **73**, *042310*, 2006.

[137] F. Dell'Anno, S. De Siena, L. Albano, and F. Illuminati. *Phys. Rev. A.* **76**, *022301*, 2007.

[138] C. Invernizzi, S. Olivares, M. G. A. Paris, and K. Banaszek. *Phys. Rev. A.* **72**, *042105*, 2005.

[139] S. Olivares and M. G. A. Paris. *J. Opt. B: Quantum and Semiclass. Opt.* **7**, *S392*, 2005.

[140] R. García-Patrón, J. Fiurásek, N. J. Cerf, J. Wenger, R. Tualle-Brouri, and P. Grangier. *Phys. Rev. Lett.* **93**, *130409*, 2004.

[141] S. Olivares and M. G. A. Paris. *Phys. Rev. A.* **70**, *032112*, 2004.

[142] J. Fiurášek, R. García-Patrón, and N. J. Cerf. *Phys. Rev. A.* **71**, *022105*, 2005.

[143] H. Jeong. *Phys. Rev. A.* **78**, *042101*, 2008.

[144] A. E. B. Nielsen and K. Mölmer. *Phys. Rev. A* **76**, *043840*, 2007.

[145] M. Sasaki, M. Takeoka, and H. Takahashi. *Phys. Rev. A* **77**, *063840*, 2008.

[146] M. Takeoka, H. Takahashi, and M. Sasaki. *Phys. Rev. A* **77**, *062315*, 2008.

[147] M. Takeoka and M. Sasaki. *Phys. Rev. A* **75**, *064302*, 2007.

[148] W. Vogel. *Phys. Rev. Lett.* **84**, *1849*, 2000.

[149] M. S. Kim, W. Son, V. Buzek, and P. L. Knight. *Phys. Rev. A.* **65**, *032323*, 2002.

[150] J. K. Asboth, J. Calsamiglia, and H. Ritsch. *Phys. Rev. Lett.* **94**, *173602*, 2005.

[151] E. Shchukin, T. Richter, and W. Vogel. *Phys. Rev. A* **71**, *011802*, 2005.

[152] M. G. Genoni, M. G. A. Paris, and K. Banaszek. *Phys. Rev. A* **76**, *042327*, 2007.

[153] M. G. Genoni, M. G. A. Paris, and K. Banaszek. *eprint:arXiv:0805.1645*, 2008.

[154] S. A. Babichev, J. Ries, and A. I. Lvovsky. *Europhys. Lett.* **64**, *1, 17*, 2003.

[155] P. Marian. *Phys. Rev. A.* **44**, *3325*, 1991.

[156] M. S. Kim, E. Park, P. L. Knight, and H. Jeong. *Phys. Rev. A.* **71**, *043805*, 2005.

[157] K. Molmer. *Phys. Rev. A.* **73**, *063804*, 1991.

[158] A. Zavatta, V. Parigi, and M. Bellini. *Phys. Rev. A* **75**, *052106*, 2007.